Accepted Manuscript

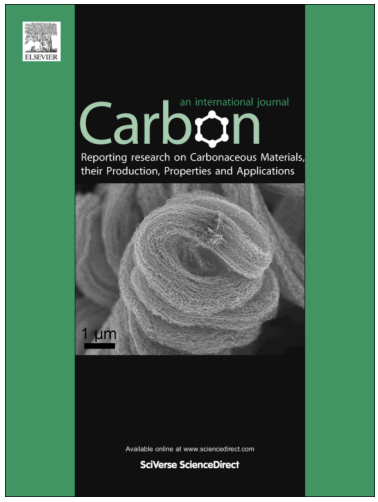

Carbon as Catalyst and Support for Electrochemical Energy Conversion

Panagiotis Trogadas, Thomas F. Fuller, Peter Strasser

PII: S0008-6223(14)00324-8
DOI: http://dx.doi.org/10.1016/j.carbon.2014.04.005
Reference: CARBON 8891

To appear in: *Carbon*

Received Date: 29 November 2013
Accepted Date: 1 April 2014

Please cite this article as: Trogadas, P., Fuller, T.F., Strasser, P., Carbon as Catalyst and Support for Electrochemical Energy Conversion, *Carbon* (2014), doi: http://dx.doi.org/10.1016/j.carbon.2014.04.005

Carbon as Catalyst and Support for Electrochemical Energy Conversion

Panagiotis Trogadas [a*], *Thomas F. Fuller* [b] *and Peter Strasser* [a*]

[a] The Electrochemical Energy, Catalysis, and Materials Science Laboratory, Department of Chemistry, Chemical Engineering Division, Technical University Berlin, Berlin, Germany 10623

[b] School of Chemical & Biomolecular Engineering, Georgia Institute of Technology, Atlanta, GA 30332-0100, USA

[*] Corresponding author: pstrasser@tu-berlin.de

Carbon has unique characteristics that make it an ideal material for use in a wide variety of electrochemical applications ranging from metal refining to electrocatalysis and fuel cells. In polymer electrolyte fuel cells (PEFCs), carbon is used as a gas diffusion layer, electrocatalyst support and oxygen reduction reaction (ORR) electrocatalyst. When used as electrocatalyst support, amorphous carbonaceous materials suffer from enhanced oxidation rates at high potentials over time. This drawback has prompted an extensive effort to improve the properties of amorphous carbon and to identify alternate carbon-based materials to replace carbon blacks. Alternate support materials are classified in carbon nanotubes and fibers, mesoporous carbon, multi-layer graphene (undoped and doped with metal nanoparticles) and reduced graphene oxide. A comparative review of all these supports is provided. Work on catalytically active carbon hybrids is focused on the development of non-precious metal electrocatalysts that will significantly reduce the cost without sacrificing catalytic activity. Of the newer electrocatalysts, nitrogen/metal-functionalized carbons and composites are emerging as possible contenders for commercial PEFCs. Nitrogen-doped carbon hybrids with transition metals and their polymer composites exhibit high ORR activity and selectivity and these catalytic properties are presented in detail in this review.

Table of Contents

1. Introduction

Carbon is distinct among chemical elements since it is found in dramatically different forms and with varying micro-textures. The diverse morphologies of carbon make it an attractive material that is widely used in a large range of electrochemical applications. Carbon exists in various allotropic forms due to its valency [1], with the most well-known being carbon black, diamond, fullerenes, graphene, and carbon nanotubes. This review is divided into five sections. In the first two sections the structure, electronic and electrochemical properties of carbon are presented along with their applications. The last three sections deal with the use of carbon in proton exchange and alkaline membrane fuel cells (PEFCs), as catalyst support and oxygen reduction reaction (ORR) electrocatalyst.

2. Carbon as Electrode and Electrocatalyst

2.1 Structure and Properties

2.1.1 Carbon Black

Carbon black is usually produced by the "furnace black" process, namely the partial combustion of petrochemical or coal tar oils [2]. Due to the nature of the source materials, heat treatment is used (250-500^{o}C) to remove impurities from the formed carbon [3-5]. Carbon black consists of spherical particles (diameter less than 50 nm) that may aggregate and form agglomerates (~ 250 nm diameter) [6]. The carbonaceous particles have para-crystallite structures [6] consisting of parallel graphitic layers with 0.35-0.38 nm interplanar spacing. The crystalline graphitic portion of carbon black has sp^2 hybridization involving a triangle in-plane formation of sp^2 orbitals while the fourth

p_z orbital lies normal to this plane forming weaker delocalized π bonds with other neighboring carbon atoms [7-9]. Chemical ($ZnCl_2$ / H_3PO_4 addition to carbon precursor) or gas (steam / CO_2) treatment of carbon black at high temperatures (800-1100ºC) and high pressure leads to the formation of activated carbon black; this form of carbon is characterized by larger and more crystalline graphitized carbon particles (~ 20-30 μm) with distinct micro-porosity and varying BET surface area (200-1200 m^2g^{-1}) [6].

Activated carbon black is often confused with activated carbon. Activated carbon is a common amorphous carbon, characterized by high pore volume (~ 2.25 cm^3g^{-1}) and surface area (~ 4100 m^2g^{-1}) [10-13]. Nitrogen adsorption isotherms revealed that activated carbons contain micro- and macro-pores with the meso-pore content being much lower [12].

The chemical characteristics (acidic / basic) of activated carbons depend on the chemical heterogeneity of the surface (the amount of non-carbon heteroatoms present in carbon structure) [14].

The presence of surface groups containing oxygen (such as carboxylic acid / anhydride, lactone, and phenolic hydroxyl [15]) on the outer surface of activated carbon increases the surface acidity and adsorption ability [16-19] of the material [13]. Gas and liquid phase oxidations are employed to incorporate oxygen containing acidic groups on the activated carbon surface [20]. Gas phase oxidation results in an increase of hydroxyl and carbonyl groups on the surface of activated carbon [13], whereas liquid phase oxidation

leads to an increased amount of carboxylic and phenolic hydroxyl groups on the surface of activated carbon [20, 21].

The presence of nitrogen groups on the surface of activated carbon increases the basicity of the material and improves the interaction between the carbon surface and acid molecules (such as covalent and hydrogen bonding) [13]. Nitrogen groups can be incorporated onto activated carbon surface via reactions with nitrogen reagents (NH_3, nitric acid, and amines) [13] or precursors [22-25].

The detection of oxygen / nitrogen groups on the surface of activated carbon is achieved by titration [15, 26-29], desorption [27, 30-36], X-ray photoelectron spectroscopy [37-42], Fourier Transform Infrared Spectroscopy (FT-IR) [43-46], NMR [47], Inverse Gas Chromatography [48] and surface imaging techniques, such as SEM and STM [32].

The high surface area (~250 m^2g^{-1} for Vulcan XC-72), low cost and availability of CBs transform it to an attractive material for fuel-cells [49]. Carbon black is widely used as electrocatalyst support but still suffers from issues that decrease the catalytic activity of the material. The presence of organo-sulphur impurities and deep micro-pores on carbon surface as well as the stability of carbon are the most important. Catalyst nanoparticles are trapped in the micro-pores and do not have access to reactants/Nafion® resulting to a decrease of catalytic activity [49]. Carbon black is also unstable under the highly acidic/alkaline conditions of a fuel-cell resulting to the corrosion of carbon support and detachment of catalyst nanoparticles [50]. As a result, extended research is being conducted on the use of other allotropic forms of carbon in fuel-cells.

2.1.2 Diamond

Diamond is another natural allotrope of carbon that has cubic structure in which each atom uses sp^3 orbitals to form four strong, covalent bonds. These bonds contribute to the hardness and high melting point of diamond [6]. On diamond {1, 0, 0} the surface atoms reconstruct and form π-bonded, symmetric dimers arranged in rows (~ 2.5 A inner distance). This causes a further splitting of the dimer orbitals and the formation of a band gap (~ 1.3eV) between occupied and unoccupied surface states [51]. On the contrary, on diamond {1, 1, 0} and {1, 1, 1} surfaces, the bonds are arranged in symmetric π-bonded chains without dimerization. Even though the inner distance between the π-orbitals (~ 1.5 and 1.4 A for {1, 1, 0} and {1, 1, 1} surfaces respectively) is smaller than the distance between π-dimers on {1, 0, 0} surface, the distance between the π-bonded chains is large (3.6 and 4.4 A respectively). As a result, a π-electron system is formed along the chains and these surfaces obtain metallic character [51].

Undoped diamond is not an attractive material for fuel-cells since it is an electrical insulator with a band gap greater than 5eV [49]. However, boron doped diamond is often used as electrocatalyst support material in fuel-cells [52-56] due to the improved conductivity, high electrochemical stability and corrosion resistance in acidic and alkaline media [57-59].

2.1.3 Fullerenes

Fullerenes are closed carbon molecules with sphere-like shape, a hollow core and diameters below 1 nm [60]. The most stable fullerene, C_{60}, is built of carbon atoms with sp^2-hybridization assembled in a truncated icosahedron. It consists of 60 carbon atoms made up of 20 hexagons and 12 pentagons, which result to the quasi-spherical structure of the molecule (Fig. 1) [60]. The molecular structure of fullerene results in a closed-shell electronic structure with highly degenerate π- and σ-derived molecular electronic states including the π-derived fivefold degenerate highest occupied molecular orbital (HOMO) and the triply degenerate lowest unoccupied molecular orbital (LUMO) [60, 61]. According to the isolated pentagon rule, separate 60-atom cages are held together by weak forces in order to avoid the contact of their surface pentagons and thus increase the stability of fullerene.

Figure 1. Structure of the C_{60} fullerene molecule consisted of 20 hexagons and 12 pentagons with carbon atoms at each corner (Reprinted from [60] with permission from Elsevier).

2.1.4 Mesoporous Carbon (MC)

Mesoporous carbon is a porous carbon material with pore size varying between 2-50 nm [62] and can be classified to ordered (OMC) and disordered (DOMC) pore structure [63-75]. The mesopores in irregular structure carbon are isolated and the pore size distribution is wider than OMC [62].

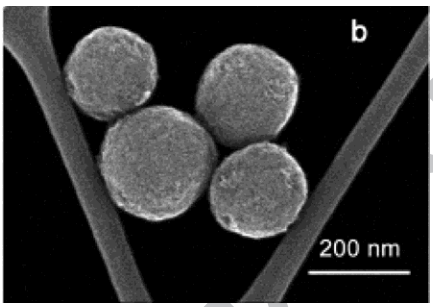

Figure 2. Mesoporous carbon nanospheres (~ 180 nm diameter) (Reprinted with permission from [76] - Copyright© 2013 American Chemical Society).

The pore structure of mesoporous carbon is controlled via the "hard-templating" method [77] where inorganic porous materials such as alumina membranes [78], zeolites [79], xerogels [22, 80], opals [81], micelles [82] and ordered mesoporous silica [83-90] are used as templates. However, the structure and morphology of the produced mesoporous carbon materials are limited to the parent template [76] and thus new alternative methods are being investigated. These novel synthesis techniques include the evaporation-induced self-assembly (EISA) [91-94] and hydrothermal method [76, 95]. Highly ordered mesoporous carbon with large uniform pores and high surface area was obtained.

Mesoporous carbon has higher surface area and very low amount of micropores compared to Carbon black (Vulcan) [72]. Hence, there is high metal dispersion and mass

transport resulting to higher catalytic activity [72]. Moreover, mesoporous carbon possess good chemical and mechanical stability as well as electrical conductivity and hence, this material has great application potential to a wide range of applications including hydrogen storage, sensors, catalysts, catalyst supports and electrochemical double layer capacitors [71, 72, 83, 96-98].

2.1.5 Carbon Nanotubes (CNTs)

CNTs consist of cylinders made of graphite layers that are closed at both ends. Both single- (SWCNTs) and multi-walled nanotubes (MWCNTs) exist, with diameters of a few nanometers and lengths of the order of 1 mm[6]. Nanotubes are classified by the wrapping vector (n, m) corresponding to the direction and distance in which the graphite layer is wrapped up [60] (Fig. 3). The arm-chair (n, n) and the zigzag (n, 0) tubes that have reflection planes are achiral, whereas all other tubes with independent n and m are chiral. Metallic nanotubes are characterized by wrapping vectors where n-m = 3·l (l=0, 1, 2, 3, etc) whereas all the other tubes are semiconductors [99, 100]. An interesting property of both fullerenes and carbon nanotubes is their ability to entrap atoms of other elements within their molecular structure. In this respect hydrogen storage in carbon nanotubes is of particular interest to fuel-cell developers.

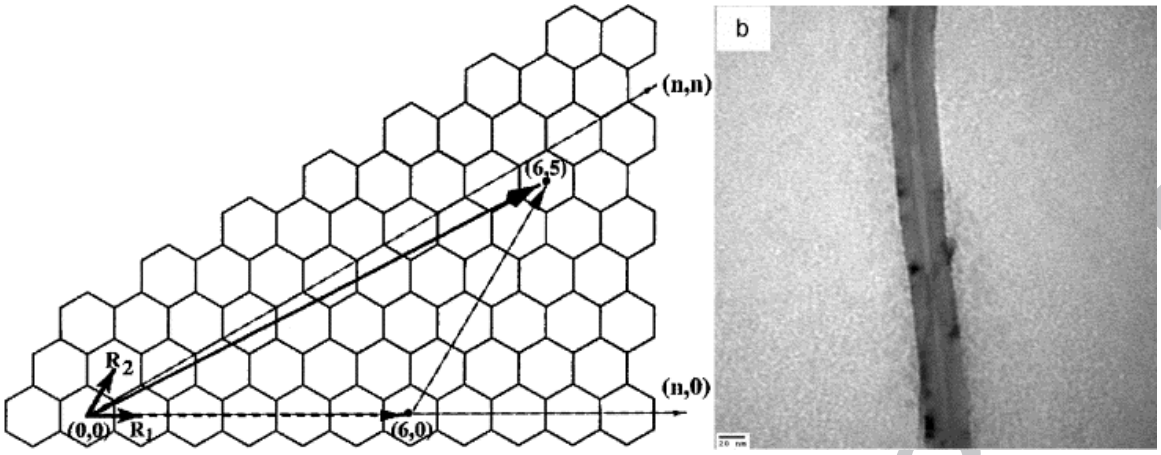

Figure 3. a) Structure of 2-D graphite layer (nanotube precursor). The primitive lattice vectors R_1 and R_2 are depicted. CNTs can be envisaged as wrapped up graphite layers whereby the wrapping direction and distance are given by a single vector. The wrapping vector (6, 5) is shown for illustration (Reprinted from [60] with permission from Elsevier); b) Transmission electron microscopy (TEM) image of CNT (Reprinted from [101] with permission from Elsevier).

2.1.6 Carbon Nanofibers (CNFs)

CNF is an industrially produced derivative of carbon formed by the decomposition and graphitization of rich organic carbon polymers (Fig. 4). The most common precursor is polyacrylonitrile (PAN), as it yields high tensile and compressive strength fibers that have high resistance to corrosion, creep, and fatigue. For these reasons, the fibers are widely used in the automotive and aerospace industries [6]. Carbon fiber is an important ingredient of carbon composite materials, which are used in fuel-cell construction, particularly in gas-diffusion layers where the fibers are woven to form a type of carbon cloth.

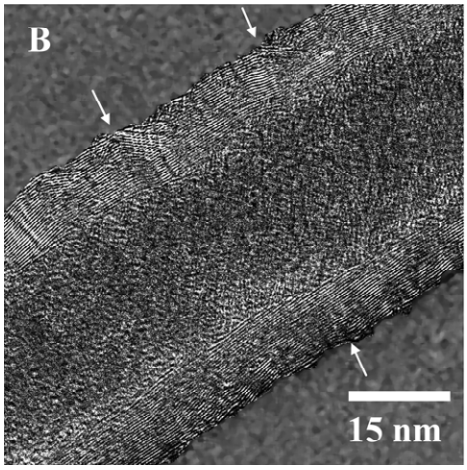

Figure 4. High resolution TEM micrograph of Carbon nanofiber (Reprinted with permission from [102] - Copyright© 2004 American Chemical Society).

2.2 Electrochemical Properties

During the last several years, extensive research has focused on the application of carbons as electrode materials because of their availability, physicochemical properties, processability, and relatively low cost. Carbon electrodes are thermally and mechanically stable, chemically resistant in different solutions (from strongly acidic to basic) as well as chemically inert [63, 103, 104].

Carbon blacks are promising electrode materials due to their relatively high activities and long lifetimes in contrast to the lower activity or rapid deactivation of the other carbonaceous materials [105-109]. These catalytic characteristics of carbon blacks are attributed to their microstructure that has many active sites consisted of edges and defects in nanosized graphitic layers [106, 107, 110].

2.2.1 Intercalation Reactions

The electrochemistry of black carbon can be described by two types of reactions, namely intercalation and surface reactions.

In the *intercalation reactions*, ions (anions X^- or cations M^+) penetrate into the van der Waals gaps between the ordered carbon layers resulting in the enlargement of their inter-layer distance [1, 111]. The corresponding charges are conducted by carbon and accepted into the carbon host lattice.

$$\begin{aligned} C_n + M^{\oplus} + e^- &\Leftrightarrow M^{\oplus}C_n^- \quad \text{Cathodic reduction} \\ C_n + X^- &\Leftrightarrow C_n^{\oplus}X^- + e^- \quad \text{Anodic oxidation} \end{aligned} \tag{1}$$

Intercalation reactions (1) represent the ideal case; there is an increase in the inter-layer distance while the carbon atom arrangement within the layers remains unchanged; that is topotactic. However, during intercalation of cations from polymer [112] and solid electrolytes [113], ternary phases ($M^{\oplus}(solv)_y C_n^- / C_n^{\oplus}(solv)_y X^-$) are produced because the solvent from the electrolyte is also accepted into the carbon lattice.

$$\begin{aligned} C_n + M^{\oplus} + e^- + y\text{solv} &\Leftrightarrow M^{\oplus}(solv)_y C_n^- \quad \text{Cathodic reduction} \\ C_n + X^- + y\text{solv} &\Leftrightarrow C_n^{\oplus}(solv)_y X^- + e^- \quad \text{Anodic oxidation} \end{aligned} \tag{2}$$

From the degree of solvation it is possible to distinguish between two-dimensional and three-dimensional solvated phases (Fig. 5) [1].

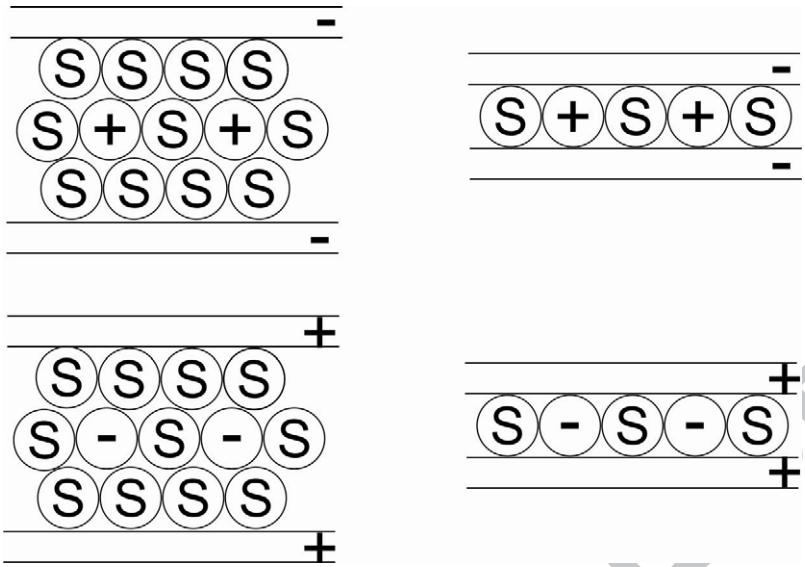

Figure 5. Three-dimensional and two-dimensional solvated and unsolvated cationic and anionic intercalation compounds; S = Solvent [1].

In the two-dimensional solvates, the distance between the carbon layers is determined either by the size of the solvent molecule [114] or by the size of the ions [115, 116].

2.2.2 Surface Reactions

The *surface reactions* of carbon black are generally reactions of C atoms at the edges of the layers or at other lattice defects, or reactions of functional groups that are bound to such C atoms. Surface reactions are of particular interest on the performance of carbon as electrochemical double layer capacitors [117-120]. The presence of oxygen groups on the surface of carbon affects its pseudo-capacitance. Pseudo-capacitance is significantly increased with an increase in the number of surface oxygen groups present [117]. The formation of CO surface complexes (hydroxyl, carbonyl, quinone) are responsible for the

enhancement in capacitance and can undergo the quinone/hydroquinone redox pair mechanism (3) [118].

$$C_xO + H^+ + e^- \Leftrightarrow C_xOH \quad (3)$$

Potential sweep measurements are employed to determine the pseudo-capacitance of carbon [117] and an increase in capacitance was reported upon carbon oxidation [117].

Electrochemical carbon oxidation during fuel-cell operation has been extensively studied [121-160] as it is detrimental to the performance and lifetime of the fuel-cell. Carbon is oxidized to carbon dioxide at potentials above its standard potential of 0.207 V (vs. NHE). Even though this potential value implies that carbon is unstable to electrochemical carbon corrosion, the slow kinetics of the reaction towards oxidation ensures the stability of carbon under fuel-cell conditions [157].

$$C + 2H_2O \rightarrow CO_2 + 4H^+ + 4e^- \quad E_o = 0.207 \text{ V (vs. NHE)} \quad (4)$$

Carbon loss can lead to a decrease in the conductivity of catalyst layer, reduction of electrochemically active surface area and aggregation/detachment of Pt particles from the support [142, 161, 162].

A mechanism for carbon oxidation reaction has been proposed by Gallagher and Fuller [146]. It is assumed that there are two sites present on carbon surface; active sites (marked with #) which are the rate determining steps of CO_2 formation and inert sites (marked with *) representing the CO_2 loss and simultaneous oxide formation.

Carbon oxidation mechanism starts with the formation of $C^{\#}(H_2O)_{ads}$ catalytic site that will eventually evolve CO_2 (eq. 5).

$$C^{\#} + H_2O \rightarrow C^{\#}(H_2O)_{ads} \quad (5)$$

$C^{\#}(H_2O)_{ads}$ further react with $C^{\#}OH$ catalytic sites leading to the formation of $C^{\#}O$ intermediates. This reaction is considered to be the rate determining step (eq. 6).

$$C^{\#}(H_2O)_{ads} + C^{\#}OH \rightarrow C^{\#}OC^{\#}OH + 2H^+ + 2e^- \quad (6)$$

The third step of the mechanism involves the reversible formation of the passive surface oxide $C^{\#}{}_xO$ (eq. 7). An electron transfer of 2.6 per oxygen atom removed was required during the reduction of chemically produced oxides on carbon [146]. This value is in accordance with previous reports in the literature [163].

$$xC^{\#} + H_2O \leftrightarrow C^{\#}{}_xO + 2H^+ + 2e^- \quad (7)$$

The next steps of the carbon oxidation mechanism describe the electrochemical reduction of the oxidized carbon surface. Catalytic oxide is consumed until the concentration of # sites reaches equilibrium (eq. 8), while C*O oxide is reduced at high potentials (> 1 V vs. SHE) resulting to the formation of quinone (eq. 9). As the quinone ($C^{\#}{}_xO_2$) production is increasing, more catalytic oxides are being consumed (eq. 10).

$$2C^{\#}OH + (x-2)C^{\#} + H_2O \rightarrow C^{\#}{}_xO_3 + 4H^+ + 4e^- \quad (8)$$

$$C^{\#}{}_xO + C^*O \rightarrow C^{\#}{}_xO_2 + C^* \quad (9)$$

$$2C^{\#}OH + (x-2)C^{\#} + H_2O + C^{\#}{}_xO_2 \rightarrow C^{\#}{}_xO_3 + C^{\#}{}_xO_2 + 4H^+ + 4e^- \quad (10)$$

The final step of the proposed carbon oxidation mechanism takes into account the oxidation-reduction reaction between quinone ($C^{\#}_xO_2$) and hydroquinone ($C^{\#}_x(OH)_2$), which is dominant in the cyclic voltammetric studies of oxidized carbons [120, 164].

$$C^{\#}_x(OH)_2 \leftrightarrow C^{\#}_xO_2 + 2H^+ + 2e^- \quad (11)$$

Even though the proposed mechanism is an important step towards understanding the carbon oxidation process, there are still limitations in the model. The most significant is the treatment of passive oxide (eq. 7). Experimental results demonstrated broad reduction peaks after extended electrochemical oxidation [165]; however this model does not reproduce that behavior. Hence, further research is needed to fully explore the formation of passive oxide.

Additional theoretical models on carbon oxidation were also developed [166-168]. It was reported that the anode Pt loading, membrane thickness and cell potential affect carbon corrosion; high Pt loading on the anode and cell potential as well as thin membranes accelerate carbon corrosion rate. The increase of carbon oxidation rate was confirmed experimentally, and it was demonstrated that the formation of intermediate PtOH species on platinum surface affect carbon oxidation rate at potentials lower than 1 V (vs. SHE) [168]. Recently, a straightforward physics-based model was constructed, proving that an increase of ORR exchange current density, RH or cell temperature increases carbon corrosion rate [167].

Potentiodynamic and constant potential measurements are used to investigate carbon corrosion [148-151]. The rate of corrosion under varying potentials is higher than under constant potential [160]. At constant potential, only the fraction of carbon with low activation energy is energetically favored to undergo corrosion [160], while surface oxide layers may build up reducing the carbon corrosion rate [162]. In contrast, under varying potentials, the rate of carbon corrosion is high since the time duration of applied high potentials is not enough to produce irreversible oxide layers [160].

Carbon corrosion rate depends on the upper and lower potential limit [160]; an increase in carbon oxidation rate was observed when anodic potential limit was increased and cathodic potential limit was decreased (Fig. 6). This phenomenon is due to the strong electro-oxidation at high potentials and to the creation of new defects by chemical oxidation in the low potential region [160]. Progressing from these newly generated defects, carbon corrosion is enhanced even at less degrading potentials [160].

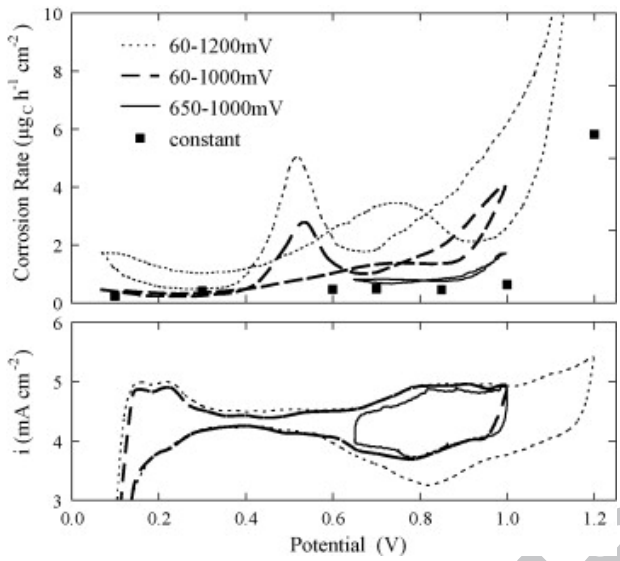

Figure 6. Carbon corrosion rates during dynamic and constant-potential measurements (Reprinted from [160] with permission from Elsevier).

Despite the previous efforts on carbon oxidation, further research is needed to fully explore the effect of potential cycling and start-up/shut-down cycles on carbon oxidation mechanism [158]. The rate determining step for carbon corrosion (oxidation of surface CO_{ad} species to CO_2) is also reported to be catalyzed by the presence of Pt [138, 160, 169], even though more research is needed to verify this claim.

Carbon corrosion under Phosphoric Acid Fuel Cells (PAFCs) conditions. Carbon corrosion is also a detrimental factor to the performance of PAFCs. At constant potential, two anodic processes occur during the electro-oxidation of carbon in H_3PO_4 solution at 135^{o}C; formation of surface oxide on carbon and CO_2 evolution, both decreasing with time. These processes are independent of each other as surface oxide formation does not inhibit CO_2 formation. As the surface oxide coverage of carbon is increasing, CO_2

evolution becomes the rate determining step [149]. Assuming a four electron corrosion process [141], carbon reacts with H_2O to form CO_2 (eq. 12).

$$C + H_2O \rightarrow CO_2 + 4H^+ + e^- \quad (12)$$

Surface oxides consist of carboxyl and quinone groups [170, 171]. FTIR studies demonstrated a band at 1712 to 1527 cm^{-1} correlated to the C=O bonding in quinone and a band at 1335 to 1000 cm^{-1} correlated to the coupled C-O bonding and OH stretching in the carboxyl groups (COOH) [170, 172]. The concentration of these surface oxides on carbon black (Vulcan XC-72) was measured by potentiodynamic sweep technique and it was approximately 10^{-10}-10^{-11} moles/cm^2 [120].

Comparison of the corrosion characteristics of Vulcan XC-72 and acetylene black after heat treatment at 200^{o}C demonstrated an increase of the carbon corrosive resistance, even though the dispersion of the supported metal catalyst is decreased [173].

2.3 Applications

The above mentioned unique properties of carbon make it to an attractive material that is widely used in various electrolytic processes in chemical industry such as reduction of Nitrobenzene [174-177] and Nitraniline [178], Chlorine [179-183] and Aluminum [184-189] production, metal refining [190-194], etc. A few representative applications of carbon are reviewed below.

2.3.1 Batteries and Capacitors

Nowadays, there is high demand for high power and high energy sources due to the numerous portable electronic devices and emerging electric vehicles. The most common energy source that can provide the required power is the Li-ion battery as it can store large amount of energy in a small volume and low weight [195-199].

Carbonaceous materials are used nearly exclusively as negative electrodes in Li-ion batteries and as fillers to improve the electrical conductivity of the composite material. Carbonaceous materials are characterized by good cycling behavior and electronic conductivity, low redox potentials and Li storage capability depending on carbon type [199] (disordered carbon can store higher amount of Li than graphitic carbon [199]). Corrosion resistance in aqueous systems (acid/alkaline) is the most important property of the material as it affects significantly the battery performance. CNTs composites (such as Si, Sn, SnO, and TiO_2) showed increased stability in aqueous systems and enhancement of reversible capacity [196, 200]. However, batteries suffer from slow power delivery and hence, their use in energy storage systems with fast storage and high power demand, is limited [201].

Electrochemical capacitors are best suited for these energy storage systems since they can provide high specific power ($10 kW kg^{-1}$), long cycle life (greater than 10^5) and fast charge/discharge [202]. Currently, electrochemical capacitors are widely used in electronics and industrial power systems [203, 204]. Carbon materials are mainly used in these devices due to their high surface area, high electrical conductivity and low cost.

Carbon composites with metal oxides [205-210] and conducting polymers [211-214] improve significantly the capacity of the system and electrical conductivity of electrodes.

2.3.2 Biosensors

A biosensor is a device that can provide specific analytical information (DNA, viruses, antigens, enzyme, and cells detection) by using a biological recognition element in direct contact with a transduction element [215]. Carbon nanomaterials and specifically CNTs are widely used in these electrochemical sensors due to their attractive characteristics (high conductivity and sensitivity, good selectivity and reversibility, fast response time, chemical and thermal stability, electronic and optical properties) [215-217] and their ability to promote electron transfer in electrochemical reactions [218, 219].

Graphene layer and reduced graphene oxide are also used for the fabrication of gas sensors as they can exhibit extremely low detection limits (ppb) for a variety of gases and vapors [220-233].

Graphene layer is very sensitive to changes in the chemical environment due to its high electron mobility at room temperature, high surface area resulting to high sensitivity to adsorbed molecular species and high electrical conductivity [228]. Gas molecules act as donors or acceptors and they are adsorbed on the surface of graphene layer altering the electrical conductivity of the gas sensor [228]. Several synthesis methods are being used for the fabrication of graphene layer based gas sensors including i) mechanical exfoliation of graphite leading to the formation of graphene layer [234]; ii) chemical

vapor deposition [235-237]; iii) epitaxial growth [238, 239]; and iv) chemical exfoliation of graphene oxide to graphene layer [240-242].

Moreover, chemically reduced (hydrazine) graphene oxide (rGO) demonstrated excellent performance for the detection of nitric oxide, warfare and explosive agents at very low concentrations (ppb) [220, 229]. However, hydrazine is extremely toxic and incorporates extra nitrogen functional groups on the graphene layer surface [230], reducing the response time of the sensor [231].

Alternative rGO synthesis routes involve the i) partial reduction of graphene oxide via low temperature annealing (~ 300^{o}C) under inert atmosphere [232]; and ii) partial reduction of graphene oxide with ascorbic acid [233].

In the case of rGO synthesized by thermal annealing, rGO demonstrated p-type semiconducting behavior and good performance for the detection of nitric oxide (ppm) [232]. The sensitivity was attributed to the electron transfer from rGO to NO_2 resulting to enhanced electrical conduction and to thermal annealing during rGO synthesis procedure; the latter leads to the formation of additional defects on the surface of rGO acting as adsorption sites for gaseous molecules [232]. On the contrary, rGO synthesis via ascorbic acid reduction of graphene oxide resulted to a highly sensitive gas sensor able to detect chemically aggressive vapors such as NO_2 and Cl_2 at very low concentrations (100 ppm-500 ppb) [233].

Despite their potential, graphene layer / reduced graphene oxide as well as CNTs still face challenges. The most severe drawback for the application of these carbon materials is heterogeneity as it is not possible to fabricate consistent and reproducible sensors [243]. Further research in the synthesis, purification and biofunctionalization of CNTs will increase their usefulness in biosensors [243]. On the graphene-based gas sensors front, further research is needed to simplify the fabrication and operation of these devices. Reduced graphene oxide based sensors in particular are expensive as it is required to oxidize graphite to graphene oxide and successively reduce it into reduced graphene oxide using strong reducing agents.

2.3.3 Photo-electrochemical Water Splitting

Photo-electrochemical water splitting (capturing and storing solar energy into the chemical bond of hydrogen) is a promising way to produce clean energy and is expected to play a significant role in the future with the depletion of fossil fuel supplies [244-251]. Many materials have been investigated to discover a suitable photo-anode [252-259]; among them, titanium oxide (TiO_2) is promising due to its low cost, chemical inertness, UV photo-activity and chemical stability [244, 245, 260-263]. However, due to the large band gap (~ 3-3.2eV) and short carrier diffusion length, the conversion efficiency of titanium oxide is reduced [244]. In an attempt to shift the optical response of titanium oxide from ultraviolet to visible spectra range, titanium oxide was doped with nitrogen [264], carbon [244, 245, 265-267] and sulfur [268]. The incorporation of carbon into titanium oxide resulted in the formation of an intragap band (~ 1.3-1.6eV) [265, 269] into

the band gap of TiO_2 that can be used to absorb photons at low band gap energy [266, 267, 270]. This effect resulted in high photo-conversion efficiency under visible light [267, 269]. Moreover, carbon modified TiO_2 synthesized by wet process using glucose solution as the carbon source demonstrated a 13-fold increase in photo-catalytic activity compared to titanium oxide while it increased only 8-fold when tetrabutylammonium hydroxide was used as the carbon source [267].

Apart from titanium oxide, two other carbon modified semiconductors were studied in water photo-electrolysis due to their low band gap energy, namely iron (Fe_2O_3) and tungsten oxide (WO_3) [245, 271]. Carbon modified iron oxide demonstrated promising photo-conversion efficiency; ~ 4% and 7% for modified oxides synthesized in oven and by thermal oxidation respectively [271]. Also, carbon modified tungsten oxide (C-WO_3) photo-catalysts exhibited a ~ 2 % photo-conversion efficiency [245].

2.3.4 Electrolytic Synthesis of Hydrogen Peroxide (H_2O_2)

Another application of carbon and carbon hybrids is their use as electrode material in proton exchange membrane (PEM) electrochemical flow reactor for the production of hydrogen peroxide (H_2O_2).

Tatapudi and Fenton [272] investigated three different catalysts, namely gold, graphite and activated carbon, for the production of H_2O_2 by oxygen reduction at the cathode of a PEM flow reactor. Graphite (10 $mgcm^{-2}$ catalyst loading with 20% Teflon binder) produced the highest amount of peroxide (25 mgL^{-1} at 2.5 V vs. SHE) while gold and

activated carbon produced lower peroxide at higher applied voltages (~ 3.5 V vs. SHE) than the graphite. It was also reported that an increase in the percentage of Teflon binder results in an enhanced electrode resistance leading to lower cell current and hence lower cell performance [272, 273].

Mesoporous nitrogen-doped carbon was also used as catalyst for the production of hydrogen peroxide [274]. H_2O_2 was produced in a three electrode setup at 1600 rpm rotation speed and ~ 325 $\mu g cm_{geo}^{-2}$ catalyst loading. H_2O_2 concentration (Fig. 7) was approximately 20 mgL^{-1} at constant potential of 0.1 V (vs. reversible hydrogen electrode (RHE)) showing that nitrogen-doped carbon is a promising catalyst for the electrochemical production of H_2O_2 [274].

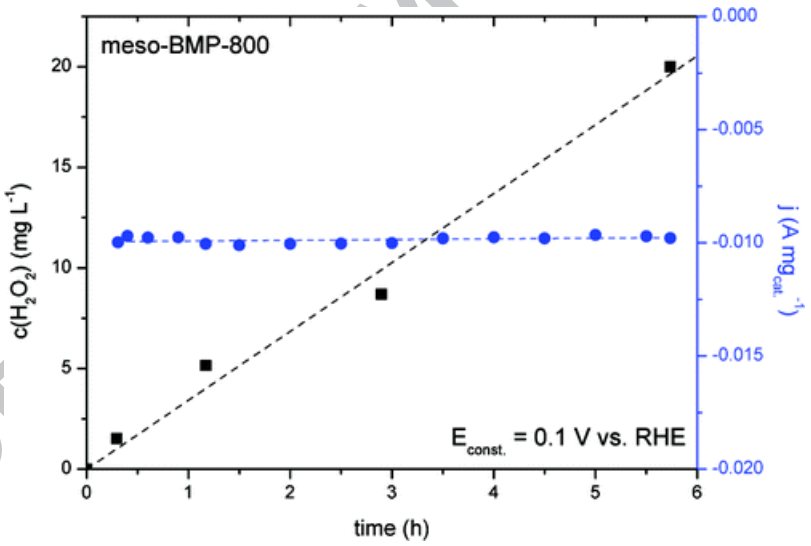

Figure 7. Photometric determination of H_2O_2 as a function of time; current (circle) and concentration (square) behavior with time for the electrochemical H_2O_2 production is shown (Reprinted with permission from [274] - Copyright© 2012 American Chemical Society).

Moreover, the effect of operating conditions (applied current, electrolyte concentration, air flow rate and pH) on the amount of electro-generated H_2O_2 was investigated [275]:

i) *Effect of applied current*. H_2O_2 production rate is increased as the applied current is increasing from 60mA to 100mA. However, above 100mA the peroxide production rate is decreasing. At 60mA the cell potential is 3 V (vs. saturated calomel electrode (SCE)) while at 100, 200, 300 and 500mA is 3.4, 4.3, 5.4 and 6.6 V (vs. SCE) respectively [275]. At potentials higher than 4.3 V (vs. SCE) the reduction of oxygen leads to the formation of water [276] and not H_2O_2 and thus the amount of electro-generated peroxide is reduced [275].

ii) *Effect of electrolyte concentration*. Sodium sulfate (Na_2SO_4) is used as the electrolyte solution; low electrolyte concentration results to low conductivity of the solution and thus higher cell potential is needed to reach the required current density [275]. Cell potential was 6.7 V and 3.4 V (vs. SCE) for sodium sulfate concentration of 0.025 and 0.05 M respectively. Thus, increasing the electrolyte solution enhanced the electro-generation rate of H_2O_2. However, increasing the sodium sulfate concentration from 0.05 M to 0.1 M had no significant effect on the electrochemical generation of hydrogen peroxide [275].

iii) *Effect of pH*. At pH values below 3, reduction of H_2O_2 to water and hydrogen gas evolution takes place (eq. 13) reducing the amount of H_2O_2 generated in the medium, while at pH values above 3, proton concentration is decreasing and hence H_2O_2 production rate is reduced as well [275].

$$H_2O_2 + 2H^+ + 2e^- \rightarrow 2H_2O$$
$$2H^+ + 2e^- \rightarrow H_2 \quad (13)$$

iv) *Effect of air flow rate*. Air was used instead of pure oxygen due to its low cost. An increase in the air flow rate results to an increase of the amount of H_2O_2 produced. High flow rate leads to high mass transfer rate of dissolved oxygen and hence enhanced peroxide production [275].

Based on these results, it was concluded that the optimum conditions for H_2O_2 electro-generation are 0.05 M sodium sulfate, 100 A applied current, pH = 3 and 2.5 $Lmin^{-1}$ air flow rate [275]. These conditions were used to investigate the electrochemical generation of H_2O_2 of three different carbon based cathode materials: graphite, activated carbon on graphite (AC/graphite) and carbon nanotubes on graphite. The amount of electro-generated H_2O_2 using CNTs/graphite was three times higher than that of AC/ graphite and seven times higher than that of bare graphite (Fig. 8). CNTs/graphite has large specific area and high amount of meso-porous pores leading to facile oxygen reduction on the cathode and hence increased H_2O_2 production [275].

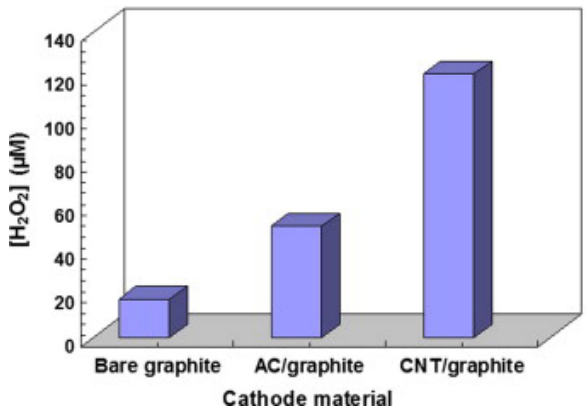

Figure 8. Electro-generated H_2O_2 on bare graphite, AC/graphite and CNTs/graphite (Experimental conditions: 180 min electrolysis, room temperature, 0.05 M Na_2SO_4,

100mA, pH = 3, air flow rate = 2.5 $Lmin^{-1}$ - Reprinted from [275] with permission from Elsevier).

3. Carbon, Carbon Hybrids and Carbon Composites in PEFCs

3.1 Carbon as Structural Component in PEFCs

A PEFC consists of two electrodes in contact with an electrolyte membrane (Fig. 9). The membrane is designed as an electronic insulator that separates the reactants (H_2 and O_2/air) and allows only the transport of protons / hydroxyl ions and water between the electrodes. The electrodes are constituted of a porous gas diffusion layer (GDL) and a catalyst (usually platinum supported on high surface area carbon) containing active layer. This assembly is sandwiched between two electrically conducting bipolar plates within which gas distribution channels are integrated [277].

The function of the electrolyte membrane is to facilitate transport of protons / hydroxyl ions from anode to cathode and to serve as an effective barrier to reactant crossover. The electrodes host the electrochemical reactions within the catalyst layer and provide electronic conductivity, and pathways for reactant supply to the catalyst and removal of products from the catalyst [277]. The GDL is a carbon paper or cloth of 0.2-0.5 mm thickness that provides rigidity and support to the membrane electrode assembly (MEA). It incorporates hydrophobic material that facilitates the product water drainage and prevents the gas paths from flooding [277]. The amount of hydrophobic resin used for carbon coating is also important. Resin at high concentrations blocks the micro-pores on the surface of carbon improving the hydrophobicity of the material at the expense of conductivity [278, 279]. The active layer consists of catalyst particles, ionomer and pore

spaces which form a three-phase boundary where the electrochemical reaction takes place. A good electrode has to effectively facilitate the trade-off between enabling high catalytic activity, retaining enough water to guarantee good proton conductivity in the ionomer phase, and having an optimal pore size distribution to facilitate rapid gas transport [277]. All the components of the MEA need to be stable (under both chemical and mechanical stresses) for several thousands of hours in the fuel-cell under the prevailing operating and transient conditions.

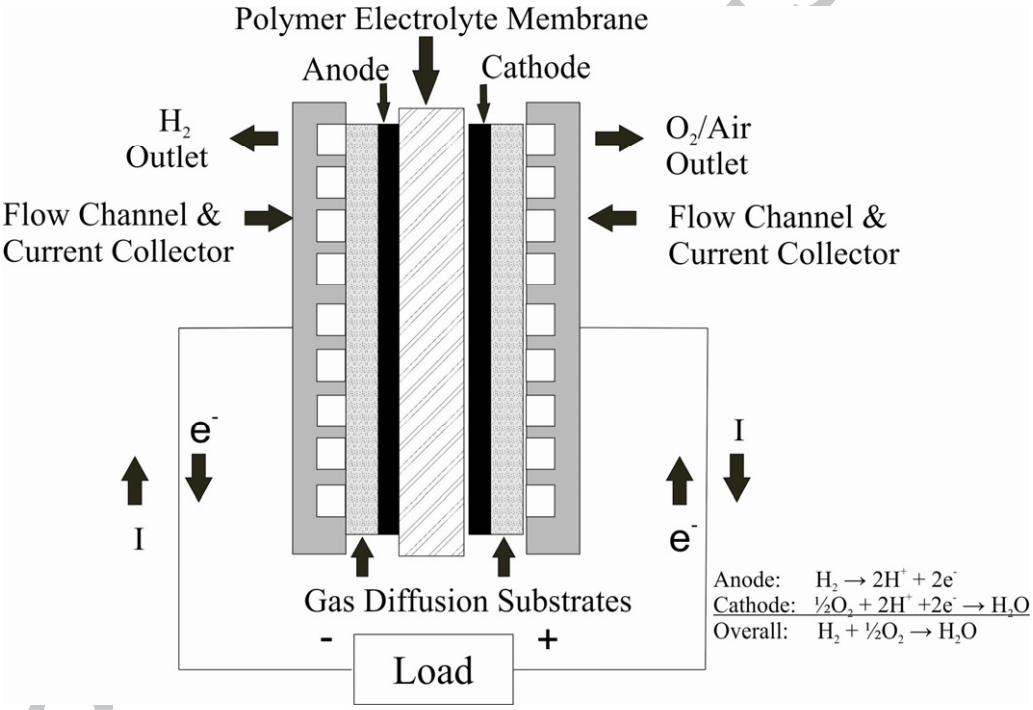

Figure 9. Cross section of a PEFC.

3.2 Carbon as PEFC Catalyst Support

The basic function of the catalyst support is to: i) provide good electrical conductivity with high surface area, ii) bring the catalyst particles close to the reactants via the pore structure and iii) provide corrosion stability under oxidizing conditions [6, 49, 280-284].

The choice of support material is vital in determining the performance and durability of the catalyst [280].

Carbon black (Vulcan XC-72R) is the most commonly used support for Pt and Pt-alloy catalysts for fuel cells due to its high surface area (~ 250 m^2g^{-1}) and low cost. It consists of spherical graphite particles (less than 50 nm diameter) [49] with ~ 0.35 nm interplanar spacing [49]. However, carbon black is susceptible to oxidation in low (potential greater than 1.2 V vs. SHE) and high temperature (potential lower than 0.9 V vs. SHE) fuel cells resulting in active surface area loss [122] and alteration of pore surface characteristics (generation of surface oxides CO_{ad}) [136]. In automotive applications, high potentials occur during *i) complete fuel starvation* of a cell in the stack; and *ii)* during *partial fuel starvation* on the anode side of a cell in the stack due to limited supply of hydrogen [131, 285] or the presence of hydrogen-air over the active area during start up and shut down of the fuel cell [131]. During complete fuel starvation, the anode potential of the starved cell is greater than the cathode resulting to water electrolysis and carbon oxidation on the anode to form the required electrons and protons for the oxygen reduction reaction at the cathode [286]. During partial fuel starvation, oxygen is present in the hydrogen deficient areas on the anode causing a decrease of the in-plane membrane potential and hence potential shifts [129, 131]. The above mentioned high potential conditions result to facile oxidation of the carbon support and thus significant performance losses [160].

$$C + H_2O \rightarrow CO_{ad} + 2H^+ + 2e^-$$

$$CO_{ad} + H_2O \rightarrow CO_2 + 2H^+ + 2e^- \quad (14)$$

Transmission (TEM) and Scanning electron microscopy (SEM), X-ray diffraction (XRD) as well as BET measurements are usually employed for the physical characterization of the carbon supports. Cyclic voltammetry is used to characterize the stability of the carbon supports [133] along with chronoamperometry (corrosion current measurement) [120, 173], while electrochemical quartz crystal microbalance (EQCM) measurements monitor the carbon mass loss during the CV potential scans [287, 288]. Mass spectroscopy [130, 132] and non-dispersive infrared spectroscopy [160] are also utilized to monitor the generation of CO_2 under electrochemical oxidation conditions.

Alternate support materials are investigated to replace carbon black as support in order to provide higher corrosion resistance and surface area. These supports can be classified into *i*) carbon nanotubes and fibers; *ii*) mesoporous carbon; and *iii*) multi-layer graphene / reduced graphene oxide; and they are presented in detail in the following section. Mesoporous carbon is characterized by high surface area and porosity leading to higher activity and stability than carbon black [62, 289-291]. The introduction of CNTs [96, 292-294] and multi-layer graphene / reduced graphene oxide [295-303] as electrocatalyst supports resulted to high catalyst utilization and thus high ORR activity. The high crystallinity and surface area of those materials effectively provide the suitable support for the dispersion of catalyst nanoparticles. Moreover, the two dimensional nature of graphene allows both the edge and basal planes to interact with the catalyst leading to high conductivity and electron transfer.

3.2.1 Carbon Nanotubes (CNTs) and Fibers (CNFs)

CNTs (single- or multi-walled) are also used as catalyst support in PEFCs. SWCNTs have large surface areas while MWCNTs are more conductive than SWCNTs [96, 160, 292].

Pristine CNTs are chemically inert and metal nanoparticles cannot be attached [160]. Hence, research is focused on the functionalization of CNTs in order to incorporate oxygen groups on their surface that will increase their hydrophilicity and improve the catalyst support interaction [160]. These fabrication methods include impregnation [304, 305], ultrasound [306], acid treatment (such as H_2SO_4) [293, 307-309], polyol processing [310, 311], ion-exchange [312, 313] and electrochemical deposition [293, 314, 315]. Acid-functionalized CNTs provide better dispersion and distribution of the catalysts nanoparticles [293, 307-309].

Conjugated polymers such as polypyrrole (Ppy) and polyaniline (PANI) form covalent bonds between Pt atoms and N atoms in PANI enabling strong adhesion of Pt nanoparticles onto the polymer [316-318]. Electron conducting PANI was used to bridge the Pt nanoparticles and CNT walls with the presence of platinum-nitride (Pt-N) bonding and π-π bonding. The synthesized PANI binds across the CNT as a result of π-π bonding while Pt nanoparticles (~ 2-4 nm diameter) are loaded onto the CNT due to polymer stabilization and existence of Pt-N bonding [316] (Fig. 10). These materials have high electro-activity, and accelerated degradation tests revealed the electrochemical stability of

Pt-PANI/CNT catalysts compared to non-functionalized MWCNTs and commercial carbon black supports [316].

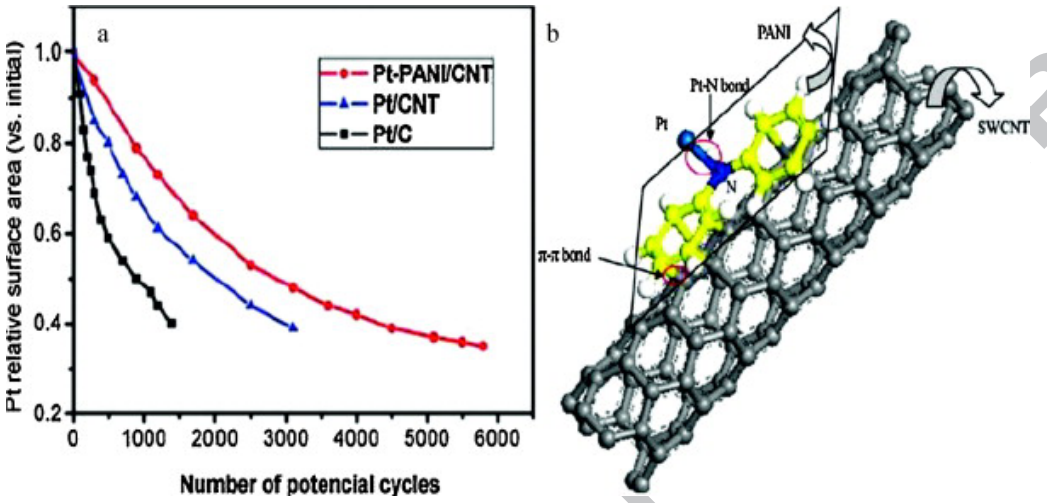

Figure 10. a) ECA of the catalysts as a function of the number of potential cycles. b) Schematic showing molecular interactions in the synthesized Pt-PANI/CNT catalyst (Reprinted from [316] with permission from Elsevier).

Another technique to modify the surface of CNTs is the use of ultrasound as it enables the formation of smaller and more uniform nanoparticles [306]. Yang and coworkers [306] compared the effect of ultrasonic treatment and reflux on the surface functionalization of MWCNTs. Ultrasonically fabricated MWCNTs demonstrated higher active surface area and improved CO tolerance due to better dispersion and utilization of the electrocatalyst [306].

Tang and coworkers [319] synthesized Pt-CNT layer acting both as gas diffusion and catalyst layer. CNT was grown in-situ on carbon paper followed by sputter deposition of the Pt catalyst. A maximum power density of 595 $mWcm^{-2}$ (Pt loading ~ 0.04 $mgcm^{-2}$)

was achieved (Fig. 11), which was higher than the power density of both Pt-Vulcan and Pt-CNT-Vulcan electrodes tested (~ 435 and 530 $mWcm^{-2}$ respectively) [319]. Hydroxyl radicals cannot easily penetrate the rigid structure of CNTs, while carbon black has excess of dangling bonds and defects that oxygen atoms can easily penetrate into [320, 321]. Dangling bonds form surface oxides that lead to higher corrosion rates [320, 321].

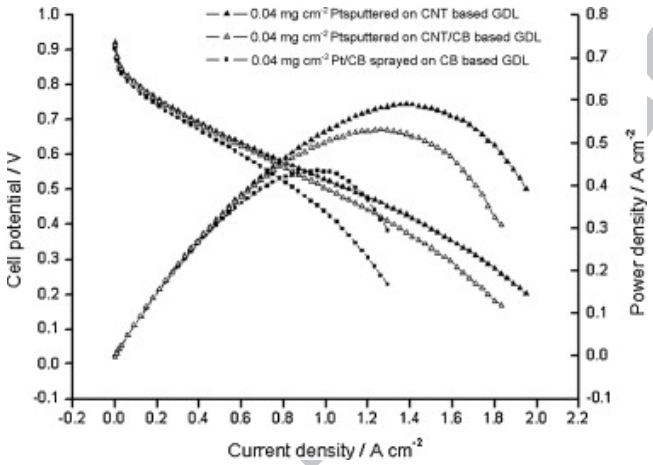

Figure 11. Polarization curves of MEA Pt-CNT, Pt-Vulcan and Pt-CNT-Vulcan based MEAs (Reprinted from [319] with permission from Elsevier).

The polarization losses of Pt supported on MWCNTs were also examined [133, 322]. Pt-MWCNTs exhibited higher corrosion resistance and retention of electrochemical active surface area compared to Pt-Vulcan electrocatalysts. Only the outer graphene layers of MWCNTs were damaged, forming defects on the surface of nanotubes [133]. Moreover, MWCNTs prevented the water flooding of cathode catalyst layer by maintaining the electrode structure and hydrophobicity for a long period under continuous anodic potential stress. Ohmic losses were found to be the major cause contributing to the performance loss [322].

The degree of graphitization also plays a significant role on the oxidation resistance of carbon black [164] and MWCNTs; the number of defects on the surface of nanotubes decreases as graphitization % increases resulting in higher electrochemical stability [323]. The higher graphitic content has also been linked to a stronger interaction between metal and carbon support. An increase in degree of graphitization results in stronger π-sites (sp^2 hybridized carbon) on the support (which are the anchoring sites for the electrocatalyst), strengthening the metal-support interaction [324].

The stability during potential cycling and ORR activity of Pt (20 wt %) supported on MWCNTs and carbon black was also investigated [325, 326]. Two different potential cycling conditions were used, namely lifetime (0.5 to 1.0 V vs. RHE) and start-up (0.5 to 1.5 V vs. RHE). Pt supported on MWCNTs catalyst exhibited a significantly lower drop in normalized electrochemically active surface area (ECA) values compared to Pt supported on Vulcan (Fig. 12), showing that MWCNTs possess superior stability than commercial carbon black under normal and severe potential cycling conditions [325].

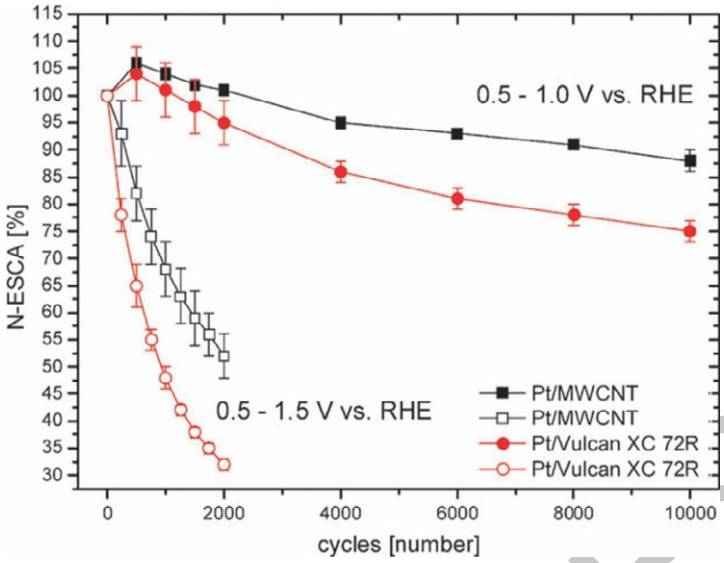

Figure 12. Normalized ECA loss due to voltage cycling for Pt/MWCNT (square) and commercial Pt/Vulcan XC-72R (circle); Experimental conditions: 0.5-1.0 V vs. RHE (solid) and 0.5-1.5 V vs. RHE (hollow); 50 mVs^{-1} scan rate - Reprinted with permission from [325] - Copyright© 2010 Royal Society of Chemistry).

Carbon nanofibers. CNFs are also used as catalyst support in PEFCs. Unlike CNTs, CNFs have a very thin or no hollow cavity. Their diameters are larger than CNTs and can be classified into three types: *i*) ribbon-like CNF; *ii*) platelet CNF; and *iii*) herringbone depending upon the orientation of the nanofibers with respect to the growth axis [49]. Herringbone CNFs are known to have intermediate characteristics between parallel and platelet types, thereby exhibiting higher catalytic activity than the parallel and better durability than the platelet forms [327]. The main difference between CNTs and CNFs lies on the exposure of active edge planes. A predominant basal plane is exposed in CNTs while only the edge planes with anchoring sites for the electrocatalyst are exposed in CNFs [49].

Pt (5 wt %) supported on platelet and ribbon graphite nanofibers exhibited similar activities to those observed by Pt (25 wt %) on carbon black [328]. This phenomenon was attributed to the crystallographic orientations adopted by the catalyst particles dispersed on graphitic nanofiber structures [328]. Also, the electrocatalyst supported on CNFs were less susceptible to CO poisoning than Pt supported on carbon black.

Pt (5-30 wt %) nanoparticles supported on CNFs were also prepared by a modified ethylene glycol method [329]. Pt-CNF based MEAs with 50 wt% Nafion® exhibited higher cell performance than the carbon black based MEAs with an optimized 30 wt% Nafion® content (Fig. 13). This was attributed to the larger length to diameter ratio of CNFs that allows the formation of conductive networks in the Nafion® matrix [329].

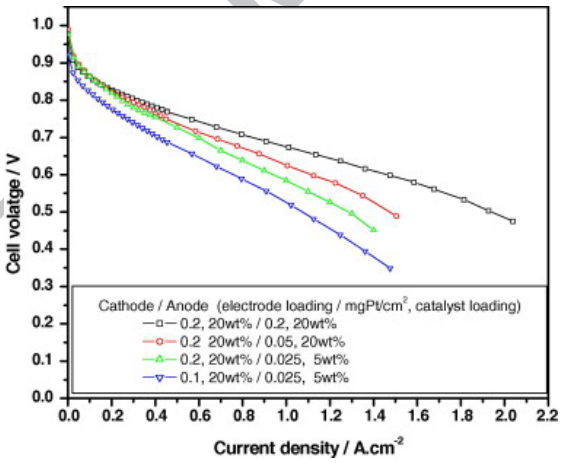

Figure 13. Polarization curves of Pt/C (BASF-Fuel Cell, 20 wt.%) or Pt/SC-CNFs (home-made, 20 wt.%) based MEAs with varying Nafion® amount in the cathode. Experimental conditions: 70°C cell temperature, 100% relative humidity (RH); anode/cathode: H_2/O_2, 200 $mLmin^{-1}$ flow rate - Reprinted from [329] with permission from Elsevier.

3.2.2 Mesoporous carbon (MC)

Despite the advantages offered by CNTs and CNFs, there are still many obstacles (cost, synthesis methods) to overcome to allow large-scale production. Another type of catalyst support material is mesoporous carbon, which provides high surface area and high conductivity [49]. It can be classified into ordered (OMC) and disordered (DOMC) mesoporous carbon [49]. OMCs have been extensively used as catalyst support materials for fuel cells [62, 72, 289, 290, 330-334]. The large surface area and 3D connected mono-dispersed mesospheres facilitates diffusion of the reactants, making them very attractive materials as catalyst supports [49].

The effect of MCs pore morphology in the electrocatalytic activity of Pt has been also studied [335]. Pt (20 wt %) was supported on OMC (CMK-3) and disordered wormhole mesoporous carbon (WMC) using microwave polyol process. Both support materials had similar pore characteristics (~ 4 nm pore size) except pore morphology. It was discovered that CMK-3 support provided more electrochemically active Pt support sites and higher active surface area than WMC, leading to superior ORR activity and fuel-cell performance. This enhanced catalytic activity was attributed to the highly ordered structure and good 3D interconnection of the nano-spacings of carbon nanorods, resulting to higher catalyst utilization efficiency compared to WMCs (Fig. 14) [335]. Hence, pore morphology of catalyst support plays an important role in the activity of the supported electrocatalyst.

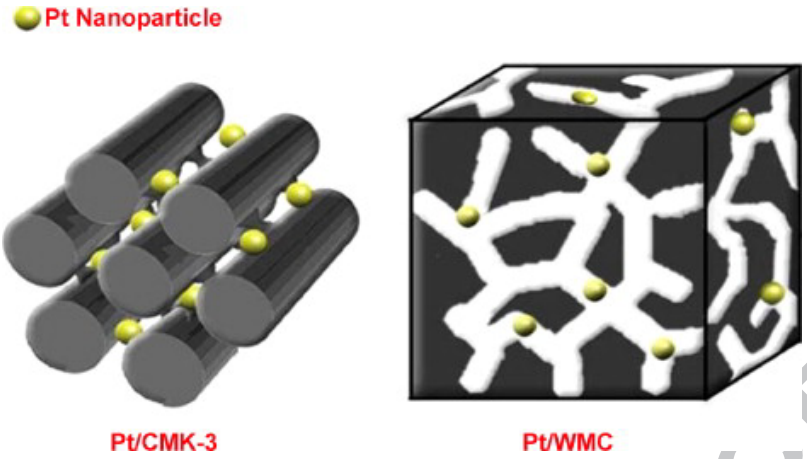

Figure 14. Effect of pore morphology of the carbon support (CMK-3 and WMC) on the activity of Pt electrocatalyst (Reprinted from [335] with permission from Elsevier).

The effect of surface chemistry of OMCs (CMK-3) has also been investigated [336]. OMCs were functionalized by diluted nitric acid (HNO_3) to modify the morphological and textural properties of the support via the introduction of surface oxygen groups. The average size of Pt nanoparticles on the CMK-3 supports was 7-8 nm; in contrast, larger catalyst particles (~ 22-23 nm) were observed (Fig. 15) when CMK-3 supports were treated with concentrated HNO_3. Nitrogen adsorption-desorption isotherms revealed lower specific surface area and total pore volume for CMK-3 support (treated with concentrated HNO_3), which led to a significant increase of the catalyst particle size. Polarization and power density curves (Fig. 16) exhibited better electrocatalytic behavior for CMK-3 based electrodes (~ 13-27 $mWcm^{-2}$) compared to commercial E-TEK electrodes (9.5 $mWcm^{-2}$), despite their lower electrical conductivity and larger Pt nanoparticles [336]. Ohmic and mass-transfer losses were greater for supports functionalized with concentrated HNO_3 due to their decreased electrical conductivity, higher agglomeration, and lower specific surface area [336, 337].

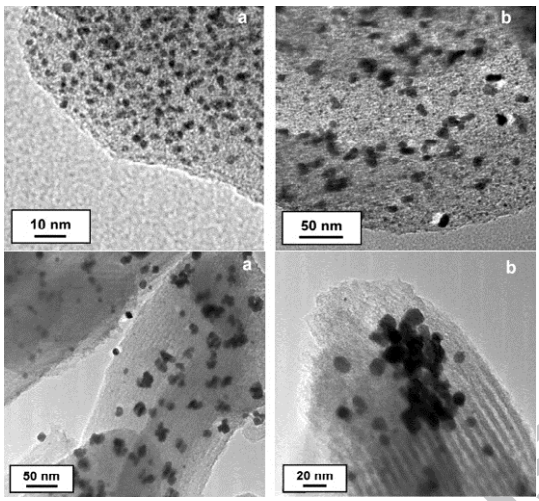

Figure 15. a) TEM images for Pt supported on CMK-3 catalysts treated with diluted HNO_3 for 2 h (Pt/CMK-3 Nd2); b) TEM images for Pt supported on CMK-3 catalysts treated with concentrated HNO_3 for 2 h (Pt/CMK-3 Nc2) (Reprinted from [336] with permission from Elsevier).

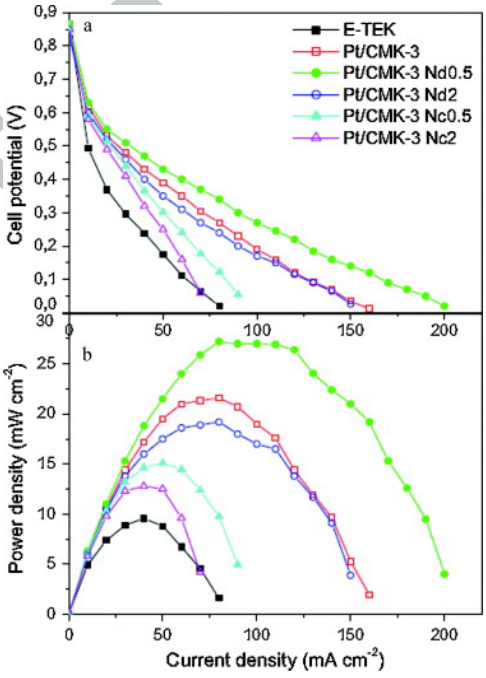

Figure 16. Polarization (a) and power density (b) curves of Pt supported on CMK-3 catalysts with different surface chemistry at the anode side of a PEFC working at room

temperature and atmospheric pressure (Reprinted from [336] with permission from Elsevier).

Hayashi and coworkers [331] built an ideal triple-phase boundary inside the mesopores of carbon support in order to examine the electrochemical reactions occurring in nanoscale. Depending on the solvent used (2-propanol) to dilute Nafion®, the reactivity toward oxygen reduction was different. Nafion® dissolved in 2-propanol was able to penetrate deeper into the mesopores and contact with more Pt particles resulting in higher oxygen reduction activity. By changing the Pt precursor, ORR current started to increase at more positive potential, indicating enhanced ORR activity (Fig. 17). Platinum (II) acetylacetonate has been chosen as the new precursor since it is soluble in various organic solvents, increasing the number of Pt particles deposited on the mesopores [330-332].

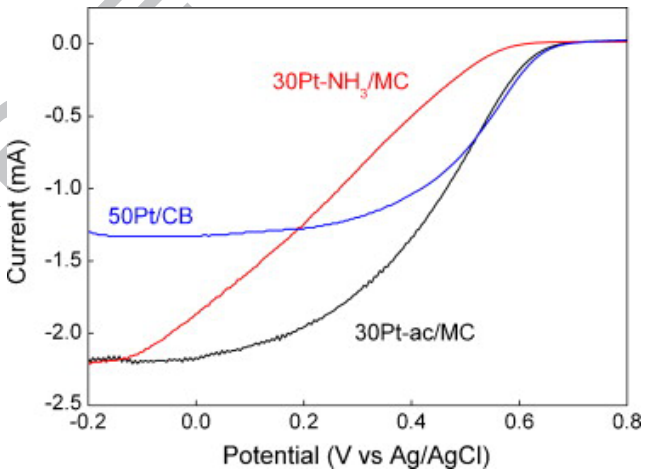

Figure 17. Linear sweep voltammograms of (50 wt %) Pt/Carbon black, (30 wt %) Pt-NH_3/MC, and (30 wt %) Ptac/MC. Catalyst loading 14μgcm^{-2}; experimental conditions: 1600rpm rotating speed and 20 mVs^{-1} sweep rate (Reprinted from [331] with permission from Elsevier).

MCs have also been doped with nitrogen and their stability was investigated [338]. These catalysts were subjected to long-term potential cycling (10,000 cycles between 0.5 and 1 V vs. RHE, 50 mVs^{-1} scan rate) and their ECA results were compared to Pt supported on high surface area carbon black (Fig. 18). The ECA values of Pt supported on nitrogen doped MCs were higher that Pt-carbon black before and after the testing (90 m^2g^{-1} to 67 m^2g^{-1} and 75 m^2g^{-1} to 55 m^2g^{-1} respectively). The mean particle size growth was the main factor of the ECA loss as well as carbon corrosion [338].

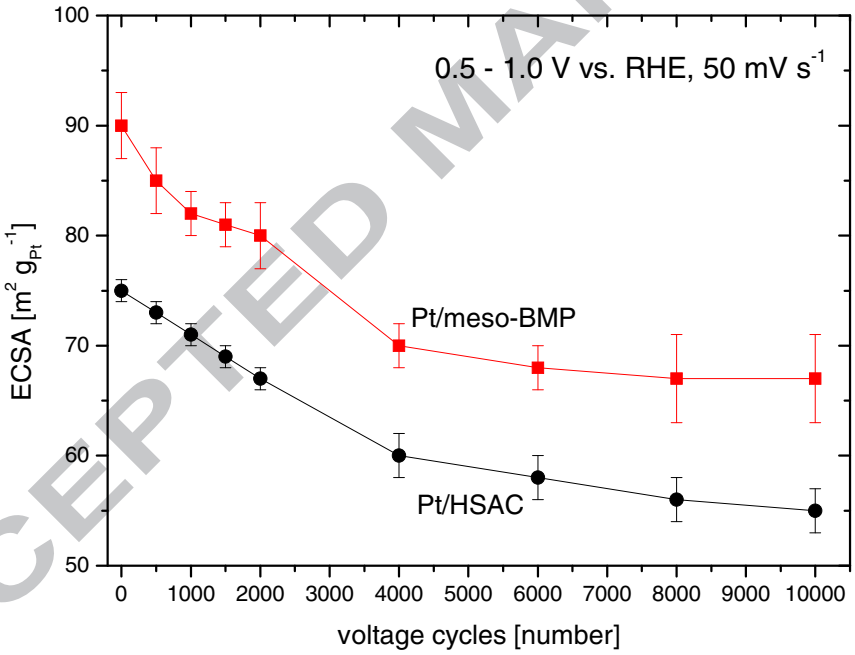

Figure 18. ECA evolution for Pt supported on nitrogen doped MC (square) and Pt supported on high surface area carbon black (circle). Experimental conditions: voltage cycling between 0.5 to 1.0 V vs. RHE, 50 mVs^{-1} scan rate, room temperature, 0.1 M $HClO_4$ (Reprinted with permission from [338] - Copyright© 2012 Wiley).

3.2.3 Multi-layer Graphene and reduced Graphene Oxide doped with Metals / Metal Oxides

Superior to the other carbon forms, the 2-D planar structure of graphene facilitates electron transport and offers high conductivity (10^3-10^4 Sm^{-1}) and enormous surface area (2630 m^2g^{-1}) [228, 242, 295, 298, 339-343].

Multi-layer graphene can be synthesized by i) epitaxial growth [344], ii) chemical vapor deposition [299, 345]; iii) solvothermal synthesis [346] and iv) electrochemical exfoliation [347-349]. However, the most common method used for the production of multi-layer graphene involves graphite oxidation to graphene oxide, followed by exfoliation and reduction of graphene oxide to multi-layer graphene [343]. The oxidation of graphite to graphene oxide can be achieved by the analytical methods developed by Brodie [350], Staudenmaier [351] and Hummers and Offeman [352]. Briefly, graphite is oxidized in concentrated acid with strong oxidizing agents (sodium nitrate, potassium permanganate) and graphene oxide is exfoliated in water due to the hydrophilic property of the material [300, 303, 343]. Finally, graphene oxide is chemically / electrochemically reduced to multi-layer graphene with various reducing agents including hydroquinone [353], hydrogen sulphide [354], sodium borohydride [353] and hydrazine hydrate [355].

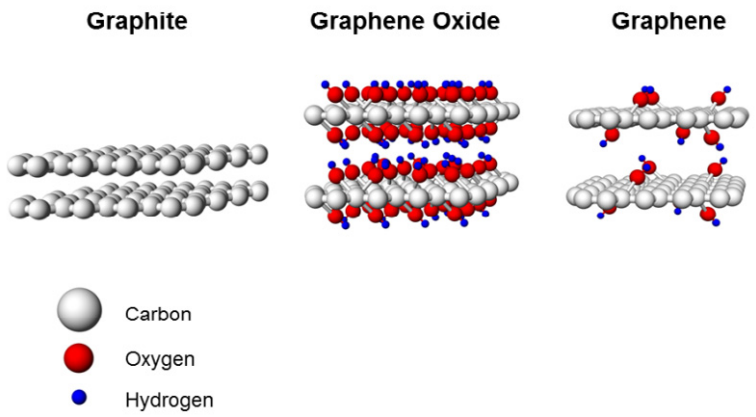

Figure 19. Multi-layer graphene synthesis from graphite: a) Chemical oxidation of graphite to graphene oxide; b) Chemical / electrochemical reduction of graphene oxide to multi-layer graphene [343].

However, the multi-layer graphene produced by exfoliation exhibits low conductivity due to chemical process-induced defects and attached chemical groups [356]. To circumvent this issue, highly conductive metal nanoparticles are attached onto multi-layer graphene increasing the electrical conductivity of the material [356]; silver nanoparticles are the most commonly used material to dope multi-layer graphene due to the high electrical and thermal conductivity as well as catalytic activity of silver [356, 357].

Ag doped multi-layer graphene was synthesized by the reduction of silver salt ($Ag(NH_3)_2$) / graphene oxide under rapid heating (room temperature to 1000^oC at 100$^oCmin^{-1}$ under inert atmosphere; 15 min at 1000^oC) [356]. A 3-fold increase in the electrical conductivity of Ag doped multi-layer graphene was exhibited compared to multi-layer graphene due to the fact that Ag nanoparticles act as an electrical bridge

between graphene layers [356]. Moreover, the capacitance of Ag doped multi-layer graphene was significantly increased compared to multi-layer graphene (326 Fg^{-1} and 109 Fg^{-1} respectively) [356].

Furthermore, cobalt oxide (Co_3O_4) doped reduced mildly oxidized graphene oxide (rmGO) demonstrated high performance in alkaline solutions [358, 359], even though Co_3O_4 itself has very low ORR activity [358, 359]. Co_3O_4 doped rmGO demonstrated similar ORR catalytic activity to pristine Pt/C in alkaline media and superior stability [359]. The electron transfer number was approximately 3.9 showing that this material favors $4e^-$ oxygen reduction pathway in alkaline solution [359].

Mildly oxidized graphene oxide (mGO) was produced by a modified Hummers method [359], in which a six times lower concentration of potassium permanganate ($KMnO_4$) was used (500 mg compared to 3 g in Hummers method) [359]. During the synthesis of Co_3O_4 doped rmGO, $Co(OAc)_2$ solution was added into ethanol / GO dispersion and the mixture was stirred for 10 h at 80^oC [359]. Then, the reaction mixture was transferred to an autoclave for hydrothermal reaction at 150^oC for 3 h [359]. During this step, mildly oxidized graphene oxide was reduced to rmGO [359]. The resulted product was centrifuged and washed with ethanol and water [359].

Nitrogen doped multi-layer graphene was prepared by thermal exfoliation of graphitic oxide followed by nitrogen plasma treatment [360]. Pt-multi-layer graphene (PtG) and Pt-nitrogen doped multi-layer graphene (PtNG) based MEAs demonstrated a maximum

power density of 390 and 440 $mWcm^{-2}$ respectively. The improved performance of PtNG was attributed to the formation of pyrrolic nitrogen defects that increased the anchoring sites for the deposition of Pt on the surface leading to increased electrical conductivity and carbon-catalyst binding [360].

3.2.4 Interaction between the Carbon Support and the Catalyst

Carbon support plays a vital role in the preparation and performance of catalysts since it influences the shape, size and dispersion of catalyst particles as well as the electronic interactions between catalyst and support [125, 361].

Carbon support is a heterogeneous surface consisting of a mixture of basal and edge planes exposed to the surface [362]. Metal particles on the heterogeneous surface are in dispersed state increasing their stability; particles are arranged on the carbon surface at graphene layer edge sites [125]. The charge transfer from metal (catalyst) to carbon support is equal to the number of surface states in the carbon support [363].

i) *Effect of the nature of the support.* The size and morphology of platinum particles depend on the nature of the support. Analysis of X-ray diffractograms (XRD) of different supports prepared by the same method and with the same metal loading demonstrated that Pt crystallites supported on CNFs were ~ 3 nm while Pt crystallites supported on Vulcan and OMCs were approximately 5.6 and 7.6 nm [364]. Thus, higher crystalline grades of the support are conductive to smaller platinum particle size and higher crystalline structures, which are associated with a strong metal-carbon interaction [364].

The crystalline structure of the metal is also affected by the metal-support interaction. Metal particles supported on CNFs have a highly crystalline structure due to strong metal-support interaction [125], whereas Pt particles supported on Vulcan and OMCs have a more dense globular morphology due to weak metal-support interaction [364]. Hence, the more amorphous the carbon support, the higher the platinum size and the more dense the globular morphology [364].

ii) *Effect of the surface chemistry of the support*. Fig. 19 shows the relationship between the total number of surface oxygen groups of the support and the Pt crystallite size for each carbon material tested. An increase in the platinum crystallite size is observed as the number of surface oxygen groups is increasing [365].

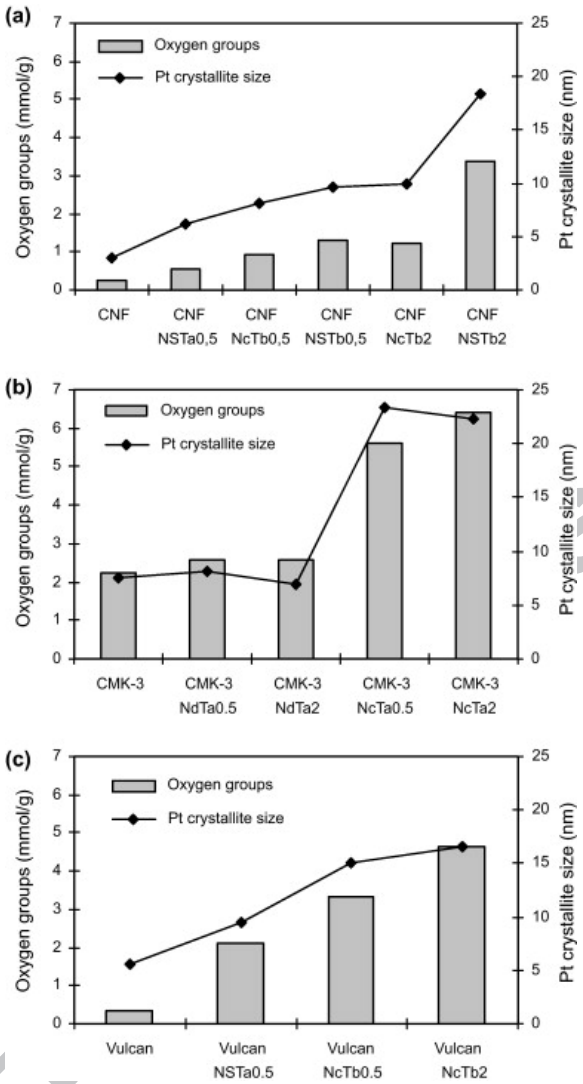

Figure 20. Effect of the surface chemistry of the support on catalyst properties: relationship between the total number of surface oxygen groups of the support and the average Pt crystallite size for oxidized and non-oxidized (a) CNF; (b) CMK-3; and (c) Vulcan (Reprinted from [364] with permission from Elsevier).

In summary, carbon black is extensively used as catalyst support in PEFCs due to low cost and high availability. However, chemical activation of carbon is required in order to increase the number of anchoring sites for catalyst particles on its surface resulting to high catalyst dispersion and catalyst utilization. Thus, new carbon support materials are

being investigated and are categorized into carbon nanotubes, multi-layer graphene (undoped and doped with metal nanoparticles), reduced graphene oxide (doped with metal oxides), mesoporous carbon and carbon nanofibers. The issue of low catalyst utilization was solved by the introduction of CNTs. Their high crystallinity, surface area and long-term stability made them an attractive substitute of carbon black. Multi-layer graphene and reduced graphene oxide as supports provide facile electron transfer and high conductivity while the high surface area and tailored meso-porosity of ordered MCs allows high metal dispersion in the support. CNFs do not require any chemical pretreatment due to the presence of highly active edge planes on which the catalyst nanoparticles can be attached. Even though the properties on the new support materials are extremely promising, further PEFC testing is required with respect to ORR activity and long-term stability.

4. Carbon Hybrids and Composites as ORR Electrocatalysts in Proton Exchange Membrane Fuel Cells

4.1 Nitrogen-doped Carbon

PEFCs are an attractive alternative power source for mobile and stationary application characterized by low emissions, good energy conversion efficiency and high power density. One of the main obstacles towards the commercialization of this technology is the high cost of component materials (catalyst, membrane, etc.) [366-368].

To circumvent this issue, extensive research has been carried out to either reduce the Pt catalyst usage (or improve catalyst utilization) [369, 370] or to identify alternative non-noble metal catalysts with similar catalytic activity [371]. A promising alternative electrocatalyst are heteroatom-doped carbon nanostructures involving Nitrogen, Sulphur, Phosphorus or other non-metallic elements [372-376]. The most prominent and popular dopant is nitrogen. Nitrogen doping of carbon nanostructure materials can be done directly during the synthesis of porous carbon materials [377-388] or with treatment of already synthesized carbon nanostructures with nitrogen containing precursors (NH_3) [389-392].

Nitrogen-doped CNFs [393] prepared via chemical vapor deposition (CVD) demonstrated improved ORR activity. It was attributed to the presence of edge plane defects and nitrogen functionalities within the CNF structure [393, 394]. Fig. 20 shows the measured hydroperoxide (HO_2^-) decomposition rates at N-doped and non-doped CNFs according to the chemical decomposition of HO_2^- reaction. The more rapid the hydroperoxide ions decompose, the more facile the ORR kinetics will be, resulting to higher cathode potential [395]

$$HO_2^- \leftrightarrow \frac{1}{2}O_2 + OH^- \tag{15}$$

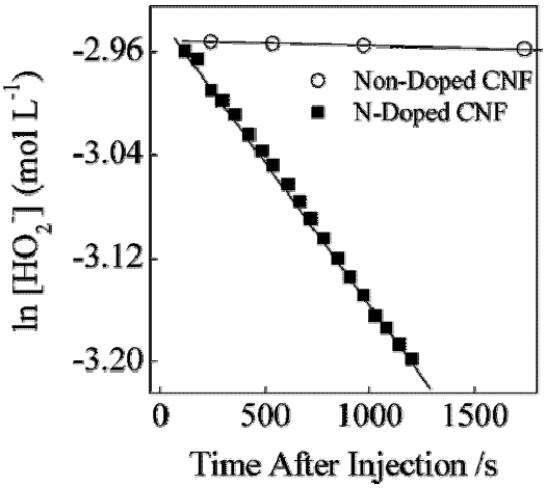

Figure 21. Gasometric analysis of the heterogeneous decomposition of hydroperoxide at non-doped CNFs (circle) and N-doped CNFs (square) in 1 M KNO_3 (Reprinted with permission from [393] - Copyright© 2005 American Chemical Society).

In potassium nitrate solution (1 M KNO_3, pH ~ 7) the forward reaction rate for N-doped CNFs was approximately $5 \cdot 10^{-6}$ cms^{-1} and $3 \cdot 10^{-8}$ cms^{-1} for non-doped CNFs. In potassium hydroxide solution (1 M KOH, pH ~ 14), the forward reaction rate was ~ $1.8 \cdot 10^{-5}$ cms^{-1} and $1 \cdot 10^{-7}$ cms^{-1} for N-doped and non-doped CNFs respectively. Thus, in both neutral and alkaline solutions, N-doped CNFs exhibited a 100-fold increase in H_2O_2 decomposition [393], with values similar to Pt black [396].

Nitrogen doping has repeatedly been reported to increase the basic nature [37, 397] and catalytic activity [398-401] of the graphitic carbon, which is attributed to the presence of nitrogen [402]. Nitrogen-doping in a basal plane of carbon may be more favorable than that in edge sites because the number of available doping sites is greater in the basal plane than in the edge [403]. Geng and coworkers [101] studied the relationship between structure and activity in nitrogen-doped CNTs. ORR activity in acid and alkaline

solutions increased as the nitrogen content on the surface was increasing (Fig. 21). Similar results were obtained by density functional calculations [403] demonstrating that oxygen adsorption becomes more energetically favorable as the number of nitrogen around C=C bond increases.

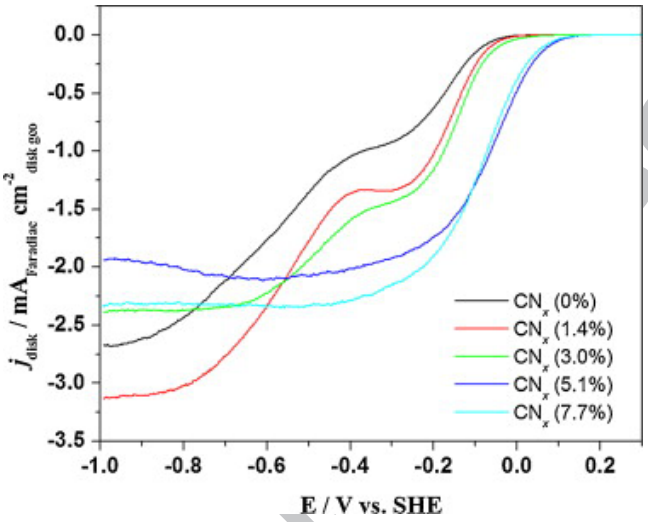

Figure 22. Polarization curves of oxygen reduction on nitrogen-doped CNTs with different nitrogen content (Experimental conditions: 0.1 M KOH, 5 mVs^{-1} scan rate, 1600 rpm rotation speed, 160 μgcm^{-2} catalyst loading - Reprinted from [101] with permission from Elsevier).

The basicity of carbon surface derives from the π electron delocalization in graphite carbon layers and the antioxidant character of carbon forming oxygen containing groups [393]. Delocalized π electrons are capable of nucleophilic attack giving Lewis basicity to the carbon [393, 404].

4.2 Nitrogen-doped Carbon Hybrids with Non-Precious Metals

Non-noble metals supported on nitrogen-doped carbon supports are synthesized by pyrolysis of nitrogen [405-411] and transition metal (such as Fe, Co) [408, 409, 412-427] precursors at high temperatures (~ 600-900^{o}C). Nitrogen precursors are ammonia (NH_3) [405, 406, 410, 411] or acetonitrile (CH_3CN) [407-409, 425] while transition metal precursors include metal salts [408, 409, 424], metal [409, 412], Prussian metal [413, 415] and N_4 macrocyclic complexes [414, 416-423]. Dodelet and coworkers [428] determined the structural parameters of carbon black that are important to maximize its catalytic activity during pyrolysis in NH_3. These parameters are the average particle diameter of carbon black, the amount of disordered phase and the mean size of graphene layers that constitute the ordered regions in carbon black. The microporosity and nitrogen content on the surface of carbon black is proportional to the amount of available disordered phase in the pristine carbon black [428]. When the mean size of graphene layers in carbon black is large, ammonia can react for an extended amount of time with the disordered carbon phase, resulting to a thick porous material. Consequently, the synthesized porous material leads to an increased catalytic activity since the catalytic sites are hosted in the micropores of carbon black [428].

For Fe-based nitrogen doped catalysts, the catalytic activity is directly related to iron content; the number of catalytic sites is increasing as Fe content is increasing until all phenanthroline nitrogens are coordinated with iron [429].

Two different catalytic sites exist at all pyrolysis temperatures in Fe-based catalysts made with Fe salt or porphyrin, namely FeN_4/C and FeN_2/C [430, 431]. FeN_2/C is an iron ion coordinated to two pyridinic nitrogen atoms while FeN_4/C is coordinated to four pyrrole nitrogen atoms. Rotating disk electrode (RDE) measurements revealed that FeN_2/C has higher activity and selectivity than FeN_4/C due to the better electrical contact of FeN_2/C catalytic site with the graphene plane [430]. However, further investigation is needed to fully comprehend the reasons for the higher activity of FeN_2/C catalytic sites.

Zelenay and coworkers [432] used cyanamide as the nitrogen precursor to synthesize transition metal-nitrogen-doped carbon ORR catalysts. Cyanamide forms graphitic C_3N_4 under pyrolysis with high nitrogen content resulting in high catalytic activity. The best performing catalyst was obtained after heat treatment at 1050^{o}C yielding an open circuit voltage of 1 V (vs. SHE) and ~ 105 $mAcm^{-2}$ current density at 0.8 V vs. SHE (Fig. 22). Cyanamide reduces sulfur evolution from the iron source ($FeSO_4$) during heat treatment indicating that an interaction between cyanamide and sulfate-derived species exists and stabilizes the sulfur through the formation of C-S bonds. However, this mechanism is still being investigated [432].

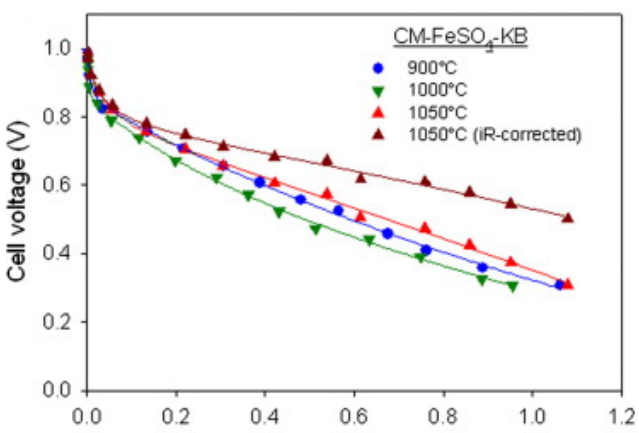

Figure 23. Fuel-cell polarization curves for CM-$FeSO_4$-KB (cyanamide-$FeSO_4$-Ketjeblack) ORR catalysts obtained at different heat-treatment temperatures. Experimental conditions: H_2/O_2, 100% RH, 4 $mgcm^{-2}$ transition metal catalyst loading (Reprinted from [432] with permission from Elsevier).

Iron and cobalt nitrogen-doped catalysts ($TM_xC_{1-x-y}N_y$; TM = Fe, Co; $0<x<0.09$; $0<y<0.5$) were also prepared by sputter deposition [433, 434]. Grazing-incidence X-ray diffraction and scanning electron microscopy (SEM) were used to observe the structural changes as a function of temperature [434]. At temperatures above 700°C, the catalyst transformed to a heterogeneous mixture of partially graphitized nitrogen-containing carbon and Fe_3C or β-Co accompanied by a rapid decrease in nitrogen content [434]. Fe-N-C catalyst exhibited the highest activity at 800°C since the thermal annealing at this temperature causes graphitization and retains sufficient amount of nitrogen to form active sites [434].

However, the instability of transition metal nitrogen-doped carbon catalysts in the highly acidic environment of PEFCs still remains a challenge. The origin of instability in acidic

medium is due to the formation of H_2O_2 (product of the incomplete reduction of oxygen) [435]. Lefevre and Dodelet [435] submitted iron-nitrogen doped carbon catalysts to peroxide treatment to quantify the effect of peroxide on their catalytic activity. Even 5 vol% of peroxide is detrimental to the activity due to the loss of iron content from the catalytic sites (Fig. 23) [435]. A partial solution to this instability issue is the heat treatment of catalysts at high temperatures. Even though stability is improved, the catalytic activity is decreased due to the loss on nitrogen content [435]. Thus, further research is needed to develop stable transition metal-nitrogen doped carbon catalysts in the acidic environment of PEFC.

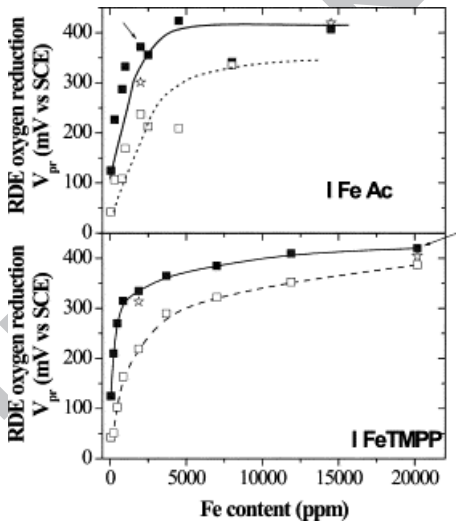

Figure 24. Effect of H_2SO_4 (stars) and of H_2SO_4 + 5 vol% H_2O_2 (open squares) on the initial catalytic activity (dark squares) for type FeAc (Iron acetate) and IFeTMPP (Fe tetramethoxyphenylporphyrin) catalysts (Reprinted from [435] with permission from Elsevier).

4.3 Polymer Composites with Nitrogen-doped Carbon Hybrids

Research is also focused on non-precious metal catalysts synthesized with conjugated heterocyclic conducting polymers such as Ppy, Pani, poly-(3-methylthiophene (P3MT)) and poly-(ethyleneimine) [371, 436-441].

The ORR activity and stability of carbon-supported materials with or without cobalt based on different heterocyclic polymers were investigated [437]. Energy dispersive atomic X-ray spectrometry (EDAX), Fourier transform infrared spectroscopy (FTIR) and Thermogravimetric analysis (TGA) studies demonstrated that the addition of cobalt modifies the chemical structure of all carbon-supported materials studied by the introduction of Co-N (Ppy-C-Co and Pani-C-Co) and Co-S (P3MT-C-Co) bonds [437]. The addition of cobalt results in improved electrocatalytic activity of C-P3MT and C-Pani catalysts even though their thermal stability is slightly reduced at lower temperatures due to the degradation of cobalt oxides (Fig. 24a) [437]. The potential at which ORR occurs was determined to be the highest for Ppy-C-Co (-0.2 to 1 V vs. normal hydrogen electrode (NHE)), followed by Ppy-C, and P3MT-C-Co. Potentiostatic measurements were conducted for 48 hrs to determine the stability of these materials at the maximum potential in the ORR peak (obtained from cyclic voltammogram). Ppy-C-Co and P3MT-C-Co were stable (after a small current decrease during the first 2 hrs) while Ppy-C exhibited a continuous current decrease throughout the experiment (Fig. 24b) [437]. Based on these results, it was reported that Ppy-C-Co catalyst was the most suitable

material for use in PEFCs, even though the potential range in which ORR occurs needs to be further improved.

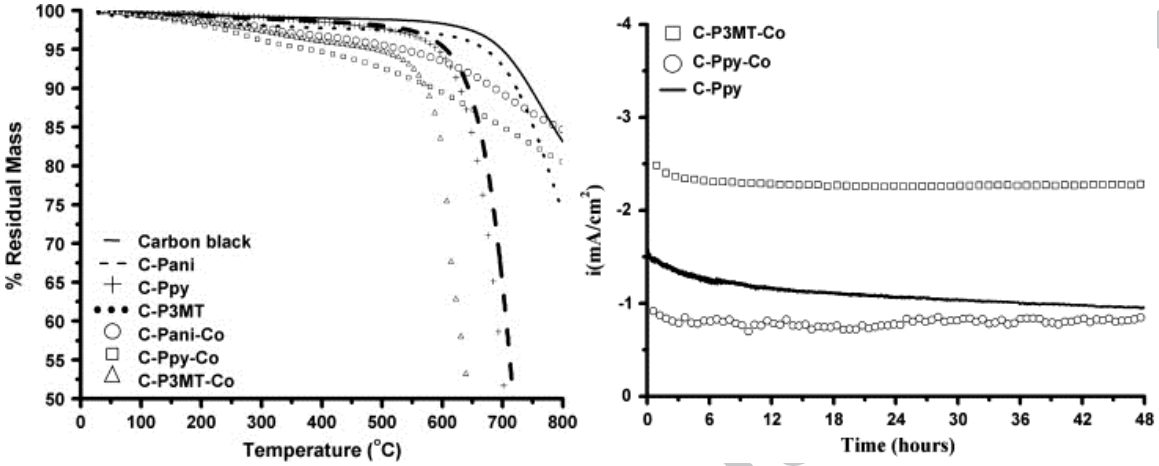

Figure 25. a) TGA curves of carbon-supported materials with or without cobalt obtained in nitrogen atmosphere; b) Chronoamperometry results for Results from chronoamperometry for Ppy-C-Co, P3MT-C-Co and Ppy-C in 0.5 M H_2SO_4 under oxygen (Reprinted from [437] with permission from Elsevier).

The activity of Ppy-C-Co catalyst was thoroughly examined by the synthesis of pyrolyzed and un-pyrolyzed Ppy-C-Co with oxidative polymerization (80^{o}C). Pyrolyzed Ppy-C-Co catalyst demonstrated significantly improved ORR activity over the un-pyrolyzed catalyst indicating that the heat treatment enhanced the catalytic activity. X-ray photoelectron spectroscopy (XPS) revealed that new nitrogen peaks corresponding to pyrrolic and graphitic nitrogen were observed. Both these groups are ORR active increasing the catalytic activity and changing the ORR mechanism from two- (H_2O_2 production) to four-electron reduction (H_2O production) process compared to un-pyrolyzed catalyst [439]. The Koutecky-Levich plot for un-pyrolyzed Ppy-C-Co showed a slope close to the theoretical value for a two-electron transfer reaction, whereas

pyrolyzed Ppy-C-Co catalysts had slope similar to the theoretical four-electron transfer reaction. Based on these data, the calculated ORR electron number (n) was 2.4 for the un-pyrolyzed Ppy-C-Co and 3.2 for the pyrolyzed (Fig. 25).

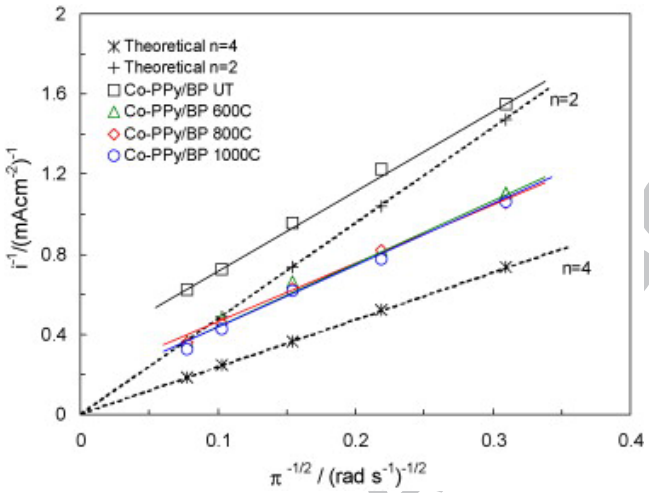

Figure 26. Koutecky-Levich plots for the ORR of un-pyrolyzed and pyrolyzed Ppy-C-Co catalysts; experimental conditions: 0.3 V (vs. RHE) in 0.5 M H_2SO_4 under saturated O_2 and 0.122 $mgcm^{-2}$ Ppy-C-Co loading. The current densities were normalized to the geometric area (Reprinted from [439] with permission from Elsevier).

The effect of the weight and molar ratio of Ppy:Co on the ORR activity of these catalysts was recently investigated [442]. Ppy:Co molar ratio of 4 increased the ORR activity as it favors the formation of complexes in which Co is coordinated to 3 or 4 nitrogen atoms. Calcination of these complexes led to the generation of CoN_{x-2} sites characterized by high ORR activity since the coordination on Co in them favors the adsorption of oxygen on them. The ORR activity of Ppy-Co-C (molar ratio 4 and weight ratio 2) was adequate, being 200 mV lower than pristine Pt-C, and produced less H_2O_2 than Pt [442].

The electrocatalytic activity of composite carbon supported materials based on heterocyclic polymers and nickel (Pani-C-Ni, Ppy-C-Ni, and P3MT-C-Ni) was also studied [438]. FTIR revealed that the modification with nickel altered the polymer bonds creating Ni-AN (for Pani and Ppy-based catalysts) and Ni-AS bonds (for P3MT -based catalysts), while TGA showed that the incorporation of nickel improved the thermal stability of the catalysts at high temperatures (above 400^{o}C). The Tafel slopes were similar for all catalysts tested (~ 0.11-0.2); however, Ppy-C-Ni had the highest exchange current density (~ $4 \cdot 10^{-5}$ mAcm^{-2} followed by P3MT-C-Ni and Ppy-C (~ $3.5 \cdot 10^{-5}$ and $2.5 \cdot 10^{-5}$ mAcm^{-2} respectively). Based on these results, it was concluded that Ppy-C-Ni was the most suitable catalyst for ORR in acidic medium [438].

Popov and coworkers [443] synthesized N-doped ordered porous carbon (CN_x) via a nanocasting process using polyacrylonitrile (Pan) as the carbon and nitrogen precursor and mesoporous silica as hard template [443]. The non-precious metal ORR catalysts were prepared by pyrolyzing CN_x at 1000^{o}C in argon after iron acetate was adsorbed onto it, followed by post-treatments. RDE measurements demonstrated a ~ 0.88 V (vs. NHE) onset potential for ORR in 0.5 M H_2SO_4, while a current density of 0.6 Acm^{-2} at 0.5 V was obtained in a H_2/O_2 PEFC using 2 mgcm^{-2} catalyst loading [443].

To sum up, nitrogen doping of nanostructured carbon is a promising strategy to obtain low cost PEFC catalysts with good cell performance. Nitrogen-doped carbon with or without transition metal catalysts exhibit enhanced catalytic activity and durability toward ORR. Nitrogen is the indispensable element in many non-Pt metal catalysts (Fe,

Co, etc.) for potential application in PEFCs. Research is also focused on the development of non-precious metal catalysts synthesized with conjugated heterocyclic conducting polymers (such as polypyrrole). Initial results show adequate ORR activity and fuel-cell performance, but further research is needed to increase the stability in acidic medium and the potential range in which ORR occurs.

5. Carbon Hybrids as ORR Electrocatalysts in Alkaline Fuel Cells

Pt and Pt alloys are undoubtedly the most widely used fuel cell ORR catalysts for acidic conditions of phosphoric acid or proton exchange membrane fuel cells [248, 325, 444-473]. Alkaline fuel cells (AFCs) allow the use of non-precious metal catalysts as cathode electrodes due to the faster ORR kinetics and better stability of these materials under basic conditions [474]. This unique characteristic transforms AFCs to a promising candidate for portable power sources and electric vehicles applications [475-479]. However, further research is needed in order to improve the low activity and poor durability of AFCs electrocatalysts, before the commercialization of this technology [479].

5.1 Nitrogen-doped Carbon

Nitrogen doped carbon materials were among the first that were studied as electrocatalysts for AFCs [296, 374, 480-485]. Nitrogen doping of carbon leads to similar

ORR kinetics with commercial Pt/C electrocatalyst, and higher kinetics than commercial Ag/C catalysts [393, 483, 486].

Nitrogen doped carbon nanotubes synthesized by catalytic growth and post treatment with ammonia (NH_3) and aniline were tested as ORR electrocatalysts in alkaline solution [480]. Nitrogen CNT-NH_3 demonstrated the highest ORR activity in alkaline solution (0.1 M KOH) [480]. However, after the alkaline treatment of the samples (10 M KOH for 5 h at 80^{o}C), nitrogen doped CNTs (by catalytic growth) exhibited enhanced catalytic activity in contrast to the decreased performances of nitrogen doped CNT-NH_3 and -aniline catalysts. This improved activity was attributed to the formation of oxygen groups by alkaline treatment and their interaction with existing nitrogen groups [480]. XPS analysis demonstrated that the treatment in 10 M KOH led to a slight decrease of the N/C ratio for all three nitrogen doped CNT samples and changes to the concentration of quaternary, pyridinic and pyrrolic nitrogen [480]. In the case of nitrogen doped CNTs (by catalytic growth), the concentrations of quaternary and pyridinic nitrogen increased, whereas pyrrolic nitrogen decreased. Nitrogen doped CNTs -NH_3 and -aniline samples exhibited the opposite trend. These results showed that high concentrations of pyridinic and quaternary-nitrogen are beneficial for the ORR catalysis. On the contrary, pyrrolic type nitrogen is also considered to be among the active sites of N-doped nanocarbons for ORR [487, 488] but it has negative effects on the ORR activity in alkaline media [489, 490].

This result is in accordance with previous reports in the literature indicating that quaternary [372, 491-496] and pyridinic [372, 492, 497-504] nitrogen are the most active forms for ORR catalysis in alkaline media. Theoretical studies support the hypothesis that the presence of quaternary-type nitrogen favors O_2 adsorption at carbon sites on the zigzag edges located adjacent to quaternary-type nitrogen [505]. The incorporation of electron-accepting nitrogen atoms creates a relatively high positive charge density on adjacent carbon atoms; nitrogen becomes more electronegative and creates a net positive charge on the adjacent carbon atoms [506]. As a result, the adsorption of O_2 on nitrogen doped CNTs becomes easier leading to an improved electrocatalytic activity of these materials towards ORR in alkaline media (higher than that of Pt/C catalyst) [506].

Apart from the contribution of quaternary and pyridinic type nitrogen, there are reports in the literature attributing the ORR activity in alkaline media to the number of defects and edge sites of carbon upon nitrogen doping [373, 507, 508], which are also considered as active sites for ORR [366].

Hence, despite the fact that the physicochemical origin of the ORR activity of N-doped nanocarbons is still unclear, nitrogen-doped CNTs are a promising candidate as cathode catalysts in AFCs. However, extensive *in-situ* fuel-cell testing of these materials is required to obtain more information about their stability and activity during fuel-cell operation.

5.2 Nitrogen-doped multi-layer Graphene / reduced Graphene Oxide

Multi-layer graphene and reduced graphene oxide are potential candidates as cathode material for AFCs due to the large surface area and good mechanical properties of the material [296, 299].

As in the case of nitrogen doped CNTs, the ORR activity of nitrogen doped multi-layer graphene / reduced graphene oxide also depends on nitrogen functionality (pyridinic, quaternary and pyrrolic nitrogen and pyridine-nitrogen-oxide) [481, 509-512]. However, there is a debate on which of the four nitrogen functionalities is the most influential factor on ORR activity in alkaline media. Nitrogen (~ 8 wt %) doped graphene oxide with high percentage of quaternary nitrogen (~ 24%) exhibited high ORR activity whereas the other three functionalities reported to have small impact [513]. Nitrogen doped reduced graphene oxide was prepared by graphene oxide (produced by Hummers method [352]) and urea (N precursor; 46 wt% N_2) [513]. Graphene oxide was dispersed in water and urea was then added in the solution under continuous stirring until complete dissolution of urea. The solution was dried at 55^{o}C and then pyrolyzed at 800^{o}C in Ar atmosphere; during pyrolysis, graphene oxide was thermally reduced and N atoms were incorporated into the graphitic structure producing nitrogen doped reduced graphene oxide [513].

On the other hand, there are reports in the literature stating that pyridinic N and the small pores of the catalyst are responsible for ORR electrocatalysis [514]. XPS and Raman measurements of the nitrogen-doped reduced graphene oxide indicated that the pyridinic

nitrogen introduced disordered edge planes into the graphene structure [485]. BET analysis demonstrated that the surface area of reduced graphene oxide was increased due to the exposure of disordered edge planes [485]. These observations led to the assumption that the defects introduced by pyridinic nitrogen act as active sites for the ORR [485].

RRDE measurements showed that nitrogen doped multi-layer graphene (2-8 layers; 0.3-0.4 nm interlayer distance and 0.9-1.1 nm layer thickness) exhibited high ORR activity in alkaline media (0.1 M KOH) [296]. The steady-state catalytic current density was approximately three times higher than that of Pt/C over a wide potential range (Fig. 26). The transferred electron number per oxygen molecule was 3.6-4 between -0.4 and -0.8 V (vs. SHE), showing that nitrogen doped multi-layer graphene exhibited a four electron pathway to ORR [296].

Chemical vapor deposition was used for the facile synthesis of multi-layer graphene. A thin layer (~ 300 nm) of nickel was deposited on a silica substrate by sputter coating and the sample was heated up to 1000^{o}C under inert atmosphere (Argon) [296]. A nitrogen-containing reaction gas mixture (NH_3:CH_4:H_2:Ar = 10:50:65:200 cm^3min^{-1}) was introduced into the furnace for 5 min followed by purging with NH_3 and Ar for another 5 min [296]. The resulting multilayer-graphene could be etched off the substrate by dissolution of the residual Ni catalyst layer in HCl solution [296].

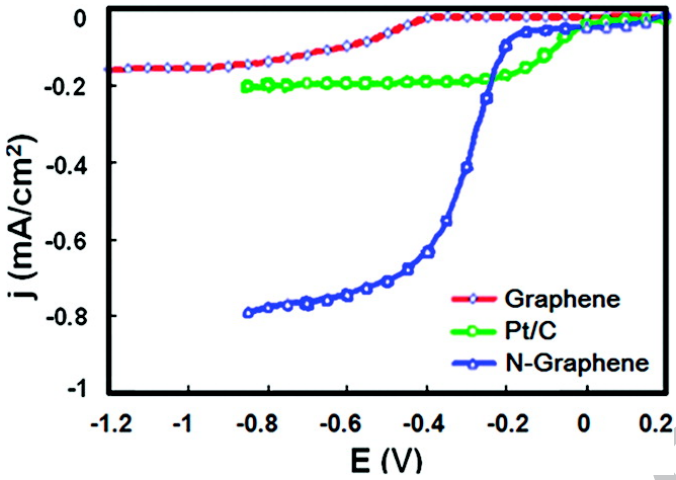

Figure 27. Rotating ring disk electrode voltammograms for multi-layer graphene (red), Pt/C (green), and nitrogen doped multi-layer graphene (blue). Experimental conditions: 0.1 M KOH, 0.01 Vs^{-1} scan rate, 1000 rpm rotation rate, Mass (multi-layer graphene) = Mass (Pt/C) = Mass (nitrogen doped multi-layer graphene) = 7.5µg (Reprinted from [296] - Copyright® 2010 American Chemical Society).

5.3 Carbon with Non-Precious Metals

Ag and Ag-alloys are used as catalysts in AFCs due to their low cost and similar ORR activities to Pt and Pt alloys [515, 516]. However, the performance of Ag based catalysts is affected by the agglomeration of the Ag nanoparticles and the electrochemical corrosion of the catalyst supports [517]. The incorporation of Ag catalysts into CNTs is a very promising method to increase the stability and ORR activity of these catalysts in alkaline environment [516]. It was reported that an increase of Ag content (from 5 to 9 wt%) and CNT surface area results to higher amount of active sites per geometric surface area of the electrode and thus, faster ORR kinetics [516].

The ORR activity of Ag/C catalysts can be predicted by the intensity of the anodic peak (Fig. 27; A_1 peak at 0.23 V vs. Hg/HgO in 0.1 M NaOH) which is correlated to silver dissolution and formation of a surface monolayer of Ag_2O [518, 519]. As the Ag loading increases (10 to 60 wt%), peak intensity increases linearly and ORR onset potential shifts positively 60 mV [519].

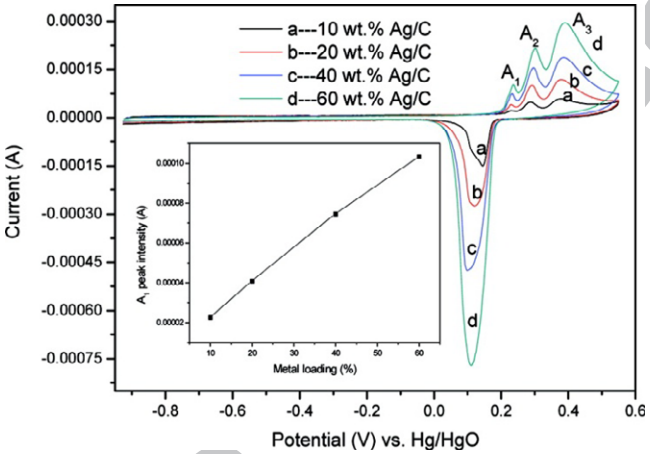

Figure 28. Cyclic voltammograms of Ag/C catalysts with different metal loadings; experimental conditions: Argon atmosphere, 0.1 M NaOH solution, and 20mVs^{-1} scan rate. Inset: curves of A_1 anodic peak intensities with metal loading (Reprinted from [519] - Copyright® 2010 American Chemical Society).

Recently, Ag nanoparticles were deposited directly on MWCNTs by sputter deposition [520] and in-situ growth [517]. Ag/MWCNTs catalyst exhibited high ORR activity in alkaline media and the reduction process proceeded via a four-electron pathway [517, 520]. The high ORR activity of Ag/MWCNTs was attributed to the ability of dispersed Ag nanoparticles on the surface of MWCNTs to further reduce HO_2^- formed at the surface of NTs [517, 520]. Even though the ORR activity of Ag/MWCNTs is still lower

than pristine PT/C (20 wt %) [517], Ag/MWCNTs are promising ORR catalysts for AFCs.

Moreover, Pd and Pd alloys are also used as non-Pt catalysts since Pd has similar properties to Pt [521]. Pd has slightly lower ORR activity than Pt, and by addition of a suitable metal, such as Co or Fe, the ORR activity of Pd can surpass that of Pt [522, 523]. The incorporation of transition metals (Co, Fe, Cr, and Ni) to Pd enhances the ORR activity due to modification of electron configuration and alteration of surface species and composition [521]. Pd has fully occupied d-orbitals while the alloyed transition metal has low occupancy of d orbitals [524]; the d-orbital coupling effect between those two metals decrease the required Gibbs free energy of the electron transfer steps in ORR, leading to an increase in ORR kinetics [524]. Among the non-Pt alloys tested, Pd-Co alloy exhibited high ORR activity in alkaline media along with Au-Co and Ag-Co alloys [525]. Cobalt is stable in alkaline media even though it dissolves from the metal alloy as cobalt oxide in acidic media [526]. A recent study demonstrated that PdCo(3:1)/C based MEAs exhibited the highest alkaline fuel-cell performance (~ 85 $mWcm^{-2}$) compared to PdCo(2:1)/C and PdCo(1:1)/C based MEAs (75 and 26 $mWcm^{-2}$ respectively) when tested at $30^{o}C$ [521].

Iron phthalocyanines (FePc), cobalt phthalocyanines (CoPc) and other similar M-N_4-macrocycles supported on different carbon nanomaterials have also attracted much attention towards ORR in alkaline medium [486, 527-534].

FePc and CoPc have the ability to promote the $4e^-$ oxygen reduction to water without the formation of peroxide intermediates [528-530]. RRDE studies (0.1 M KOH) demonstrated that the current density of CoPc was consistently higher than FePc due to the different onset potential of ORR. The onset potential for CoPc/MWCNT starts at -0.1 V (vs. SCE) and shifts towards the positive direction whereas the FePc/MWCNT onset potential begins at -0.15 V (vs. SCE) [531]. Fuel cell performance (H_2/O_2 as fuel, 45^oC) of CoPc/MWCNT based MEAs was similar (~ 100 $mWcm^{-2}$ power density) to commercial E-TEK Pt/C MEAs [531], whereas FePc/MWCNTs based MEAs exhibited poor fuel-cell performance (~ $60mWcm^{-2}$) under the same conditions [531]. However, further fuel-cell performance testing at higher temperatures could not be conducted due to water balance issues in the fuel-cell above 50^oC [531].

Manganese oxide based catalysts for the ORR in alkaline media have also attracted much attention in recent years [535-542] due to the low cost of the material. The catalytic activity of MnO_2 depends on the crystallographic structures, namely α-, β- and γ -MnO_2 [543]. ORR catalytic activity order in alkaline media is α- > β-> γ -MnO_2 and a 4 electron ORR pathway is achieved when α-MnO_2 nanostructures are used [536, 544, 545]. However MnO_2 has low electrical conductivity and it is always incorporated into a conducting carbon material such as CNTs to overcome this issue [543, 546-550].

Similar to manganese dioxide, MnOOH also shows catalytic activity toward ORR in alkaline media [544]. A recent study demonstrated that an increase of the MnOOH catalyst loading resulted to an enhancement of the catalytic activity of MnOOH/C even

though still lower than pristine Pt/C (Fig. 28). Hence, optimization of the MnOOH content in the carbon hybrid catalyst can lead to enhanced electrocatalytic properties [544].

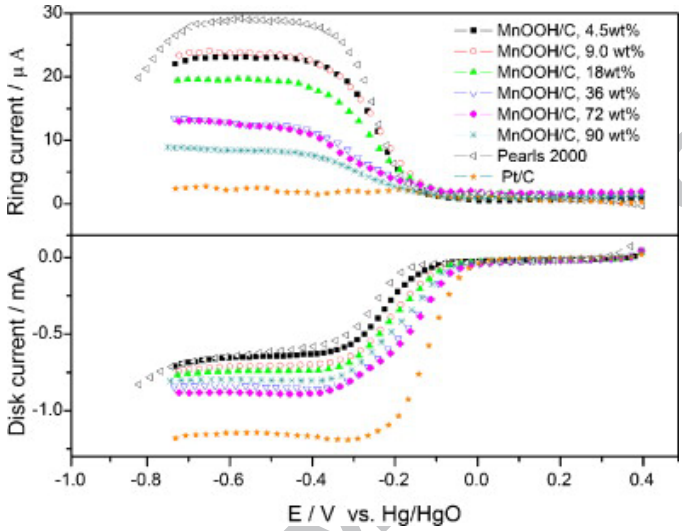

Figure 29. RRDE results of MnOOH/C catalysts with varying MnOOH content. Experimental conditions: 0.1 M KOH, 10 mVs^{-1} scan rate, 1600 rpm rotating speed (Reprinted from [544] with permission from Elsevier).

In summary, AFCs offer facile ORR kinetics in alkaline media allowing a wide range of low cost, non-platinum electrocatalysts to be used in the cathode, namely, nitrogen doped carbonaceous materials, Ag and Pd nanoparticles, transition metal oxides and M-N_4-macrocycles supported on carbon. Among these materials, nitrogen doped CNTs and nitrogen doped multi-layer graphene / reduced graphene oxide exhibit the highest ORR activity in alkaline media, even though the activity is still lower when compared to pristine Pt/C. However, it remains unclear whether the nitrogen functionality (pyridinic, quaternary and pyrrolic nitrogen) or the number of defects on carbon surface created by

nitrogen doping is the main contributor to the enhanced ORR activity of these materials. Further research is needed to clarify the main source of ORR activity of nitrogen doped carbonaceous materials in alkaline media and to improve the electrocatalytic activity and *in-situ* stability under various fuel-cell operating conditions and potential cycling profiles.

6. Conclusions and Future Outlook

Carbon is widely used in the catalytic processes of the chemical industry due to its unique characteristics, such as chemical inertness, high surface area and porosity, good mechanical properties and low cost. It is used for the production of chlorine and aluminum, in metal refining, in batteries and biosensors as well as for the electrolytic production of hydrogen peroxide and photo-electrochemical water splitting.

Carbon is a vital component of PEFCs as well and it can serve as structural component (gas diffusion layer), catalyst support and ORR electrocatalyst. However, carbon is oxidized at high potentials leading to fuel-cell performance losses and hence new carbon support materials such as carbon nanotubes and nanofibers as well as mesoporous carbon, multi-layer graphene (undoped and doped with metal nanoparticles) and reduced graphene oxide (undoped and doped with metal oxides) are being investigated. They offer high crystallinity, surface area, increased fuel cell performance and stability. However, further PEFC testing is required with respect to their ORR activity, long-term stability (continuous cycling and accelerated degradation tests) and conductivity.

Pt is currently used as the electrocatalyst for oxygen reduction in PEFCs, but its high cost and limited resources led to an extensive research for alternate, non-noble metal electrocatalysts. Among them, nitrogen doping of nanostructured carbon (with or without transition metals) demonstrated enhanced catalytic activity and durability. Nitrogen-doped non-precious metal electrocatalysts with conducting polymers (polypyrrole, polyaniline) also exhibited adequate ORR activity and fuel cell performance. However, further research is needed toward their stability in highly acidic/alkaline medium and broadening of potential range in which oxygen reduction occurs.

7. Commentary

The current review presented in detail the various forms of carbon used for electrochemical energy conversion. Carbon black has been used extensively due to low cost and high availability. Insufficient electrochemical stability and low catalyst utilization with carbon black resulted in the development of new carbon derivatives. However, which of these carbon forms are viable (based on the properties and cost of the material) and are strong contenders for large scale production?

Ordered mesoporous carbon, carbon nanotubes, multi-layer graphene and reduced graphene oxide are the most promising candidates for commercialization. As catalyst support, the large surface area of OMCs results in high dispersion of catalyst while the uniform mesopores of the material lead to high rates of mass transport and enhanced catalytic activity. As fuel cell catalysts though, OMCs exhibit low durability and activity. This issue can be resolved by nitrogen doping resulting in the formation of graphitic

framework with nitrogen content and thus high activity and stability under fuel cell conditions. Further research is needed to evaluate the electrochemical properties of N-OMCs under long term fuel-cell operation.

Moreover, the utilization of CNTs, multi-layer graphene (undoped and doped with metal nanoparticles) and reduced graphene oxide (doped with metal oxides) as catalyst supports offers high rates of mass / charge transport as well as high conductivity and stability. The two dimensional nature of these materials allows both the edge and basal planes to interact with the catalysts increasing the catalytic activity. As catalysts, nitrogen doped CNTs as well as nitrogen doped multi-layer graphene and reduced graphene oxide exhibit the highest ORR activity in alkaline media, even though the activity is still lower when compared to pristine Pt/C. Further research is needed to improve the electrocatalytic activity and *in-situ* stability under various fuel-cell operating conditions and potential cycling profiles.

Hence, nitrogen doped CNTs, OMCs, multi-layer graphene and reduced graphene oxide are the most suitable applicants (supports / catalysts) for fuel cell commercialization, even though there are still a few obstacles to overcome, namely long-term stability and development of cost-effective synthesis techniques for large scale production.

Nomenclature

Abbreviation	
AC	Activated carbon
AFC	Alkaline fuel cell
BET	Brunauer, Emmett and Teller
CIC	Carbon in column
CIL	Carbon in leach
CIP	Carbon in pulp
CNF	Carbon fiber
CNT	Carbon nanotube
CVD	Chemical vapor deposition
DOMC	Disordered mesoporous carbon
ECA	Electrochemically active surface area
EDAX	Energy dispersive atomic X-ray spectrometry
EQCM	Electrochemical quartz crystal microbalance
FTIR	Fourier transform infrared spectroscopy
GDL	Gas diffusion layer
HOMO	Highest occupied molecular orbital
LUMO	Lowest unoccupied molecular orbital
MC	Mesoporous carbon
MEA	Membrane electrode assembly
MWCNT	Multi-walled carbon nanotube
OMC	Ordered mesoporous carbon
ORR	Oxygen reduction reaction
NHE	Normal hydrogen electrode (E = 0 V)
P3MT	Poly (3-methylthiophene)
Pan	Polyacrylonitrile
Pani	Polyaniline
PEFC	Polymer electrolyte fuel cell
PEM	Proton exchange membrane
Ppy	Polypyrrole
Pt	Platinum
PtG	Platinum-graphene
PtNG	Pt-nitrogen doped graphene
RDE	Rotating disk electrode
RH	Relative humidity
RHE	Reversible hydrogen electrode (E = 0 V)
SCE	Saturated calomel electrode (E = +0.24 V vs.NHE)
SEM	Scanning electron microscopy
SHE	Standard hydrogen electrode (E = 0 V)
SWCNT	Single-walled carbon nanotube
TEM	Transmission electron microscopy
TGA	Thermogravimetric analysis
Vol	Volume percent (%)
wt	Weight percent (%)
WMC	Wormhole mesoporous carbon
XPS	X-ray photoelectron spectroscopy
XRD	X-ray diffraction

References

1. Besenhard, J.O. and H.P. Fritz, *The Electrochemistry of Black Carbons.* Angewandte Chemie International Edition in English, 1983. **22**(12): p. 950-975.
2. Harris, P.J.F., *New Perspectives on the Structure of Graphitic Carbons.* Critical Reviews in Solid State and Materials Sciences, 2005. **30**(4): p. 235-253.
3. Dementev, N., et al., *Purification of carbon nanotubes by dynamic oxidation in air.* Journal of Materials Chemistry, 2009. **19**(42): p. 7904-7908.
4. Chiang, I.W., et al., *Purification and Characterization of Single-Wall Carbon Nanotubes.* The Journal of Physical Chemistry B, 2001. **105**(6): p. 1157-1161.
5. Itkis, M.E., et al., *Purity Evaluation of As-Prepared Single-Walled Carbon Nanotube Soot by Use of Solution-Phase Near-IR Spectroscopy.* Nano Letters, 2003. **3**(3): p. 309-314.
6. Dicks, A.L., *The role of carbon in fuel cells.* Journal of Power Sources, 2006. **156**(2): p. 128-141.
7. Logothetidis, S., *Optical and electronic properties of amorphous carbon materials.* Diamond and Related Materials, 2003. **12**(2): p. 141-150.
8. Peres, N.M.R., F. Guinea, and A.H. Castro Neto, *Electronic properties of two-dimensional carbon.* Annals of Physics, 2006. **321**(7): p. 1559-1567.
9. Xanthakis, J.P., *Effects of short-range order on the electronic structure and optical properties of amorphous carbon.* Diamond and Related Materials, 2000. **9**(7): p. 1369-1373.
10. Yang, Y., K. Chiang, and N. Burke, *Porous carbon-supported catalysts for energy and environmental applications: A short review.* Catalysis Today, 2011. **178**(1): p. 197-205.
11. Velo-Gala, I., et al., *Surface modifications of activated carbon by gamma irradiation.* Carbon, 2014. **67**(0): p. 236-249.
12. Jaramillo, J., P.M. Álvarez, and V. Gómez-Serrano, *Oxidation of activated carbon by dry and wet methods: Surface chemistry and textural modifications.* Fuel Processing Technology, 2010. **91**(11): p. 1768-1775.
13. Shafeeyan, M.S., et al., *A review on surface modification of activated carbon for carbon dioxide adsorption.* Journal of Analytical and Applied Pyrolysis, 2010. **89**(2): p. 143-151.
14. László, K. and A. Szűcs, *Surface characterization of polyethyleneterephthalate (PET) based activated carbon and the effect of pH on its adsorption capacity from aqueous phenol and 2,3,4-trichlorophenol solutions.* Carbon, 2001. **39**(13): p. 1945-1953.
15. Boehm, H.P., *Some aspects of the surface chemistry of carbon blacks and other carbons.* Carbon, 1994. **32**(5): p. 759-769.
16. Karanfil, T. and J.E. Kilduff, *Role of Granular Activated Carbon Surface Chemistry on the Adsorption of Organic Compounds. 1. Priority Pollutants.* Environmental Science & Technology, 1999. **33**(18): p. 3217-3224.
17. Bansal, R.C., F.J. Vastola, and P.L. Walker Jr, *Influence of hydrogen chemisorption on the subsequent chemisorption of oxygen on activated graphon.* Carbon, 1974. **12**(3): p. 355-357.
18. Szymański, G.S., et al., *The effect of the gradual thermal decomposition of surface oxygen species on the chemical and catalytic properties of oxidized activated carbon.* Carbon, 2002. **40**(14): p. 2627-2639.
19. Menéndez, J.A., et al., *On the Modification and Characterization of Chemical Surface Properties of Activated Carbon: In the Search of Carbons with Stable Basic Properties.* Langmuir, 1996. **12**(18): p. 4404-4410.

20. Mangun, C.L., et al., *Oxidation of Activated Carbon Fibers: Effect on Pore Size, Surface Chemistry, and Adsorption Properties.* Chemistry of Materials, 1999. **11**(12): p. 3476-3483.
21. Figueiredo, J.L., et al., *Modification of the surface chemistry of activated carbons.* Carbon, 1999. **37**(9): p. 1379-1389.
22. Stoeckli, F., et al., *Porous structure of polyarylamide-based activated carbon fibres.* Carbon, 1996. **34**(10): p. 1201-1206.
23. Carrott, P.J.M., et al., *Preparation of activated carbon fibres from acrylic textile fibres.* Carbon, 2001. **39**(10): p. 1543-1555.
24. Mangun, C.L., et al., *Surface chemistry, pore sizes and adsorption properties of activated carbon fibers and precursors treated with ammonia.* Carbon, 2001. **39**(12): p. 1809-1820.
25. Pittman Jr, C.U., et al., *Chemical modification of carbon fiber surfaces by nitric acid oxidation followed by reaction with tetraethylenepentamine.* Carbon, 1997. **35**(3): p. 317-331.
26. Noh, J.S. and J.A. Schwarz, *Effect of HNO3 treatment on the surface acidity of activated carbons.* Carbon, 1990. **28**(5): p. 675-682.
27. Boehm, H.P., *Surface oxides on carbon and their analysis: a critical assessment.* Carbon, 2002. **40**(2): p. 145-149.
28. Salame, I.I. and T.J. Bandosz, *Role of surface chemistry in adsorption of phenol on activated carbons.* Journal of Colloid and Interface Science, 2003. **264**(2): p. 307-312.
29. Papirer, E., et al., *Surface groups on nitric acid oxidized carbon black samples determined by chemical and thermodesorption analyses.* Carbon, 1991. **29**(1): p. 69-72.
30. Zhou, J.-H., et al., *Characterization of surface oxygen complexes on carbon nanofibers by TPD, XPS and FT-IR.* Carbon, 2007. **45**(4): p. 785-796.
31. Otake, Y. and R.G. Jenkins, *Characterization of oxygen-containing surface complexes created on a microporous carbon by air and nitric acid treatment.* Carbon, 1993. **31**(1): p. 109-121.
32. Zielke, U., K.J. Hüttinger, and W.P. Hoffman, *Surface-oxidized carbon fibers: I. Surface structure and chemistry.* Carbon, 1996. **34**(8): p. 983-998.
33. Marchon, B., et al., *TPD and XPS studies of O2, CO2, and H2O adsorption on clean polycrystalline graphite.* Carbon, 1988. **26**(4): p. 507-514.
34. Boudou, J.P., et al., *Nitrogen in aramid-based activated carbon fibers by TPD, XPS and XANES.* Carbon, 2006. **44**(12): p. 2452-2462.
35. Proctor, A. and P.M.A. Sherwood, *X-ray photoelectron spectroscopic studies of carbon fibre surfaces—II: The effect of electrochemical treatment.* Carbon, 1983. **21**(1): p. 53-59.
36. Vickers, P.E., et al., *The surface chemistry and acid–base properties of a PAN-based carbon fibre.* Carbon, 2000. **38**(5): p. 675-689.
37. Biniak, S., et al., *The characterization of activated carbons with oxygen and nitrogen surface groups.* Carbon, 1997. **35**(12): p. 1799-1810.
38. Bradley, R.H., X. Ling, and I. Sutherland, *An investigation of carbon fibre surface chemistry and reactivity based on XPS and surface free energy.* Carbon, 1993. **31**(7): p. 1115-1120.
39. Chan, D., et al., *Surface characterization of intermediate modulus graphite fibers via surface free energy measurement and esca.* Carbon, 1991. **29**(8): p. 1091-1098.
40. Grzybek, T. and K. Kreiner, *Surface Changes in Coals after Oxidation. 1. X-ray Photoelectron Spectroscopy Studies†.* Langmuir, 1997. **13**(5): p. 909-912.

41. Gai, P.L., B.H.M. Billinge, and A.M. Brown, *Microstructure of carbons.* Carbon, 1989. **27**(1): p. 41-53.
42. Goworek, J., A. Świątkowski, and S. Biniak, *Characterization of Modified Active Carbons by Adsorption of Pure Water and Benzene Vapors and Ternary Liquid Mixture Benzene + Diethyl Ketone + n-Heptane†.* Langmuir, 1997. **13**(5): p. 1225-1228.
43. Gómez-Serrano, V., et al., *Formation of oxygen structures by air activation. A study by FT-IR spectroscopy.* Carbon, 1999. **37**(10): p. 1517-1528.
44. Moreno-Castilla, C., M.V. López-Ramón, and F. Carrasco-Marín, *Changes in surface chemistry of activated carbons by wet oxidation.* Carbon, 2000. **38**(14): p. 1995-2001.
45. Sellitti, C., J.L. Koenig, and H. Ishida, *Surface characterization of graphitized carbon fibers by attenuated total reflection fourier transform infrared spectroscopy.* Carbon, 1990. **28**(1): p. 221-228.
46. Ishizaki, C. and I. Martí, *Surface oxide structures on a commercial activated carbon.* Carbon, 1981. **19**(6): p. 409-412.
47. Sakintuna, B. and Y. Yürüm, *Preparation and characterization of mesoporous carbons using a Turkish natural zeolitic template/furfuryl alcohol system.* Microporous and Mesoporous Materials, 2006. **93**(1–3): p. 304-312.
48. Donnet, J.B., et al., *Energy site distribution of carbon black surfaces by inverse gas chromatography at finite concentration conditions.* Carbon, 2002. **40**(2): p. 163-167.
49. Sharma, S. and B.G. Pollet, *Support materials for PEMFC and DMFC electrocatalysts—A review.* Journal of Power Sources, 2012. **208**(0): p. 96-119.
50. Shao-Horn, Y., et al., *Instability of Supported Platinum Nanoparticles in Low-Temperature Fuel Cells.* Topics in Catalysis, 2007. **46**(3-4): p. 285-305.
51. Ristein, J., *Electronic properties of diamond surfaces — blessing or curse for devices?* Diamond and Related Materials, 2000. **9**(3–6): p. 1129-1137.
52. Honda, K., et al., *Electrochemical properties of Pt-modified nano-honeycomb diamond electrodes.* Journal of Electroanalytical Chemistry, 2001. **514**(1–2): p. 35-50.
53. Montilla, F., et al., *Platinum particles deposited on synthetic boron-doped diamond surfaces. Application to methanol oxidation.* Electrochimica Acta, 2003. **48**(25–26): p. 3891-3897.
54. Spătaru, N., et al., *Platinum Electrodeposition on Conductive Diamond Powder and Its Application to Methanol Oxidation in Acidic Media.* Journal of The Electrochemical Society, 2008. **155**(3): p. B264-B269.
55. Antolini, E., *Carbon supports for low-temperature fuel cell catalysts.* Applied Catalysis B: Environmental, 2009. **88**(1–2): p. 1-24.
56. Salazar-Banda, G.R., K.I.B. Eguiluz, and L.A. Avaca, *Boron-doped diamond powder as catalyst support for fuel cell applications.* Electrochemistry Communications, 2007. **9**(1): p. 59-64.
57. Swain, G.M., *The use of CVD diamond thin films in electrochemical systems.* Advanced Materials, 1994. **6**(5): p. 388-392.
58. Xu, J., et al., *Peer Reviewed: Boron-Doped Diamond Thin-Film Electrodes.* Analytical Chemistry, 1997. **69**(19): p. 591A-597A.
59. Chen, Q., et al., *Morphological and Microstructural Stability of Boron-Doped Diamond Thin Film Electrodes in an Acidic Chloride Medium at High Anodic Current Densities.* Journal of The Electrochemical Society, 1997. **144**(11): p. 3806-3812.
60. Knupfer, M., *Electronic properties of carbon nanostructures.* Surface Science Reports, 2001. **42**(1–2): p. 1-74.

61. Haddon, R.C., L.E. Brus, and K. Raghavachari, *Electronic structure and bonding in icosahedral C60.* Chemical Physics Letters, 1986. **125**(5–6): p. 459-464.
62. Chang, H., S.H. Joo, and C. Pak, *Synthesis and characterization of mesoporous carbon for fuel cell applications.* Journal of Materials Chemistry, 2007. **17**(30): p. 3078-3088.
63. Ryoo, R., et al., *Ordered Mesoporous Carbons.* Advanced Materials, 2001. **13**(9): p. 677-681.
64. Yang, H. and D. Zhao, *Synthesis of replica mesostructures by the nanocasting strategy.* Journal of Materials Chemistry, 2005. **15**(12): p. 1217-1231.
65. Lu, A.H. and F. Schüth, *Nanocasting: A Versatile Strategy for Creating Nanostructured Porous Materials.* Advanced Materials, 2006. **18**(14): p. 1793-1805.
66. Lee, J., J. Kim, and T. Hyeon, *Recent Progress in the Synthesis of Porous Carbon Materials.* Advanced Materials, 2006. **18**(16): p. 2073-2094.
67. Kyotani, T., *Control of pore structure in carbon.* Carbon, 2000. **38**(2): p. 269-286.
68. Ndamanisha, J.C. and L.-p. Guo, *Ordered mesoporous carbon for electrochemical sensing: A review.* Analytica Chimica Acta, 2012. **747**(0): p. 19-28.
69. Guo, L., et al., *Hollow mesoporous carbon spheres-an excellent bilirubin adsorbent.* Chemical Communications, 2009(40): p. 6071-6073.
70. Lang, J.-W., et al., *Study on the electrochemical properties of cubic ordered mesoporous carbon for supercapacitors.* Journal of Power Sources, 2011. **196**(23): p. 10472-10478.
71. Cheon, J.Y., et al., *Ordered mesoporous carbon-carbon nanotube nanocomposites as highly conductive and durable cathode catalyst supports for polymer electrolyte fuel cells.* Journal of Materials Chemistry A, 2013. **1**(4): p. 1270-1283.
72. Xu, J.B. and T.S. Zhao, *Mesoporous carbon with uniquely combined electrochemical and mass transport characteristics for polymer electrolyte membrane fuel cells.* RSC Advances, 2013. **3**(1): p. 16-24.
73. Xia, Y. and R. Mokaya, *Generalized and Facile Synthesis Approach to N-Doped Highly Graphitic Mesoporous Carbon Materials.* Chemistry of Materials, 2005. **17**(6): p. 1553-1560.
74. Liang, C., Z. Li, and S. Dai, *Mesoporous Carbon Materials: Synthesis and Modification.* Angewandte Chemie International Edition, 2008. **47**(20): p. 3696-3717.
75. Chen, X., et al., *Synthesis, Growth Mechanism, and Electrochemical Properties of Hollow Mesoporous Carbon Spheres with Controlled Diameter.* The Journal of Physical Chemistry C, 2011. **115**(36): p. 17717-17724.
76. Qiao, Z.-A., et al., *Controlled Synthesis of Mesoporous Carbon Nanostructures via a "Silica-Assisted" Strategy.* Nano Letters, 2012. **13**(1): p. 207-212.
77. Liu, H.-J., et al., *Highly ordered mesoporous carbon nanofiber arrays from a crab shell biological template and its application in supercapacitors and fuel cells.* Journal of Materials Chemistry, 2010. **20**(20): p. 4223-4230.
78. Kyotani, T., L.-f. Tsai, and A. Tomita, *Formation of Ultrafine Carbon Tubes by Using an Anodic Aluminum Oxide Film as a Template.* Chemistry of Materials, 1995. **7**(8): p. 1427-1428.
79. Ma, Z., T. Kyotani, and A. Tomita, *Preparation of a high surface area microporous carbon having the structural regularity of Y zeolite.* Chemical Communications, 2000(23): p. 2365-2366.
80. Fuertes, A.B., *Low-Cost Synthetic Route to Mesoporous Carbons with Narrow Pore Size Distributions and Tunable Porosity through Silica Xerogel Templates.* Chemistry of Materials, 2004. **16**(3): p. 449-455.

81. Zakhidov, A.A., et al., *Carbon Structures with Three-Dimensional Periodicity at Optical Wavelengths.* Science, 1998. **282**(5390): p. 897-901.
82. Wan, Y. and Zhao, *On the Controllable Soft-Templating Approach to Mesoporous Silicates.* Chemical Reviews, 2007. **107**(7): p. 2821-2860.
83. Joo, S.H., et al., *Ordered nanoporous arrays of carbon supporting high dispersions of platinum nanoparticles.* Nature, 2001. **412**(6843): p. 169-172.
84. Ryoo, R., S.H. Joo, and S. Jun, *Synthesis of Highly Ordered Carbon Molecular Sieves via Template-Mediated Structural Transformation.* The Journal of Physical Chemistry B, 1999. **103**(37): p. 7743-7746.
85. Jun, S., et al., *Synthesis of New, Nanoporous Carbon with Hexagonally Ordered Mesostructure.* Journal of the American Chemical Society, 2000. **122**(43): p. 10712-10713.
86. Lee, J.-S., S.H. Joo, and R. Ryoo, *Synthesis of Mesoporous Silicas of Controlled Pore Wall Thickness and Their Replication to Ordered Nanoporous Carbons with Various Pore Diameters.* Journal of the American Chemical Society, 2002. **124**(7): p. 1156-1157.
87. Tian, B., et al., *Novel approaches to synthesize self-supported ultrathin carbon nanowire arrays templated by MCM-41.* Chemical Communications, 2003(21): p. 2726-2727.
88. Barata-Rodrigues, P.M., T.J. Mays, and G.D. Moggridge, *Structured carbon adsorbents from clay, zeolite and mesoporous aluminosilicate templates.* Carbon, 2003. **41**(12): p. 2231-2246.
89. Alvarez, S. and A.B. Fuertes, *Template synthesis of mesoporous carbons with tailorable pore size and porosity.* Carbon, 2004. **42**(2): p. 433-436.
90. Lu, A., et al., *Synthesis of Polyacrylonitrile-Based Ordered Mesoporous Carbon with Tunable Pore Structures.* Chemistry of Materials, 2003. **16**(1): p. 100-103.
91. Meng, Y., et al., *A Family of Highly Ordered Mesoporous Polymer Resin and Carbon Structures from Organic−Organic Self-Assembly.* Chemistry of Materials, 2006. **18**(18): p. 4447-4464.
92. Meng, Y., et al., *Ordered Mesoporous Polymers and Homologous Carbon Frameworks: Amphiphilic Surfactant Templating and Direct Transformation.* Angewandte Chemie International Edition, 2005. **44**(43): p. 7053-7059.
93. Tanaka, S., et al., *Synthesis of ordered mesoporous carbons with channel structure from an organic-organic nanocomposite.* Chemical Communications, 2005(16): p. 2125-2127.
94. Zhang, F., et al., *A Facile Aqueous Route to Synthesize Highly Ordered Mesoporous Polymers and Carbon Frameworks with Ia3d Bicontinuous Cubic Structure.* Journal of the American Chemical Society, 2005. **127**(39): p. 13508-13509.
95. Fang, Y., et al., *A Low-Concentration Hydrothermal Synthesis of Biocompatible Ordered Mesoporous Carbon Nanospheres with Tunable and Uniform Size.* Angewandte Chemie International Edition, 2010. **49**(43): p. 7987-7991.
96. Che, G., et al., *Carbon nanotubule membranes for electrochemical energy storage and production.* Nature, 1998. **393**(6683): p. 346-349.
97. Lee, J., et al., *Synthesis of a new mesoporous carbon and its application to electrochemical double-layer capacitors.* Chemical Communications, 1999(21): p. 2177-2178.
98. Dillon, A.C., et al., *Storage of hydrogen in single-walled carbon nanotubes.* Nature, 1997. **386**(6623): p. 377-379.
99. Hamada, N., S.-i. Sawada, and A. Oshiyama, *New one-dimensional conductors: Graphitic microtubules.* Physical Review Letters, 1992. **68**(10): p. 1579-1581.

100. Mintmire, J.W., B.I. Dunlap, and C.T. White, *Are fullerene tubules metallic?* Physical Review Letters, 1992. **68**(5): p. 631-634.
101. Geng, D., et al., *Non-noble metal oxygen reduction electrocatalysts based on carbon nanotubes with controlled nitrogen contents.* Journal of Power Sources, 2011. **196**(4): p. 1795-1801.
102. Maldonado, S. and K.J. Stevenson, *Direct Preparation of Carbon Nanofiber Electrodes via Pyrolysis of Iron(II) Phthalocyanine: Electrocatalytic Aspects for Oxygen Reduction.* The Journal of Physical Chemistry B, 2004. **108**(31): p. 11375-11383.
103. Bok, S., et al., *Electrochemical Properties of Carbon Nanoparticles Entrapped in a Silica Matrix.* Journal of The Electrochemical Society, 2008. **155**(5): p. K91-K95.
104. Frackowiak, E. and F. Béguin, *Carbon materials for the electrochemical storage of energy in capacitors.* Carbon, 2001. **39**(6): p. 937-950.
105. Kameya, Y. and K. Hanamura, *Kinetic and Raman spectroscopic study on catalytic characteristics of carbon blacks in methane decomposition.* Chemical Engineering Journal, 2011. **173**(2): p. 627-635.
106. Lee, E.K., et al., *Catalytic decomposition of methane over carbon blacks for CO2-free hydrogen production.* Carbon, 2004. **42**(12–13): p. 2641-2648.
107. Lee, S.Y., et al., *Catalytic characteristics of specialty carbon blacks in decomposition of methane for hydrogen production.* Carbon, 2008. **46**(14): p. 1978-1986.
108. Muradov, N., *Catalysis of methane decomposition over elemental carbon.* Catalysis Communications, 2001. **2**(3–4): p. 89-94.
109. Muradov, N., F. Smith, and A. T-Raissi, *Catalytic activity of carbons for methane decomposition reaction.* Catalysis Today, 2005. **102–103**(0): p. 225-233.
110. Lee, S.Y., et al., *Characterization of active sites for methane decomposition on carbon black through acetylene chemisorption.* Carbon, 2008. **46**(2): p. 342-348.
111. Whittingham, M.S., *Lithium incorporation in crystalline and amorphous chalcogenides: Thermodynamics, mechanism and structure.* Journal of Electroanalytical Chemistry and Interfacial Electrochemistry, 1981. **118**(0): p. 229-239.
112. Yazami, R. and P. Touzain, *A reversible graphite-lithium negative electrode for electrochemical generators.* Journal of Power Sources, 1983. **9**(3): p. 365-371.
113. Pfluger, P., et al., *Aspects of alkali metal intercalation and deintercalation in highly oriented pyrolytic graphites.* Synthetic Metals, 1981. **3**(1–2): p. 27-39.
114. Amiell, J., et al., *Propriétés physiques des composés lamellaires KC24(THF)n.* Materials Science and Engineering, 1977. **31**(0): p. 243-247.
115. Billaud, D., A. Pron, and F. Lincoln Vogel, *Electrical resistivity and X-ray spacings of graphite tetrafluoroborate, hexafluorophosphate and hexafluoroantimonate compounds synthesized from nitronium salts.* Synthetic Metals, 1980. **2**(3–4): p. 177-184.
116. Chenite, A. and D. Billaud, *Novel graphite-Hexafluoroarsenate intercalation compounds.* Carbon, 1982. **20**(2): p. 120-121.
117. Hsieh, C.-T. and H. Teng, *Influence of oxygen treatment on electric double-layer capacitance of activated carbon fabrics.* Carbon, 2002. **40**(5): p. 667-674.
118. Bleda-Martínez, M.J., et al., *Chemical and electrochemical characterization of porous carbon materials.* Carbon, 2006. **44**(13): p. 2642-2651.
119. Lozano-Castelló, D., et al., *Influence of pore structure and surface chemistry on electric double layer capacitance in non-aqueous electrolyte.* Carbon, 2003. **41**(9): p. 1765-1775.
120. Kinoshita, K. and J.A.S. Bett, *Potentiodynamic analysis of surface oxides on carbon blacks.* Carbon, 1973. **11**(4): p. 403-411.

121. Cheng, X., et al., *Catalyst Microstructure Examination of PEMFC Membrane Electrode Assemblies vs. Time.* Journal of The Electrochemical Society, 2004. **151**(1): p. A48-A52.
122. Antolini, E., *Formation, microstructural characteristics and stability of carbon supported platinum catalysts for low temperature fuel cells.* Journal of Materials Science, 2003. **38**(14): p. 2995-3005.
123. Taniguchi, A., et al., *Analysis of degradation in PEMFC caused by cell reversal during air starvation.* International Journal of Hydrogen Energy, 2008. **33**(9): p. 2323-2329.
124. Wang, J., et al., *Effect of carbon black support corrosion on the durability of Pt/C catalyst.* Journal of Power Sources, 2007. **171**(2): p. 331-339.
125. Yu, X. and S. Ye, *Recent advances in activity and durability enhancement of Pt/C catalytic cathode in PEMFC: Part I. Physico-chemical and electronic interaction between Pt and carbon support, and activity enhancement of Pt/C catalyst.* Journal of Power Sources, 2007. **172**(1): p. 133-144.
126. Tang, H., et al., *PEM fuel cell cathode carbon corrosion due to the formation of air/fuel boundary at the anode.* Journal of Power Sources, 2006. **158**(2): p. 1306-1312.
127. Paik, C.H., G.S. Saloka, and G.W. Graham, *Influence of Cyclic Operation on PEM Fuel Cell Catalyst Stability.* Electrochemical and Solid-State Letters, 2007. **10**(2): p. B39-B42.
128. Lim, K.H., et al., *Effect of operating conditions on carbon corrosion in polymer electrolyte membrane fuel cells.* Journal of Power Sources, 2009. **193**(2): p. 575-579.
129. Reiser, C.A., et al., *A Reverse-Current Decay Mechanism for Fuel Cells.* Electrochemical and Solid-State Letters, 2005. **8**(6): p. A273-A276.
130. Roen, L.M., C.H. Paik, and T.D. Jarvi, *Electrocatalytic Corrosion of Carbon Support in PEMFC Cathodes.* Electrochemical and Solid-State Letters, 2004. **7**(1): p. A19-A22.
131. Meyers, J.P. and R.M. Darling, *Model of Carbon Corrosion in PEM Fuel Cells.* Journal of The Electrochemical Society, 2006. **153**(8): p. A1432-A1442.
132. Chaparro, A.M., et al., *Study of electrochemical instabilities of PEMFC electrodes in aqueous solution by means of membrane inlet mass spectrometry.* Journal of Electroanalytical Chemistry, 2006. **591**(1): p. 69-73.
133. Li, L. and Y. Xing, *Electrochemical Durability of Carbon Nanotubes in Noncatalyzed and Catalyzed Oxidations.* Journal of The Electrochemical Society, 2006. **153**(10): p. A1823-A1828.
134. Li, L. and Y. Xing, *Electrochemical durability of carbon nanotubes at 80 °C.* Journal of Power Sources, 2008. **178**(1): p. 75-79.
135. Stevens, D.A., et al., *Ex Situ and In Situ Stability Studies of PEMFC Catalysts: Effect of Carbon Type and Humidification on Degradation of the Carbon.* Journal of The Electrochemical Society, 2005. **152**(12): p. A2309-A2315.
136. Kangasniemi, K.H., D.A. Condit, and T.D. Jarvi, *Characterization of Vulcan Electrochemically Oxidized under Simulated PEM Fuel Cell Conditions.* Journal of The Electrochemical Society, 2004. **151**(4): p. E125-E132.
137. Meier, J.C., et al., *Degradation Mechanisms of Pt/C Fuel Cell Catalysts under Simulated Start–Stop Conditions.* ACS Catalysis, 2012. **2**(5): p. 832-843.
138. Linse, N., et al., *The effect of platinum on carbon corrosion behavior in polymer electrolyte fuel cells.* Electrochimica Acta, 2011. **56**(22): p. 7541-7549.
139. Ishigami, Y., et al., *Corrosion of carbon supports at cathode during hydrogen/air replacement at anode studied by visualization of oxygen partial pressures in a PEFC—Start-up/shut-down simulation.* Journal of Power Sources, 2011. **196**(6): p. 3003-3008.

140. Liu, Z.Y., et al., *Characterization of Carbon Corrosion-Induced Structural Damage of PEM Fuel Cell Cathode Electrodes Caused by Local Fuel Starvation.* Journal of The Electrochemical Society, 2008. **155**(10): p. B979-B984.
141. Antonucci, P.L., et al., *Electrochemical corrosion behavior of carbon black in phosphoric acid.* Carbon, 1988. **26**(2): p. 197-203.
142. Ball, S.C., et al., *An investigation into factors affecting the stability of carbons and carbon supported platinum and platinum/cobalt alloy catalysts during 1.2 V potentiostatic hold regimes at a range of temperatures.* Journal of Power Sources, 2007. **171**(1): p. 18-25.
143. Li, W. and A.M. Lane, *Investigation of Pt catalytic effects on carbon support corrosion of the cathode catalyst in PEM fuel cells using DEMS spectra.* Electrochemistry Communications, 2009. **11**(6): p. 1187-1190.
144. Bi, W., et al., *The effect of humidity and oxygen partial pressure on degradation of Pt/C catalyst in PEM fuel cell.* Electrochimica Acta, 2009. **54**(6): p. 1826-1833.
145. Yoda, T., H. Uchida, and M. Watanabe, *Effects of operating potential and temperature on degradation of electrocatalyst layer for PEFCs.* Electrochimica Acta, 2007. **52**(19): p. 5997-6005.
146. Gallagher, K.G. and T.F. Fuller, *Kinetic model of the electrochemical oxidation of graphitic carbon in acidic environments.* Physical Chemistry Chemical Physics, 2009. **11**(48): p. 11557-11567.
147. Yang, Y. and Z.-G. Lin, *In situ IR spectroscopic characterization of surface oxide species on glassy carbon electrodes.* Journal of Electroanalytical Chemistry, 1994. **364**(1–2): p. 23-30.
148. Passalacqua, E., et al., *The influence of Pt on the electrooxidation behaviour of carbon in phosphoric acid.* Electrochimica Acta, 1992. **37**(15): p. 2725-2730.
149. Kinoshita, K. and J. Bett, *Electrochemical oxidation of carbon black in concentrated phosphoric acid at 135°C.* Carbon, 1973. **11**(3): p. 237-247.
150. Gruver, G.A., *The Corrosion of Carbon Black in Phosphoric Acid.* Journal of The Electrochemical Society, 1978. **125**(10): p. 1719-1720.
151. Wei, Z., H. Guo, and Z. Tang, *Heat treatment of carbon-based powders carrying platinum alloy catalysts for oxygen reduction: influence on corrosion resistance and particle size.* Journal of Power Sources, 1996. **62**(2): p. 233-236.
152. Stevens, D.A. and J.R. Dahn, *Thermal degradation of the support in carbon-supported platinum electrocatalysts for PEM fuel cells.* Carbon, 2005. **43**(1): p. 179-188.
153. Willsau, J. and J. Heitbaum, *The influence of Pt-activation on the corrosion of carbon in gas diffusion electrodes—A dems study.* Journal of Electroanalytical Chemistry and Interfacial Electrochemistry, 1984. **161**(1): p. 93-101.
154. Binder, H., et al., *Über die anodische oxydation von aktivkohlen in wässrigen elektrolyten.* Electrochimica Acta, 1964. **9**(3): p. 255-274.
155. Hung, C.-C., et al., *Corrosion of carbon support for PEM fuel cells by electrochemical quartz crystal microbalance.* Journal of Power Sources, 2011. **196**(1): p. 140-146.
156. Jang, S.-E. and H. Kim, *Effect of Water Electrolysis Catalysts on Carbon Corrosion in Polymer Electrolyte Membrane Fuel Cells.* Journal of the American Chemical Society, 2010. **132**(42): p. 14700-14701.
157. Oh, H.-S., J.-H. Lee, and H. Kim, *Electrochemical carbon corrosion in high temperature proton exchange membrane fuel cells.* International Journal of Hydrogen Energy, 2012. **37**(14): p. 10844-10849.

158. Zana, A., et al., *Investigating the corrosion of high surface area carbons during start/stop fuel cell conditions: A Raman study.* Electrochimica Acta, 2013. **114**(0): p. 455-461.
159. Park, Y.-C., et al., *Investigation of the corrosion of carbon supports in polymer electrolyte fuel cells using simulated start-up/shutdown cycling.* Electrochimica Acta, 2013. **91**(0): p. 195-207.
160. Maass, S., et al., *Carbon support oxidation in PEM fuel cell cathodes.* Journal of Power Sources, 2008. **176**(2): p. 444-451.
161. Ferreira, P.J., et al., *Instability of Pt C Electrocatalysts in Proton Exchange Membrane Fuel Cells: A Mechanistic Investigation.* Journal of The Electrochemical Society, 2005. **152**(11): p. A2256-A2271.
162. Shao, Y., et al., *Durability Study of Pt C and Pt CNTs Catalysts under Simulated PEM Fuel Cell Conditions.* Journal of The Electrochemical Society, 2006. **153**(6): p. A1093-A1097.
163. Cheng, P.-Z. and H. Teng, *Electrochemical responses from surface oxides present on HNO3-treated carbons.* Carbon, 2003. **41**(11): p. 2057-2063.
164. Gallagher, K.G., D.T. Wong, and T.F. Fuller, *The Effect of Transient Potential Exposure on the Electrochemical Oxidation of Carbon Black in Low-Temperature Fuel Cells.* Journal of The Electrochemical Society, 2008. **155**(5): p. B488-B493.
165. Colmenares, L.C., et al., *Model study on the stability of carbon support materials under polymer electrolyte fuel cell cathode operation conditions.* Journal of Power Sources, 2009. **190**(1): p. 14-24.
166. Takeuchi, N. and T.F. Fuller, *Modeling and Investigation of Design Factors and Their Impact on Carbon Corrosion of PEMFC Electrodes.* Journal of The Electrochemical Society, 2008. **155**(7): p. B770-B775.
167. Takeuchi, N. and T.F. Fuller, *Modeling and Investigation of Carbon Loss on the Cathode Electrode during PEMFC Operation.* Journal of The Electrochemical Society, 2010. **157**(1): p. B135-B140.
168. Takeuchi, N., E. Jennings, and T.F. Fuller, *Investigation and Modeling of Carbon Oxidation of Pt/C under Dynamic Potential Condition.* ECS Transactions, 2009. **25**(1): p. 1045-1054.
169. Avasarala, B., R. Moore, and P. Haldar, *Surface oxidation of carbon supports due to potential cycling under PEM fuel cell conditions.* Electrochimica Acta, 2010. **55**(16): p. 4765-4771.
170. Su-Il, P., et al., *Role of surface oxides in corrosion of carbon black in phosphoric acid solution at elevated temperature.* Carbon, 1994. **32**(1): p. 155-159.
171. Rositani, F., et al., *Infrared analysis of carbon blacks.* Carbon, 1987. **25**(3): p. 325-332.
172. Akhter, M.S., et al., *The absorption band at 1590 cm−1 in the infrared spectrum of carbons.* Carbon, 1985. **23**(5): p. 589-591.
173. Stonehart, P., *Carbon substrates for phosphoric acid fuel cell cathodes.* Carbon, 1984. **22**(4–5): p. 423-431.
174. Winslow, N.M., *Porous Carbon Electrodes: IV . Wicking Electrodes for Utilization of Insoluble Liquid Depolarizers; Reduction of Nitrobenzene.* Transactions of The Electrochemical Society, 1945. **88**(1): p. 81-96.
175. Zhou, H., L. Shi, and Q. Sun, *Reduction of Nitrobenzene with Hydrazine Hydrate Catalyzed by Acid-Treated Activated Carbon.* Chinese Journal of Catalysis, 2012. **33**(9–10): p. 1463-1469.

176. Ling, X., et al., *Synthesis of nanoscale zero-valent iron/ordered mesoporous carbon for adsorption and synergistic reduction of nitrobenzene.* Chemosphere, 2012. **87**(6): p. 655-660.
177. Liu, C., et al., *One-step assembly of N-doped partially graphitic mesoporous carbon for nitrobenzene reduction.* Materials Letters, 2013. **108**(0): p. 285-288.
178. Winslow, N.M., *Porous Carbon Electrodes: III . Reduction of p-Nitraniline.* Transactions of The Electrochemical Society, 1941. **80**(1): p. 121-131.
179. Janes, M., *Graphite Anodes in Brine Electrolysis: II . Application to Chlorate Cells.* Transactions of The Electrochemical Society, 1947. **92**(1): p. 23-44.
180. Hine, F. and M. Yasuda, *Studies on the Mechanism of the Chlorine Electrode Process.* Journal of The Electrochemical Society, 1974. **121**(10): p. 1289-1294.
181. Janssen, L.J.J., *The mechanism of the chlorine evolution on different types of graphite anodes during the electrolysis of an acidic NaCl solution.* Electrochimica Acta, 1974. **19**(6): p. 257-265.
182. Janssen, L.J.J. and J.G. Hoogland, *The electrolysis of an acidic NaCl solution with a graphite anode—III. Mechanism of chlorine evolution.* Electrochimica Acta, 1970. **15**(6): p. 941-951.
183. Triaca, W.E., C. Solomons, and J.O.M. Bockris, *The mechanism of the electrolytic evolution and dissolution of chlorine on graphite.* Electrochimica Acta, 1968. **13**(9): p. 1949-1964.
184. Frary, F.C., *The Electrolytic Production of Aluminum.* Journal of The Electrochemical Society, 1948. **94**(1): p. 31-40.
185. Mandin, P., R. Wüthrich, and H. Roustan, *Industrial Aluminium Production: the Hall-Heroult Process Modelling.* ECS Transactions, 2009. **19**(26): p. 1-10.
186. Sum, E.Y.L. and M. Skyllas-Kazacos, *Dissolution study of electrolytically deposited aluminium at a graphite electrode.* Electrochimica Acta, 1991. **36**(5–6): p. 811-817.
187. Azari, K., et al., *Mixing variables for prebaked anodes used in aluminum production.* Powder Technology, 2013. **235**(0): p. 341-348.
188. Azari, K., et al., *Compaction properties of carbon materials used for prebaked anodes in aluminum production plants.* Powder Technology, 2013. **246**(0): p. 650-657.
189. Sum, E. and M. Skyllas-Kazacos, *Aluminium dissolution in the NaF-AlF3-Al2O3 system: Effects of alumina, temperature, gas bubbling and dissolved metal.* Journal of Applied Electrochemistry, 1989. **19**(4): p. 485-494.
190. Fleming, C.A., *Hydrometallurgy of precious metals recovery.* Hydrometallurgy, 1992. **30**(1–3): p. 127-162.
191. Ladeira, A.C.Q., M.E.M. Figueira, and V.S.T. Ciminelli, *Characterization of activated carbons utilized in the gold industry: Physical and chemical properties, and kinetic study.* Minerals Engineering, 1993. **6**(6): p. 585-596.
192. Du, J., et al., *Improvement of grain refining efficiency for Mg–Al alloy modified by the combination of carbon and calcium.* Journal of Alloys and Compounds, 2009. **470**(1–2): p. 134-140.
193. Kim, Y.M., C.D. Yim, and B.S. You, *Grain refining mechanism in Mg–Al base alloys with carbon addition.* Scripta Materialia, 2007. **57**(8): p. 691-694.
194. StJohn, D., et al., *Grain refinement of magnesium alloys.* Metallurgical and Materials Transactions A, 2005. **36**(7): p. 1669-1679.
195. Chen, W.X., J.Y. Lee, and Z. Liu, *The nanocomposites of carbon nanotube with Sb and SnSb0.5 as Li-ion battery anodes.* Carbon, 2003. **41**(5): p. 959-966.

196. Yan, J., et al., *Preparation and electrochemical properties of composites of carbon nanotubes loaded with Ag and TiO2 nanoparticle for use as anode material in lithium-ion batteries.* Electrochimica Acta, 2008. **53**(22): p. 6351-6355.
197. Majeau-Bettez, G., T.R. Hawkins, and A.H. Strømman, *Life Cycle Environmental Assessment of Lithium-Ion and Nickel Metal Hydride Batteries for Plug-In Hybrid and Battery Electric Vehicles.* Environmental Science & Technology, 2011. **45**(10): p. 4548-4554.
198. Girishkumar, G., et al., *Lithium–Air Battery: Promise and Challenges.* The Journal of Physical Chemistry Letters, 2010. **1**(14): p. 2193-2203.
199. Goodenough, J.B. and K.-S. Park, *The Li-Ion Rechargeable Battery: A Perspective.* Journal of the American Chemical Society, 2013. **135**(4): p. 1167-1176.
200. Sanjinés, R., et al., *Electrical properties and applications of carbon based nanocomposite materials: An overview.* Surface and Coatings Technology, 2011. **206**(4): p. 727-733.
201. Zhai, Y., et al., *Carbon Materials for Chemical Capacitive Energy Storage.* Advanced Materials, 2011. **23**(42): p. 4828-4850.
202. Simon, P. and Y. Gogotsi, *Materials for electrochemical capacitors.* Nat Mater, 2008. **7**(11): p. 845-854.
203. Zheng, J.P., *Theoretical Energy Density for Electrochemical Capacitors with Intercalation Electrodes.* Journal of The Electrochemical Society, 2005. **152**(9): p. A1864-A1869.
204. Yuan, C.-Z., B. Gao, and X.-G. Zhang, *Electrochemical capacitance of NiO/Ru0.35V0.65O2 asymmetric electrochemical capacitor.* Journal of Power Sources, 2007. **173**(1): p. 606-612.
205. Shimamoto, K., K. Tadanaga, and M. Tatsumisago, *All-solid-state electrochemical capacitors using MnO2/carbon nanotube composite electrode.* Electrochimica Acta, 2013. **109**(0): p. 651-655.
206. Shen, J., et al., *Asymmetric deposition of manganese oxide in single walled carbon nanotube films as electrodes for flexible high frequency response electrochemical capacitors.* Electrochimica Acta, 2012. **78**(0): p. 122-132.
207. Kim, B.-H., K.S. Yang, and D.J. Yang, *Electrochemical behavior of activated carbon nanofiber-vanadium pentoxide composites for double-layer capacitors.* Electrochimica Acta, 2013. **109**(0): p. 859-865.
208. Zhang, W., B. Mu, and A. Wang, *Preparation of manganese dioxide/multiwalled carbon nanotubes hybrid hollow microspheres via layer-by-layer assembly for supercapacitor.* Journal of Materials Science, 2013. **48**(21): p. 7581-7586.
209. Sassin, M.B., et al., *Redox Deposition of Nanoscale Metal Oxides on Carbon for Next-Generation Electrochemical Capacitors.* Accounts of Chemical Research, 2012. **46**(5): p. 1062-1074.
210. Zhao, X., et al., *Incorporation of Manganese Dioxide within Ultraporous Activated Graphene for High-Performance Electrochemical Capacitors.* ACS Nano, 2012. **6**(6): p. 5404-5412.
211. Stepniak, I. and A. Ciszewski, *Electrochemical characteristics of a new electric double layer capacitor with acidic polymer hydrogel electrolyte.* Electrochimica Acta, 2011. **56**(5): p. 2477-2482.
212. Yao, B., et al., *Paper-based solid-state supercapacitors with pencil-drawing graphite/polyaniline networks hybrid electrodes.* Nano Energy, 2013. **2**(6): p. 1071-1078.
213. Kumar, Y., G.P. Pandey, and S.A. Hashmi, *Gel Polymer Electrolyte Based Electrical Double Layer Capacitors: Comparative Study with Multiwalled Carbon Nanotubes and Activated Carbon Electrodes.* The Journal of Physical Chemistry C, 2012. **116**(50): p. 26118-26127.

214. Yuan, J.-K., et al., *Biphasic Polymer Blends Containing Carbon Nanotubes: Heterogeneous Nanotube Distribution and Its Influence on the Dielectric Properties.* The Journal of Physical Chemistry C, 2011. **116**(2): p. 2051-2058.
215. Yang, W., et al., *Carbon Nanomaterials in Biosensors: Should You Use Nanotubes or Graphene?* Angewandte Chemie International Edition, 2010. **49**(12): p. 2114-2138.
216. Krapf, D., et al., *Experimental Observation of Nonlinear Ionic Transport at the Nanometer Scale.* Nano Letters, 2006. **6**(11): p. 2531-2535.
217. Heller, I., et al., *Optimizing the Signal-to-Noise Ratio for Biosensing with Carbon Nanotube Transistors.* Nano Letters, 2008. **9**(1): p. 377-382.
218. Gooding, J.J., *Nanostructuring electrodes with carbon nanotubes: A review on electrochemistry and applications for sensing.* Electrochimica Acta, 2005. **50**(15): p. 3049-3060.
219. McCreery, R.L., *Advanced Carbon Electrode Materials for Molecular Electrochemistry.* Chemical Reviews, 2008. **108**(7): p. 2646-2687.
220. Robinson, J.T., et al., *Reduced Graphene Oxide Molecular Sensors.* Nano Letters, 2008. **8**(10): p. 3137-3140.
221. Ohno, Y., et al., *Electrolyte-Gated Graphene Field-Effect Transistors for Detecting pH and Protein Adsorption.* Nano Letters, 2009. **9**(9): p. 3318-3322.
222. Alwarappan, S., et al., *Probing the Electrochemical Properties of Graphene Nanosheets for Biosensing Applications.* The Journal of Physical Chemistry C, 2009. **113**(20): p. 8853-8857.
223. Lu, C.-H., et al., *A Graphene Platform for Sensing Biomolecules.* Angewandte Chemie, 2009. **121**(26): p. 4879-4881.
224. Lu, J., et al., *Nanometal-Decorated Exfoliated Graphite Nanoplatelet Based Glucose Biosensors with High Sensitivity and Fast Response.* ACS Nano, 2008. **2**(9): p. 1825-1832.
225. Chen, N., et al., *Enhanced room temperature sensing of Co3O4-intercalated reduced graphene oxide based gas sensors.* Sensors and Actuators B: Chemical, 2013. **188**(0): p. 902-908.
226. Huang, X., et al., *The NH3 sensing properties of gas sensors based on aniline reduced graphene oxide.* Synthetic Metals, 2013. **185–186**(0): p. 25-30.
227. Ratinac, K.R., et al., *Toward Ubiquitous Environmental Gas Sensors—Capitalizing on the Promise of Graphene.* Environmental Science & Technology, 2010. **44**(4): p. 1167-1176.
228. Yavari, F. and N. Koratkar, *Graphene-Based Chemical Sensors.* The Journal of Physical Chemistry Letters, 2012. **3**(13): p. 1746-1753.
229. Li, W., et al., *Reduced Graphene Oxide Electrically Contacted Graphene Sensor for Highly Sensitive Nitric Oxide Detection.* ACS Nano, 2011. **5**(9): p. 6955-6961.
230. Yang, D., et al., *Chemical analysis of graphene oxide films after heat and chemical treatments by X-ray photoelectron and Micro-Raman spectroscopy.* Carbon, 2009. **47**(1): p. 145-152.
231. Jung, I., et al., *Effect of Water Vapor on Electrical Properties of Individual Reduced Graphene Oxide Sheets.* The Journal of Physical Chemistry C, 2008. **112**(51): p. 20264-20268.
232. Lu, G., L.E. Ocola, and J. Chen, *Gas detection using low-temperature reduced graphene oxide sheets.* Applied Physics Letters, 2009. **94**(8): p. -.
233. Dua, V., et al., *All-Organic Vapor Sensor Using Inkjet-Printed Reduced Graphene Oxide.* Angewandte Chemie International Edition, 2010. **49**(12): p. 2154-2157.
234. Novoselov, K.S., et al., *Electric Field Effect in Atomically Thin Carbon Films.* Science, 2004. **306**(5696): p. 666-669.

235. Srivastava, A., et al., *Novel Liquid Precursor-Based Facile Synthesis of Large-Area Continuous, Single, and Few-Layer Graphene Films.* Chemistry of Materials, 2010. **22**(11): p. 3457-3461.
236. Reina, A., et al., *Large Area, Few-Layer Graphene Films on Arbitrary Substrates by Chemical Vapor Deposition.* Nano Letters, 2008. **9**(1): p. 30-35.
237. Kim, K.S., et al., *Large-scale pattern growth of graphene films for stretchable transparent electrodes.* Nature, 2009. **457**(7230): p. 706-710.
238. Sutter, P.W., J.-I. Flege, and E.A. Sutter, *Epitaxial graphene on ruthenium.* Nat Mater, 2008. **7**(5): p. 406-411.
239. Gilje, S., et al., *A Chemical Route to Graphene for Device Applications.* Nano Letters, 2007. **7**(11): p. 3394-3398.
240. Soldano, C., A. Mahmood, and E. Dujardin, *Production, properties and potential of graphene.* Carbon, 2010. **48**(8): p. 2127-2150.
241. McAllister, M.J., et al., *Single Sheet Functionalized Graphene by Oxidation and Thermal Expansion of Graphite.* Chemistry of Materials, 2007. **19**(18): p. 4396-4404.
242. Park, S. and R.S. Ruoff, *Chemical methods for the production of graphenes.* Nat Nano, 2009. **4**(4): p. 217-224.
243. Geim, A.K., *Graphene: Status and Prospects.* Science, 2009. **324**(5934): p. 1530-1534.
244. Cheng, C. and Y. Sun, *Carbon doped TiO2 nanowire arrays with improved photoelectrochemical water splitting performance.* Applied Surface Science, 2012. **263**(0): p. 273-276.
245. Shaban, Y.A. and S.U.M. Khan, *Surface grooved visible light active carbon modified (CM)-n-TiO2 thin films for efficient photoelectrochemical splitting of water.* Chemical Physics, 2007. **339**(1–3): p. 73-85.
246. Chen, X. and S.S. Mao, *Titanium Dioxide Nanomaterials: Synthesis, Properties, Modifications, and Applications.* Chemical Reviews, 2007. **107**(7): p. 2891-2959.
247. Fujishima, A. and K. Honda, *Electrochemical Photolysis of Water at a Semiconductor Electrode.* Nature, 1972. **238**(5358): p. 37-38.
248. Cui, C., et al., *Octahedral PtNi Nanoparticle Catalysts: Exceptional Oxygen Reduction Activity by Tuning the Alloy Particle Surface Composition.* Nano Letters, 2012. **12**: p. 5885-5889.
249. Oezaslan, M., F. Hasché, and P. Strasser, *In Situ Observation of Bimetallic Alloy Nanoparticle Formation and Growth Using High-Temperature XRD.* Chemistry of Materials, 2011. **23**(8): p. 2159-2165.
250. Neyerlin, K.C., et al., *Electrochemical activity and stability of dealloyed Pt-Cu and Pt-Cu-Co electrocatalysts for the oxygen reduction reaction (ORR).* J. Power Sources, 2009. **186**(2): p. 261-267.
251. Neyerlin, K.C., et al., *Combinatorial Study of High-Surface-Area Binary and Ternary Electrocatalysts for the Oxygen Evolution Reaction.* J. Electrochem. Soc., 2009. **156**(3): p. B363-B369.
252. Khan, S.U.M., M. Al-Shahry, and W.B. Ingler, *Efficient Photochemical Water Splitting by a Chemically Modified n-TiO2.* Science, 2002. **297**(5590): p. 2243-2245.
253. Licht, S., et al., *Efficient Solar Water Splitting, Exemplified by RuO2-Catalyzed AlGaAs/Si Photoelectrolysis.* The Journal of Physical Chemistry B, 2000. **104**(38): p. 8920-8924.
254. Khaselev, O. and J.A. Turner, *A Monolithic Photovoltaic-Photoelectrochemical Device for Hydrogen Production via Water Splitting.* Science, 1998. **280**(5362): p. 425-427.

255. Khan, S.U.M. and J. Akikusa, *Photoelectrochemical Splitting of Water at Nanocrystalline n-Fe2O3 Thin-Film Electrodes.* The Journal of Physical Chemistry B, 1999. **103**(34): p. 7184-7189.
256. Srivastava, O.N., R.K. Karn, and M. Misra, *Semiconductor-septum photoelectrochemical solar cell for hydrogen production.* International Journal of Hydrogen Energy, 2000. **25**(6): p. 495-503.
257. Akikusa, J. and S.U.M. Khan, *Photoelectrolysis of water to hydrogen in p-SiC/Pt and p-SiC/ n-TiO2 cells.* International Journal of Hydrogen Energy, 2002. **27**(9): p. 863-870.
258. Yu, J.-G., et al., *The Effect of Calcination Temperature on the Surface Microstructure and Photocatalytic Activity of TiO2 Thin Films Prepared by Liquid Phase Deposition.* The Journal of Physical Chemistry B, 2003. **107**(50): p. 13871-13879.
259. Gaillard, N., et al., *A nanocomposite photoelectrode made of 2.2 eV band gap copper tungstate (CuWO4) and multi-wall carbon nanotubes for solar-assisted water splitting.* International Journal of Hydrogen Energy, 2013. **38**(8): p. 3166-3176.
260. Hartmann, P., et al., *Mesoporous TiO2: Comparison of Classical Sol–Gel and Nanoparticle Based Photoelectrodes for the Water Splitting Reaction.* ACS Nano, 2010. **4**(6): p. 3147-3154.
261. Cheng, C., et al., *Solution heteroepitaxial growth of dendritic SnO2/TiO2 hybrid nanowires.* Journal of Materials Research, 2011. **26**(17): p. 2254-2260.
262. Cheng, C., et al., *Quantum-Dot-Sensitized TiO2 Inverse Opals for Photoelectrochemical Hydrogen Generation.* Small, 2012. **8**(1): p. 37-42.
263. Krengvirat, W., et al., *Single-step growth of carbon and potassium-embedded TiO2 nanotube arrays for efficient photoelectrochemical hydrogen generation.* Electrochimica Acta, 2013. **89**(0): p. 585-593.
264. Asahi, R., et al., *Visible-Light Photocatalysis in Nitrogen-Doped Titanium Oxides.* Science, 2001. **293**(5528): p. 269-271.
265. Xu, C., et al., *Nanotube enhanced photoresponse of carbon modified (CM)-n-TiO2 for efficient water splitting.* Solar Energy Materials and Solar Cells, 2007. **91**(10): p. 938-943.
266. Nakano, Y., et al., *Electrical characterization of band gap states in C-doped TiO[sub 2] films.* Applied Physics Letters, 2005. **87**(5): p. 052111-3.
267. Xu, C., et al., *Photocatalytic effect of carbon-modified n-TiO2 nanoparticles under visible light illumination.* Applied Catalysis B: Environmental, 2006. **64**(3–4): p. 312-317.
268. Umebayashi, T., et al., *Band gap narrowing of titanium dioxide by sulfur doping.* Applied Physics Letters, 2002. **81**(3): p. 454-456.
269. Shaban, Y.A. and S.U.M. Khan, *Visible light active carbon modified n-TiO2 for efficient hydrogen production by photoelectrochemical splitting of water.* International Journal of Hydrogen Energy, 2008. **33**(4): p. 1118-1126.
270. Xu, C., et al., *Enhanced carbon doping of n-TiO2 thin films for photoelectrochemical water splitting.* Electrochemistry Communications, 2006. **8**(10): p. 1650-1654.
271. Khan, S.U. and Y.A. Shaban, *Carbon Modified (CM)- n-Fe2O3 Thin Films for Efficient Photoelectrochemical Splitting of Water.* ECS Transactions, 2006. **3**(5): p. 87-94.
272. Tatapudi, P. and J.M. Fenton, *Synthesis of Hydrogen Peroxide in a Proton Exchange Membrane Electrochemical Reactor.* Journal of The Electrochemical Society, 1993. **140**(4): p. L55-L57.
273. Ridge, S.J., et al., *Oxygen Reduction in a Proton Exchange Membrane Test Cell.* Journal of The Electrochemical Society, 1989. **136**(7): p. 1902-1909.

274. Fellinger, T.-P., et al., *Mesoporous Nitrogen-Doped Carbon for the Electrocatalytic Synthesis of Hydrogen Peroxide.* Journal of the American Chemical Society, 2012. **134**(9): p. 4072-4075.
275. Khataee, A.R., et al., *Electrochemical generation of H2O2 using immobilized carbon nanotubes on graphite electrode fed with air: Investigation of operational parameters.* Journal of Electroanalytical Chemistry, 2011. **659**(1): p. 63-68.
276. Özcan, A., Y. Şahin, and M.A. Oturan, *Removal of propham from water by using electro-Fenton technology: Kinetics and mechanism.* Chemosphere, 2008. **73**(5): p. 737-744.
277. Yousfi-Steiner, N., et al., *A review on PEM voltage degradation associated with water management: Impacts, influent factors and characterization.* Journal of Power Sources, 2008. **183**(1): p. 260-274.
278. Bevers, D., R. Rogers, and M. von Bradke, *Examination of the influence of PTFE coating on the properties of carbon paper in polymer electrolyte fuel cells.* Journal of Power Sources, 1996. **63**(2): p. 193-201.
279. Lim, C. and C.Y. Wang, *Effects of hydrophobic polymer content in GDL on power performance of a PEM fuel cell.* Electrochimica Acta, 2004. **49**(24): p. 4149-4156.
280. Jha, N., et al., *Pt–Ru/multi-walled carbon nanotubes as electrocatalysts for direct methanol fuel cell.* International Journal of Hydrogen Energy, 2008. **33**(1): p. 427-433.
281. Anderson, M.L., R.M. Stroud, and D.R. Rolison, *Enhancing the Activity of Fuel-cell Reactions by Designing Three-dimensional Nanostructured Architectures: Catalyst-modified Carbon−Silica Composite Aerogels.* Nano Letters, 2002. **2**(3): p. 235-240.
282. Job, N., et al., *Carbon xerogels as catalyst supports for PEM fuel cell cathode.* Energy Conversion and Management, 2008. **49**(9): p. 2461-2470.
283. Liu, B. and S. Creager, *Carbon xerogels as Pt catalyst supports for polymer electrolyte membrane fuel-cell applications.* Journal of Power Sources, 2010. **195**(7): p. 1812-1820.
284. Pérez-Cadenas, M.a., et al., *Surface Chemistry, Porous Texture, and Morphology of N-Doped Carbon Xerogels.* Langmuir, 2008. **25**(1): p. 466-470.
285. Mitsuda, K. and T. Murahashi, *Polarization Study of a Fuel Cell with Four Reference Electrodes.* Journal of The Electrochemical Society, 1990. **137**(10): p. 3079-3085.
286. Taniguchi, A., et al., *Analysis of electrocatalyst degradation in PEMFC caused by cell reversal during fuel starvation.* Journal of Power Sources, 2004. **130**(1–2): p. 42-49.
287. Yadav, A.P., et al., *Electrochemical Stability and Oxidation Mechanism of Carbon Support for PEM Fuel Cell.* ECS Transactions, 2008. **16**(2): p. 2093-2099.
288. Dam, V.A.T., K. Jayasayee, and F.A. de Bruijn, *Determination of the Potentiostatic Stability of PEMFC Electro Catalysts at Elevated Temperatures.* Fuel Cells, 2009. **9**(4): p. 453-462.
289. Ding, J., et al., *Platinum and platinum–ruthenium nanoparticles supported on ordered mesoporous carbon and their electrocatalytic performance for fuel cell reactions.* Electrochimica Acta, 2005. **50**(15): p. 3131-3141.
290. Su, F., et al., *Preparation and Characterization of Highly Ordered Graphitic Mesoporous Carbon as a Pt Catalyst Support for Direct Methanol Fuel Cells.* Chemistry of Materials, 2005. **17**(15): p. 3960-3967.
291. Joo, S.H., et al., *Ordered mesoporous carbons (OMC) as supports of electrocatalysts for direct methanol fuel cells (DMFC): Effect of carbon precursors of OMC on DMFC performances.* Electrochimica Acta, 2006. **52**(4): p. 1618-1626.
292. Mawhinney, D.B., et al., *Infrared Spectral Evidence for the Etching of Carbon Nanotubes: Ozone Oxidation at 298 K.* Journal of the American Chemical Society, 2000. **122**(10): p. 2383-2384.

293. Dudin, P.V., P.R. Unwin, and J.V. Macpherson, *Electrochemical Nucleation and Growth of Gold Nanoparticles on Single-Walled Carbon Nanotubes: New Mechanistic Insights.* The Journal of Physical Chemistry C, 2010. **114**(31): p. 13241-13248.
294. Wu, G., et al., *A carbon-nanotube-supported graphene-rich non-precious metal oxygen reduction catalyst with enhanced performance durability.* Chemical Communications, 2013. **49**(32): p. 3291-3293.
295. Liu, S., et al., *"Green" electrochemical synthesis of Pt/graphene sheet nanocomposite film and its electrocatalytic property.* Journal of Power Sources, 2010. **195**(15): p. 4628-4633.
296. Qu, L., et al., *Nitrogen-Doped Graphene as Efficient Metal-Free Electrocatalyst for Oxygen Reduction in Fuel Cells.* ACS Nano, 2010. **4**(3): p. 1321-1326.
297. Soin, N., et al., *Microstructural and electrochemical properties of vertically aligned few layered graphene (FLG) nanoflakes and their application in methanol oxidation.* Materials Chemistry and Physics, 2011. **129**(3): p. 1051-1057.
298. Guo, S., S. Dong, and E. Wang, *Three-Dimensional Pt-on-Pd Bimetallic Nanodendrites Supported on Graphene Nanosheet: Facile Synthesis and Used as an Advanced Nanoelectrocatalyst for Methanol Oxidation.* ACS Nano, 2009. **4**(1): p. 547-555.
299. Gao, H., et al., *A simple method to synthesize continuous large area nitrogen-doped graphene.* Carbon, 2012. **50**(12): p. 4476-4482.
300. Gao, W., et al., *New insights into the structure and reduction of graphite oxide.* Nat Chem, 2009. **1**(5): p. 403-408.
301. Song, L., et al., *Effect of high-temperature thermal treatment on the structure and adsorption properties of reduced graphene oxide.* Carbon, 2013. **52**(0): p. 608-612.
302. Li, Y., et al., *Catalytic performance of Pt nanoparticles on reduced graphene oxide for methanol electro-oxidation.* Carbon, 2010. **48**(4): p. 1124-1130.
303. Gao, W., *Graphite Oxide*, in *Springer Handbook of Nanomaterials*, R. Vajtai, Editor. 2013, Springer Berlin Heidelberg. p. 571-604.
304. Matsumoto, T., et al., *Reduction of Pt usage in fuel cell electrocatalysts with carbon nanotube electrodes.* Chemical Communications, 2004(7): p. 840-841.
305. Li, X. and I.M. Hsing, *The effect of the Pt deposition method and the support on Pt dispersion on carbon nanotubes.* Electrochimica Acta, 2006. **51**(25): p. 5250-5258.
306. Yang, C., et al., *Ultrasonically treated multi-walled carbon nanotubes (MWCNTs) as PtRu catalyst supports for methanol electrooxidation.* Journal of Power Sources, 2006. **160**(1): p. 187-193.
307. Ebbesen, T.W., et al., *Decoration of carbon nanotubes.* Advanced Materials, 1996. **8**(2): p. 155-157.
308. Liu, Z., et al., *Preparation and Characterization of Platinum-Based Electrocatalysts on Multiwalled Carbon Nanotubes for Proton Exchange Membrane Fuel Cells.* Langmuir, 2002. **18**(10): p. 4054-4060.
309. Wang, C.H., et al., *High performance of low electrocatalysts loading on CNT directly grown on carbon cloth for DMFC.* Journal of Power Sources, 2007. **171**(1): p. 55-62.
310. Knupp, S.L., et al., *The effect of experimental parameters on the synthesis of carbon nanotube/nanofiber supported platinum by polyol processing techniques.* Carbon, 2008. **46**(10): p. 1276-1284.
311. Liu, Z., et al., *Physical and Electrochemical Characterizations of Microwave-Assisted Polyol Preparation of Carbon-Supported PtRu Nanoparticles.* Langmuir, 2003. **20**(1): p. 181-187.

312. Yasuda, K. and Y. Nishimura, *The deposition of ultrafine platinum particles on carbon black by surface ion exchange—increase in loading amount.* Materials Chemistry and Physics, 2003. **82**(3): p. 921-928.
313. Shao, Y., et al., *Multi-walled carbon nanotubes based Pt electrodes prepared with in situ ion exchange method for oxygen reduction.* Journal of Power Sources, 2006. **161**(1): p. 47-53.
314. Day, T.M., P.R. Unwin, and J.V. Macpherson, *Factors Controlling the Electrodeposition of Metal Nanoparticles on Pristine Single Walled Carbon Nanotubes.* Nano Letters, 2006. **7**(1): p. 51-57.
315. Day, T.M., et al., *Electrochemical Templating of Metal Nanoparticles and Nanowires on Single-Walled Carbon Nanotube Networks.* Journal of the American Chemical Society, 2005. **127**(30): p. 10639-10647.
316. He, D., et al., *Polyaniline-Functionalized Carbon Nanotube Supported Platinum Catalysts.* Langmuir, 2011. **27**(9): p. 5582-5588.
317. Oh, H.-S., K. Kim, and H. Kim, *Polypyrrole-modified hydrophobic carbon nanotubes as promising electrocatalyst supports in polymer electrolyte membrane fuel cells.* International Journal of Hydrogen Energy, 2011. **36**(18): p. 11564-11571.
318. Zhao, Y., et al., *A facile and novel approach toward synthetic polypyrrole oligomers functionalization of multi-walled carbon nanotubes as PtRu catalyst support for methanol electro-oxidation.* Journal of Power Sources, 2010. **195**(15): p. 4634-4640.
319. Tang, Z., et al., *Enhanced catalytic properties from platinum nanodots covered carbon nanotubes for proton-exchange membrane fuel cells.* Journal of Power Sources, 2010. **195**(1): p. 155-159.
320. Fang, H.-T., et al., *Purification of Single-Wall Carbon Nanotubes by Electrochemical Oxidation.* Chemistry of Materials, 2004. **16**(26): p. 5744-5750.
321. Shao, Y., et al., *Comparative investigation of the resistance to electrochemical oxidation of carbon black and carbon nanotubes in aqueous sulfuric acid solution.* Electrochimica Acta, 2006. **51**(26): p. 5853-5857.
322. Park, S., et al., *Polarization Losses under Accelerated Stress Test Using Multiwalled Carbon Nanotube Supported Pt Catalyst in PEM Fuel Cells.* Journal of The Electrochemical Society, 2011. **158**(3): p. B297-B302.
323. Wang, J., et al., *Investigation of Further Improvement of Platinum Catalyst Durability with Highly Graphitized Carbon Nanotubes Support.* The Journal of Physical Chemistry C, 2008. **112**(15): p. 5784-5789.
324. Coloma, F., et al., *Preparation of Platinum Supported on Pregraphitized Carbon Blacks.* Langmuir, 1994. **10**(3): p. 750-755.
325. Hasche, F., M. Oezaslan, and P. Strasser, *Activity, stability and degradation of multi walled carbon nanotube (MWCNT) supported Pt fuel cell electrocatalysts.* Physical Chemistry Chemical Physics, 2010. **12**(46): p. 15251-15258.
326. Andersen, S.M., et al., *Durability of carbon nanofiber (CNF) & carbon nanotube (CNT) as catalyst support for Proton Exchange Membrane Fuel Cells.* Solid State Ionics, 2013. **231**(0): p. 94-101.
327. Zheng, J.-S., et al., *Effect of carbon nanofiber microstructure on oxygen reduction activity of supported palladium electrocatalyst.* Electrochemistry Communications, 2007. **9**(5): p. 895-900.
328. Bessel, C.A., et al., *Graphite Nanofibers as an Electrode for Fuel Cell Applications.* The Journal of Physical Chemistry B, 2001. **105**(6): p. 1115-1118.

329. Li, W., et al., *Platinum nanopaticles supported on stacked-cup carbon nanofibers as electrocatalysts for proton exchange membrane fuel cell.* Carbon, 2010. **48**(4): p. 995-1003.
330. Hayashi, A., et al., *Oxygen Transfer and Storage Processes inside the Mesopores of Platinum-Deposited Mesoporous Carbon Catalyst Thin-Layer Electrode.* The Journal of Physical Chemistry C, 2009. **113**(28): p. 12149-12153.
331. Hayashi, A., et al., *Preparation of Pt/mesoporous carbon (MC) electrode catalyst and its reactivity toward oxygen reduction.* Electrochimica Acta, 2008. **53**(21): p. 6117-6125.
332. Kimijima, K.i., et al., *Oxygen Reduction Reactivity of Precisely Controlled Nanostructured Model Catalysts.* The Journal of Physical Chemistry C, 2010. **114**(35): p. 14675-14683.
333. Zeng, J., et al., *Electrochemical Performance of Pt-Based Catalysts Supported on Different Ordered Mesoporous Carbons (Pt/OMCs) for Oxygen Reduction Reaction.* Industrial & Engineering Chemistry Research, 2011. **51**(22): p. 7500-7509.
334. Ahn, C.-Y., et al., *Effects of ionomer content on Pt catalyst/ordered mesoporous carbon support in polymer electrolyte membrane fuel cells.* Journal of Power Sources, 2013. **222**(0): p. 477-482.
335. Song, S., et al., *Effect of pore morphology of mesoporous carbons on the electrocatalytic activity of Pt nanoparticles for fuel cell reactions.* Applied Catalysis B: Environmental, 2010. **98**(3–4): p. 132-137.
336. Calvillo, L., et al., *Synthesis and performance of platinum supported on ordered mesoporous carbons as catalyst for PEM fuel cells: Effect of the surface chemistry of the support.* International Journal of Hydrogen Energy, 2011. **36**(16): p. 9805-9814.
337. Liu, B. and S. Creager, *Silica–sol-templated mesoporous carbon as catalyst support for polymer electrolyte membrane fuel cell applications.* Electrochimica Acta, 2010. **55**(8): p. 2721-2726.
338. Hasché, F., et al., *Mesoporous Nitrogen Doped Carbon Supported Platinum PEM Fuel Cell Electrocatalyst Made From Ionic Liquids.* ChemCatChem, 2012. **4**(4): p. 479-483.
339. Kim, G. and S.-H. Jhi, *Carbon Monoxide-Tolerant Platinum Nanoparticle Catalysts on Defect-Engineered Graphene.* ACS Nano, 2011. **5**(2): p. 805-810.
340. Jiang, Y., et al., *Enhanced Catalytic Performance of Pt-Free Iron Phthalocyanine by Graphene Support for Efficient Oxygen Reduction Reaction.* ACS Catalysis, 2013. **3**(6): p. 1263-1271.
341. Bianco, A., et al., *All in the graphene family – A recommended nomenclature for two-dimensional carbon materials.* Carbon, 2013. **65**(0): p. 1-6.
342. Geim, A.K. and K.S. Novoselov, *The rise of graphene.* Nat Mater, 2007. **6**(3): p. 183-191.
343. Antolini, E., *Graphene as a new carbon support for low-temperature fuel cell catalysts.* Applied Catalysis B: Environmental, 2012. **123–124**(0): p. 52-68.
344. Berger, C., et al., *Electronic Confinement and Coherence in Patterned Epitaxial Graphene.* Science, 2006. **312**(5777): p. 1191-1196.
345. Dato, A., et al., *Substrate-Free Gas-Phase Synthesis of Graphene Sheets.* Nano Letters, 2008. **8**(7): p. 2012-2016.
346. Choucair, M., P. Thordarson, and J.A. Stride, *Gram-scale production of graphene based on solvothermal synthesis and sonication.* Nat Nano, 2009. **4**(1): p. 30-33.
347. Liu, N., et al., *One-Step Ionic-Liquid-Assisted Electrochemical Synthesis of Ionic-Liquid-Functionalized Graphene Sheets Directly from Graphite.* Advanced Functional Materials, 2008. **18**(10): p. 1518-1525.
348. Wang, G., et al., *Highly efficient and large-scale synthesis of graphene by electrolytic exfoliation.* Carbon, 2009. **47**(14): p. 3242-3246.

349. Lee, S.-H., et al., *A graphite foil electrode covered with electrochemically exfoliated graphene nanosheets.* Electrochemistry Communications, 2010. **12**(10): p. 1419-1422.
350. Brodie, B.C., *Sur le poids atomique du graphite.* Ann. Chim. Phys., 1860. **59**: p. 466-472.
351. Staudenmaier, L., *Verfahren zur Darstellung der Graphitsäure.* Berichte der deutschen chemischen Gesellschaft, 1899. **32**(2): p. 1394-1399.
352. Hummers, W.S. and R.E. Offeman, *Preparation of Graphitic Oxide.* Journal of the American Chemical Society, 1958. **80**(6): p. 1339-1339.
353. Bourlinos, A.B., et al., *Graphite Oxide: Chemical Reduction to Graphite and Surface Modification with Primary Aliphatic Amines and Amino Acids.* Langmuir, 2003. **19**(15): p. 6050-6055.
354. Hofmann, U. and A. Frenzel, *Die Reduktion von Graphitoxyd mit Schwefelwasserstoff.* Kolloid-Zeitschrift, 1934. **68**(2): p. 149-151.
355. Stankovich, S., et al., *Synthesis of graphene-based nanosheets via chemical reduction of exfoliated graphite oxide.* Carbon, 2007. **45**(7): p. 1558-1565.
356. Zhang, Y., et al., *Tuning electrical conductivity and surface area of chemically-exfoliated graphene through nanocrystal functionalization.* Materials Chemistry and Physics, 2012. **135**(2–3): p. 1057-1063.
357. Lu, G., et al., *Facile, noncovalent decoration of graphene oxide sheets with nanocrystals.* Nano Research, 2009. **2**(3): p. 192-200.
358. Cui, S., et al., *Graphene Coupled with Nanocrystals: Opportunities and Challenges for Energy and Sensing Applications.* The Journal of Physical Chemistry Letters, 2013. **4**(15): p. 2441-2454.
359. Liang, Y., et al., *Co3O4 nanocrystals on graphene as a synergistic catalyst for oxygen reduction reaction.* Nat Mater, 2011. **10**(10): p. 780-786.
360. Imran Jafri, R., N. Rajalakshmi, and S. Ramaprabhu, *Nitrogen doped graphene nanoplatelets as catalyst support for oxygen reduction reaction in proton exchange membrane fuel cell.* Journal of Materials Chemistry, 2010. **20**(34): p. 7114-7117.
361. Kim, M., et al., *The preparation of Pt/C catalysts using various carbon materials for the cathode of PEMFC.* Journal of Power Sources, 2006. **163**(1): p. 93-97.
362. Viswanathan, B., *Architecture of carbon support for Pt anodes in direct methanol fuel cells.* Catalysis Today, 2009. **141**(1–2): p. 52-55.
363. Hegenberger, E., N.L. Wu, and J. Phillips, *Evidence of strong interaction between iron particles and an activated carbon support.* The Journal of Physical Chemistry, 1987. **91**(19): p. 5067-5071.
364. Calvillo, L., et al., *Influence of the support on the physicochemical properties of Pt electrocatalysts: Comparison of catalysts supported on different carbon materials.* Materials Chemistry and Physics, 2011. **127**(1–2): p. 335-341.
365. Calvillo, L., et al., *Effect of the support properties on the preparation and performance of platinum catalysts supported on carbon nanofibers.* Journal of Power Sources, 2009. **192**(1): p. 144-150.
366. Shao, Y., et al., *Nitrogen-doped carbon nanostructures and their composites as catalytic materials for proton exchange membrane fuel cell.* Applied Catalysis B: Environmental, 2008. **79**(1): p. 89-99.
367. Prehn, K., et al., *Towards nitrogen-containing CNTs for fuel cell electrodes.* Composites Science and Technology, 2009. **69**(10): p. 1570-1579.
368. Gasteiger, H.A., et al., *Activity benchmarks and requirements for Pt, Pt-alloy, and non-Pt oxygen reduction catalysts for PEMFCs.* Applied Catalysis B: Environmental, 2005. **56**(1–2): p. 9-35.

369. Litster, S. and G. McLean, *PEM fuel cell electrodes.* Journal of Power Sources, 2004. **130**(1–2): p. 61-76.
370. Wang, C., et al., *Proton Exchange Membrane Fuel Cells with Carbon Nanotube Based Electrodes.* Nano Letters, 2003. **4**(2): p. 345-348.
371. Bashyam, R. and P. Zelenay, *A class of non-precious metal composite catalysts for fuel cells.* Nature, 2006. **443**(7107): p. 63-66.
372. Sidik, R.A., et al., *O2 Reduction on Graphite and Nitrogen-Doped Graphite: Experiment and Theory.* The Journal of Physical Chemistry B, 2006. **110**(4): p. 1787-1793.
373. Matter, P.H., L. Zhang, and U.S. Ozkan, *The role of nanostructure in nitrogen-containing carbon catalysts for the oxygen reduction reaction.* Journal of Catalysis, 2006. **239**(1): p. 83-96.
374. Wong, W.Y., et al., *Recent progress in nitrogen-doped carbon and its composites as electrocatalysts for fuel cell applications.* International Journal of Hydrogen Energy, 2013. **38**(22): p. 9370-9386.
375. Wohlgemuth, S.-A., et al., *Tunable nitrogen-doped carbon aerogels as sustainable electrocatalysts in the oxygen reduction reaction.* Journal of Materials Chemistry A, 2013. **1**(12): p. 4002-4009.
376. Wu, J., et al., *Phosphorus-doped porous carbons as efficient electrocatalysts for oxygen reduction.* Journal of Materials Chemistry A, 2013. **1**(34): p. 9889-9896.
377. Glerup, M., et al., *Synthesis of N-doped SWNT using the arc-discharge procedure.* Chemical Physics Letters, 2004. **387**(1–3): p. 193-197.
378. Droppa Jr, R., et al., *Incorporation of nitrogen in carbon nanotubes.* Journal of Non-Crystalline Solids, 2002. **299–302, Part 2**(0): p. 874-879.
379. Hummelen, J.C., et al., *Isolation of the Heterofullerene C59N as Its Dimer (C59N)2.* Science, 1995. **269**(5230): p. 1554-1556.
380. Yudasaka, M., et al., *Nitrogen-containing carbon nanotube growth from Ni phthalocyanine by chemical vapor deposition.* Carbon, 1997. **35**(2): p. 195-201.
381. Terrones, M., et al., *Novel nanoscale gas containers: encapsulation of N in CN nanotubes.* Chemical Communications, 2000(23): p. 2335-2336.
382. Wang, E.-G., *A New Development in Covalently Bonded Carbon Nitride and Related Materials.* Advanced Materials, 1999. **11**(13): p. 1129-1133.
383. Tang, C., et al., *Structure and nitrogen incorporation of carbon nanotubes synthesized by catalytic pyrolysis of dimethylformamide.* Carbon, 2004. **42**(12–13): p. 2625-2633.
384. CaoCao, et al., *Synthesis of Carbon Nitride Nanotubes via a Catalytic-Assembly Solvothermal Route.* Chemistry of Materials, 2004. **16**(25): p. 5213-5215.
385. Wong, W.Y., et al., *Influence of nitrogen doping on carbon nanotubes towards the structure, composition and oxygen reduction reaction.* International Journal of Hydrogen Energy, 2013. **38**(22): p. 9421-9430.
386. Yun, Y.S., et al., *3D hierarchical porous carbons containing numerous nitrogen atoms as catalyst supports for PEMFCs.* Synthetic Metals, 2012. **162**(24): p. 2337-2341.
387. Lu, J., et al., *Nitrogen-doped ordered mesoporous carbons synthesized from honey as metal-free catalyst for oxygen reduction reaction.* Electrochimica Acta, 2013. **108**(0): p. 10-16.
388. Choi, C.H., S.H. Park, and S.I. Woo, *Binary and Ternary Doping of Nitrogen, Boron, and Phosphorus into Carbon for Enhancing Electrochemical Oxygen Reduction Activity.* ACS Nano, 2012. **6**(8): p. 7084-7091.
389. Jiang, L. and L. Gao, *Modified carbon nanotubes: an effective way to selective attachment of gold nanoparticles.* Carbon, 2003. **41**(15): p. 2923-2929.

390. Roy, S.C., et al., *Spectroelectrochemical Study of the Role Played by Carbon Functionality in Fuel Cell Electrodes.* Journal of The Electrochemical Society, 1997. **144**(7): p. 2323-2328.
391. Jaouen, F., et al., *Heat-Treated Fe/N/C Catalysts for O2 Electroreduction: Are Active Sites Hosted in Micropores?* The Journal of Physical Chemistry B, 2006. **110**(11): p. 5553-5558.
392. Yin, J., Y. Qiu, and J. Yu, *Porous nitrogen-doped carbon nanofibers as highly efficient metal-free electrocatalyst for oxygen reduction reaction.* Journal of Electroanalytical Chemistry, 2013. **702**(0): p. 56-59.
393. Maldonado, S. and K.J. Stevenson, *Influence of Nitrogen Doping on Oxygen Reduction Electrocatalysis at Carbon Nanofiber Electrodes.* The Journal of Physical Chemistry B, 2005. **109**(10): p. 4707-4716.
394. Sjöström, H., et al., *Superhard and Elastic Carbon Nitride Thin Films Having Fullerenelike Microstructure.* Physical Review Letters, 1995. **75**(7): p. 1336-1339.
395. Yeager, E., *Electrocatalysts for O2 reduction.* Electrochimica Acta, 1984. **29**(11): p. 1527-1537.
396. Venkatachalapathy, R., G.P. Davila, and J. Prakash, *Catalytic decomposition of hydrogen peroxide in alkaline solutions.* Electrochemistry Communications, 1999. **1**(12): p. 614-617.
397. Szymański, G.S., T. Grzybek, and H. Papp, *Influence of nitrogen surface functionalities on the catalytic activity of activated carbon in low temperature SCR of NOx with NH3.* Catalysis Today, 2004. **90**(1–2): p. 51-59.
398. Matzner, S. and H.P. Boehm, *Influence of nitrogen doping on the adsorption and reduction of nitric oxide by activated carbons.* Carbon, 1998. **36**(11): p. 1697-1703.
399. Huang, M.-C. and H. Teng, *Nitrogen-containing carbons from phenol–formaldehyde resins and their catalytic activity in NO reduction with NH3.* Carbon, 2003. **41**(5): p. 951-957.
400. Zhang, L., et al., *Effect of Microstructure of Nitrogen-Doped Graphene on Oxygen Reduction Activity in Fuel Cells.* Langmuir, 2012. **28**(19): p. 7542-7550.
401. Zhang, L. and Z. Xia, *Mechanisms of Oxygen Reduction Reaction on Nitrogen-Doped Graphene for Fuel Cells.* The Journal of Physical Chemistry C, 2011. **115**(22): p. 11170-11176.
402. Ozaki, J.-i., et al., *Simultaneous doping of boron and nitrogen into a carbon to enhance its oxygen reduction activity in proton exchange membrane fuel cells.* Carbon, 2006. **44**(15): p. 3358-3361.
403. Okamoto, Y., *First-principles molecular dynamics simulation of O2 reduction on nitrogen-doped carbon.* Applied Surface Science, 2009. **256**(1): p. 335-341.
404. Leon y Leon, C.A., et al., *Evidence for the protonation of basal plane sites on carbon.* Carbon, 1992. **30**(5): p. 797-811.
405. Médard, C., et al., *Oxygen reduction by Fe-based catalysts in PEM fuel cell conditions: Activity and selectivity of the catalysts obtained with two Fe precursors and various carbon supports.* Electrochimica Acta, 2006. **51**(16): p. 3202-3213.
406. Co⁄té, R., et al., *Influence of Nitrogen-Containing Precursors on the Electrocatalytic Activity of Heat-Treated Fe (OH) 2 on Carbon Black for O 2 Reduction.* Journal of The Electrochemical Society, 1998. **145**(7): p. 2411-2418.
407. Jaouen, F., F. Charreteur, and J.P. Dodelet, *Fe-Based Catalysts for Oxygen Reduction in PEMFCs: Importance of the Disordered Phase of the Carbon Support.* Journal of The Electrochemical Society, 2006. **153**(4): p. A689-A698.

408. Faubert, G., et al., *Oxygen reduction catalysts for polymer electrolyte fuel cells from the pyrolysis of FeII acetate adsorbed on 3,4,9,10-perylenetetracarboxylic dianhydride.* Electrochimica Acta, 1999. **44**(15): p. 2589-2603.
409. Bron, M., et al., *Catalysts for oxygen reduction from heat-treated carbon-supported iron phenantroline complexes.* Journal of Applied Electrochemistry, 2002. **32**(2): p. 211-216.
410. Kramm, U.I., et al., *Structure of the catalytic sites in Fe/N/C-catalysts for O2-reduction in PEM fuel cells.* Physical Chemistry Chemical Physics, 2012. **14**(33): p. 11673-11688.
411. Herranz, J., et al., *Unveiling N-Protonation and Anion-Binding Effects on Fe/N/C Catalysts for O2 Reduction in Proton-Exchange-Membrane Fuel Cells.* The Journal of Physical Chemistry C, 2011. **115**(32): p. 16087-16097.
412. Sawai, K. and N. Suzuki *Heat-Treated Transition Metal Hexacyanometallates as Electrocatalysts for Oxygen Reduction Insensitive to Methanol.* Journal of The Electrochemical Society, 2004. **151**(5): p. A682-A688.
413. Lalande, G., et al., *Catalytic activity and stability of heat-treated iron phthalocyanines for the electroreduction of oxygen in polymer electrolyte fuel cells.* Journal of Power Sources, 1996. **61**(1–2): p. 227-237.
414. Lalande, G., et al., *Electroreduction of Oxygen in Polymer Electrolyte Fuel Cells by Activated Carbon Coated Cobalt Nanocrystallites Produced by Electric Arc Discharge.* Chemistry of Materials, 1997. **9**(3): p. 784-790.
415. Biloul, A., et al., *Oxygen reduction in acid media: effect of iron substitution by cobalt on heat-treated naphthalocyanine impregnations supported on preselected carbon blacks.* Journal of Electroanalytical Chemistry, 1992. **335**(1–2): p. 163-186.
416. Bouwkamp-Wijnoltz, A.L., et al., *On Active-Site Heterogeneity in Pyrolyzed Carbon-Supported Iron Porphyrin Catalysts for the Electrochemical Reduction of Oxygen: An In Situ Mössbauer Study.* The Journal of Physical Chemistry B, 2002. **106**(50): p. 12993-13001.
417. Gojković, S.L., S. Gupta, and R.F. Savinell, *Heat-Treated Iron(III) Tetramethoxyphenyl Porphyrin Supported on High-Area Carbon as an Electrocatalyst for Oxygen Reduction: I. Characterization of the Electrocatalyst.* Journal of The Electrochemical Society, 1998. **145**(10): p. 3493-3499.
418. Gojković, S.L., S. Gupta, and R.F. Savinell, *Heat-treated iron(III) tetramethoxyphenyl porphyrin chloride supported on high-area carbon as an electrocatalyst for oxygen reduction: Part II. Kinetics of oxygen reduction.* Journal of Electroanalytical Chemistry, 1999. **462**(1): p. 63-72.
419. Gouérec, P., et al., *Dioxygen reduction electrocatalysis in acidic media: effect of peripheral ligand substitution on cobalt tetraphenylporphyrin.* Journal of Electroanalytical Chemistry, 1995. **398**(1–2): p. 67-75.
420. Gouérec, P., et al., *Oxygen reduction in acid media catalyzed by heat treated cobalt tetraazaannulene supported on an active charcoal: correlations between the performances after longevity tests and the active site configuration as seen by XPS and ToF-SIMS.* Journal of Electroanalytical Chemistry, 1997. **422**(1–2): p. 61-75.
421. Gouérec, P., M. Savy, and J. Riga, *Oxygen reduction in acidic media catalyzed by pyrolyzed cobalt macrocycles dispersed on an active carbon: The importance of the content of oxygen surface groups on the evolution of the chelate structure during the heat treatment.* Electrochimica Acta, 1997. **43**(7): p. 743-753.
422. Faubert, G., et al., *Iron catalysts prepared by high-temperature pyrolysis of tetraphenylporphyrins adsorbed on carbon black for oxygen reduction in polymer electrolyte fuel cells.* Electrochimica Acta, 1998. **43**(3–4): p. 341-353.

423. Faubert, G., et al., *Activation and characterization of Fe-based catalysts for the reduction of oxygen in polymer electrolyte fuel cells.* Electrochimica Acta, 1998. **43**(14–15): p. 1969-1984.
424. Serov, A., et al., *Tri-metallic transition metal–nitrogen–carbon catalysts derived by sacrificial support method synthesis.* Electrochimica Acta, 2013. **109**(0): p. 433-439.
425. Di Noto, V., et al., *Preparation, characterization and single-cell performance of a new class of Pd-carbon nitride electrocatalysts for oxygen reduction reaction in PEMFCs.* Applied Catalysis B: Environmental, 2012. **111–112**(0): p. 185-199.
426. Alessio, R., et al., *N,N-dialkylcarbamato complexes of the d(10) cations of copper, silver, and gold.* Helvetica Chimica Acta, 1998. **81**(2): p. 219-230.
427. Eiswirth, M., et al., *Oscillating Langmuir Hinshelwood Mechanisms.* J. Phys. Chem., 1996. **100**: p. 19118.
428. Charreteur, F., et al., *Fe/N/C non-precious catalysts for PEM fuel cells: Influence of the structural parameters of pristine commercial carbon blacks on their activity for oxygen reduction.* Electrochimica Acta, 2008. **53**(6): p. 2925-2938.
429. Lefèvre, M., J.P. Dodelet, and P. Bertrand, *O2 Reduction in PEM Fuel Cells: Activity and Active Site Structural Information for Catalysts Obtained by the Pyrolysis at High Temperature of Fe Precursors.* The Journal of Physical Chemistry B, 2000. **104**(47): p. 11238-11247.
430. Lefèvre, M., J.P. Dodelet, and P. Bertrand, *Molecular Oxygen Reduction in PEM Fuel Cells: Evidence for the Simultaneous Presence of Two Active Sites in Fe-Based Catalysts.* The Journal of Physical Chemistry B, 2002. **106**(34): p. 8705-8713.
431. Jaouen, F., et al., *Oxygen Reduction Catalysts for Polymer Electrolyte Fuel Cells from the Pyrolysis of Iron Acetate Adsorbed on Various Carbon Supports.* The Journal of Physical Chemistry B, 2003. **107**(6): p. 1376-1386.
432. Chung, H.T., et al., *Cyanamide-derived non-precious metal catalyst for oxygen reduction.* Electrochemistry Communications, 2010. **12**(12): p. 1792-1795.
433. Easton, E.B., A. Bonakdarpour, and J.R. Dahn, *Fe-C-N Oxygen Reduction Catalysts Prepared by Combinatorial Sputter Deposition.* Electrochemical and Solid-State Letters, 2006. **9**(10): p. A463-A467.
434. Easton, E.B., et al., *Thermal Evolution of the Structure and Activity of Magnetron-Sputtered TM–C–N (TM = Fe , Co) Oxygen Reduction Catalysts.* Electrochemical and Solid-State Letters, 2007. **10**(1): p. B6-B10.
435. Lefèvre, M. and J.-P. Dodelet, *Fe-based catalysts for the reduction of oxygen in polymer electrolyte membrane fuel cell conditions: determination of the amount of peroxide released during electroreduction and its influence on the stability of the catalysts.* Electrochimica Acta, 2003. **48**(19): p. 2749-2760.
436. Othman, R., A.L. Dicks, and Z. Zhu, *Non precious metal catalysts for the PEM fuel cell cathode.* International Journal of Hydrogen Energy, 2012. **37**(1): p. 357-372.
437. Martínez Millán, W., et al., *Characterization of composite materials of electroconductive polymer and cobalt as electrocatalysts for the oxygen reduction reaction.* International Journal of Hydrogen Energy, 2009. **34**(2): p. 694-702.
438. Millán, W.M. and M.A. Smit, *Study of electrocatalysts for oxygen reduction based on electroconducting polymer and nickel.* Journal of Applied Polymer Science, 2009. **112**(5): p. 2959-2967.
439. Lee, K., et al., *Oxygen reduction reaction (ORR) catalyzed by carbon-supported cobalt polypyrrole (Co-PPy/C) electrocatalysts.* Electrochimica Acta, 2009. **54**(20): p. 4704-4711.

440. Mo, Z., et al., *Vesicular nitrogen doped carbon material derived from Fe2O3 templated polyaniline as improved non-platinum fuel cell cathode catalyst.* Electrochimica Acta, 2013. **99**(0): p. 30-37.
441. Serov, A., et al., *Templated non-PGM cathode catalysts derived from iron and poly(ethyleneimine) precursors.* Applied Catalysis B: Environmental, 2012. **127**(0): p. 300-306.
442. Nguyen-Thanh, D., et al., *Cobalt–polypyrrole–carbon black (Co–PPY–CB) electrocatalysts for the oxygen reduction reaction (ORR) in fuel cells: Composition and kinetic activity.* Applied Catalysis B: Environmental, 2011. **105**(1–2): p. 50-60.
443. Liu, G., et al., *Development of non-precious metal oxygen-reduction catalysts for PEM fuel cells based on N-doped ordered porous carbon.* Applied Catalysis B: Environmental, 2009. **93**(1–2): p. 156-165.
444. Siahrostami, S., et al., *Tandem cathode for proton exchange membrane fuel cells.* Physical Chemistry Chemical Physics, 2013. **15**(23): p. 9326-9334.
445. Oezaslan, M., F. Hasche, and P. Strasser, *Pt-Based Core-Shell Catalyst Architectures for Oxygen Fuel Cell Electrodes.* Journal of Physical Chemistry Letters, 2013. **4**(19): p. 3273-3291.
446. Gan, L. and P. Strasser, *Dealloyed Pt-Based Core–Shell Catalysts for Oxygen Reduction*, in *Electrocatalysis for fuel cells: a non and low Platinum approach*, M. Shao, Editor. 2013, Springer: London. p. 533-560.
447. Gan, L., et al., *Understanding and Controlling Nanoporosity Formation for Improving the Stability of Bimetallic Fuel Cell Catalysts.* Nano Lett., 2013. **13**: p. 1131-1138.
448. Cui, C., et al., *Compositional segregation in shaped Pt alloy nanoparticles and their structural behavior during electrocatalysis.* Nature Mat., 2013. **12**: p. 765.
449. Cui, C., et al., *Shape-selected bimetallic nanoparticle electrocatalysts: evolution of their atomic-scale structure, chemical composition, and electrochemical reactivity under various chemical environments.* Faraday Disc., 2013. **162**(1): p. 91-112.
450. Tuaev, X., et al., *Nitrogen-doped coatings on carbon nanotubes and their stabilizing effect on Pt nanoparticles.* Physical Chemistry Chemical Physics, 2012. **14**(18): p. 6437-6440.
451. Rudi, S., X. Tuaev, and P. Strasser, *Electrocatalytic Oxygen Reduction on Dealloyed Pt1-xNix Alloy Nanoparticle Electrocatalysts.* Electrocatalysis, 2012. **3**: p. 265-273.
452. Oezaslan, M., M. Heggen, and P. Strasser, *Size-Dependent Morphology of Dealloyed Bimetallic Catalysts: Linking the Nano to the Macro Scale.* Journal of the American Chemical Society, 2012. **134**(1): p. 514-524.
453. Oezaslan, M., F. Hasché, and P. Strasser, *Oxygen Electroreduction on PtCo3, PtCo and Pt3Co Alloy Nanoparticles for Alkaline and Acidic PEM Fuel Cells.* Jounal of The Electrochemical Society, 2012. **159**(4): p. B394-B405.
454. Oezaslan, M., F. Hasche, and P. Strasser, *PtCu3, PtCu and Pt3Cu Alloy Nanoparticle Electrocatalysts for Oxygen Reduction Reaction in Alkaline and Acidic Media.* Journal of the Electrochemical Society, 2012. **159**(4): p. B444-B454.
455. Heggen, M., et al., *Formation and Analysis of Core–Shell Fine Structures in Pt Bimetallic Nanoparticle Fuel Cell Electrocatalysts.* Journal of Physical Chemistry C, 2012. **116**(36): p. 19073-19083.
456. Hasche, F., M. Oezaslan, and P. Strasser, *Activity, Structure and Degradation of Dealloyed PtNi3 Nanoparticle Electrocatalyst for the Oxygen Reduction Reaction in PEMFC.* Journal of the Electrochemical Society, 2012. **159**(1): p. B25-B34.

457. Gan, L., et al., *Core-shell Compositional Fine Structures of Dealloyed PtxNi1-x Nanoparticles and their Impact on Oxygen Reduction Catalysis.* Nano Letters, 2012. **12**: p. 5423−5430.
458. Yang, R., P. Strasser, and M.F. Toney, *Dealloying of Cu3Pt (111) Studied by Surface X-ray Scattering.* The Journal of Physical Chemistry C, 2011. **115**(18): p. 9074-9080.
459. Oezaslan, M. and P. Strasser, *Activity of dealloyed PtCo3 and PtCu3 nanoparticle electrocatalyst for oxygen reduction reaction in polymer electrolyte membrane fuel cell.* Journal of Power Sources, 2011. **196**(12): p. 5240-5249.
460. Mani, P., R. Srivastava, and P. Strasser, *Dealloyed binary PtM3 (M=Cu, Co, Ni) and ternary PtNi3M (M=Cu, Co, Fe, Cr) electrocatalysts for the oxygen reduction reaction: performance in polymer electrolyte membrane fuel cells.* J. Pow. Sourc., 2011. **196**: p. 666-673.
461. Hasché, F., M. Oezaslan, and P. Strasser, *Activity, Stability, and Degradation Mechanisms of Dealloyed PtCu3 and PtCo3 Nanoparticle Fuel Cell Catalysts.* ChemCatChem, 2011. **3**(11): p. 1805-1813.
462. Yang, R.Y., Ruizhi); Leisch, J (Leisch, Jennifer); Strasser, P (Strasser, Peter); Toney, MF (Toney, Michael F.), *Structure of Dealloyed PtCu3 Thin Films and Catalytic Activity for Oxygen Reduction.* CHEMISTRY OF MATERIALS, 2010. **22**: p. 4712-4720.
463. Strasser, P., et al., *Lattice-strain control of the activity in dealloyed core-shell fuel cell catalysts.* Nature Chemistry, 2010. **2**(6): p. 454-460.
464. Strasser, P., *Dealloyed Core-Shell Fuel Cell Electrocatalysts.* Reviews in Chemical Engineering, 2009. **25**(4): p. 255-295.
465. Strasser, P., *Dealloyed Pt bimetallic electrocatalysts for oxygen reduction*, in *Handbook of Fuel Cells:Advances in Electrocatalysis, Materials, Diagnostics and Durability*, W. Vielstich, H.A. Gasteiger, and H. Yokokawa, Editors. 2009, John Wiley & Sons Ltd: Chichester, West Sussex, UK. p. 30-47.
466. Strasser, P., S. Koh, and J. Greeley, *Voltammetric surface dealloying of Pt bimetallic nanoparticles: an experimental and DFT computational analysis.* Physical Chemistry Chemical Physics, 2008. **10**(25): p. 3670-3683.
467. Neyerlin, K.C., R. Srivastava, and P. Strasser, *Electrochemical Stability of PtCu and PtCuCo Core-Shell Oxygen Reduction Reaction Electrocatalysts in Liquid Electrolyte.* ECS Transactions, 2008. **16**(2): p. 509-514.
468. Mani, P., R. Srivastava, and P. Strasser, *Dealloyed Pt-Cu core-shell nanoparticle electrocatalysts for use in PEM fuel cell cathodes.* Journal of Physical Chemistry C, 2008. **112**(7): p. 2770-2778.
469. Koh, S., et al., *Effects of Composition and Annealing Conditions on Catalytic Activities of Dealloyed Pt-Cu Nanoparticle Electrocatalysts for PEMFC.* Journal of the Electrochemical Society, 2008. **155**(12): p. B1281-B1288.
470. Srivastava, R., et al., *Efficient oxygen reduction fuel cell electrocatalysis on voltammetrically dealloyed Pt-Cu-Co nanoparticles.* Angewandte Chemie International Edition, 2007. **46**(47): p. 8988-8991.
471. Koh, S.K., Shirlaine); Toney, MF (Toney, Michael F.); Strasser, P (Strasser, Peter), *Activity-stability relationships of ordered and disordered alloy phases of Pt3Co electrocatalysts for the oxygen reduction reaction (ORR).* ELECTROCHIMICA ACTA 2007. **52**: p. 2765-2774.
472. Koh, S., et al., *Activity of ordered and disordered Pt-Co alloy phases for the electroreduction of oxygen in catalysts with multiple coexisting phases.* Journal of Power Sources, 2007. **172**(1): p. 50-56.

473. Koh, S. and P. Strasser, *Electrocatalysis on bimetallic surfaces: Modifying catalytic reactivity for oxygen reduction by voltammetric surface dealloying.* Journal of the American Chemical Society, 2007. **129**(42): p. 12624-+.
474. Jo, G. and S. Shanmugam, *Single-step synthetic approach for boron-doped carbons as a non-precious catalyst for oxygen reduction in alkaline medium.* Electrochemistry Communications, 2012. **25**(0): p. 101-104.
475. Hu, F. and W. Chen, *End-opened carbon nanotube array supported Pd as anode for alkaline fuel cell.* Electrochemistry Communications, 2011. **13**(9): p. 955-958.
476. Duerr, M., et al., *Dynamic electrochemical model of an alkaline fuel cell stack.* Journal of Power Sources, 2007. **171**(2): p. 1023-1032.
477. McLean, G.F., et al., *An assessment of alkaline fuel cell technology.* International Journal of Hydrogen Energy, 2002. **27**(5): p. 507-526.
478. Dillon, R., et al., *International activities in DMFC R&D: status of technologies and potential applications.* Journal of Power Sources, 2004. **127**(1–2): p. 112-126.
479. Bidault, F., et al., *Review of gas diffusion cathodes for alkaline fuel cells.* Journal of Power Sources, 2009. **187**(1): p. 39-48.
480. Zhao, A., et al., *Activation and Stabilization of Nitrogen-Doped Carbon Nanotubes as Electrocatalysts in the Oxygen Reduction Reaction at Strongly Alkaline Conditions.* The Journal of Physical Chemistry C, 2013.
481. Vikkisk, M., et al., *Electrocatalytic oxygen reduction on nitrogen-doped graphene in alkaline media.* Applied Catalysis B: Environmental, 2014. **147**(0): p. 369-376.
482. Vikkisk, M., et al., *Electrocatalysis of oxygen reduction on nitrogen-containing multi-walled carbon nanotube modified glassy carbon electrodes.* Electrochimica Acta, 2013. **87**(0): p. 709-716.
483. Li, H., et al., *Nitrogen-doped carbon nanotubes with high activity for oxygen reduction in alkaline media.* International Journal of Hydrogen Energy, 2011. **36**(3): p. 2258-2265.
484. Huang, T., et al., *Nitrogen-doped graphene-vanadium carbide hybrids as a high-performance oxygen reduction reaction electrocatalyst support in alkaline media.* Journal of Materials Chemistry A, 2013. **1**(43): p. 13404-13410.
485. Hibino, T., K. Kobayashi, and P. Heo, *Oxygen reduction reaction over nitrogen-doped graphene oxide cathodes in acid and alkaline fuel cells at intermediate temperatures.* Electrochimica Acta, 2013. **112**(0): p. 82-89.
486. Jiang, R. and D. Chu, *Comparative study of CoFeNx/C catalyst obtained by pyrolysis of hemin and cobalt porphyrin for catalytic oxygen reduction in alkaline and acidic electrolytes.* Journal of Power Sources, 2014. **245**(0): p. 352-361.
487. Xia, W., et al., *Highly active metal-free nitrogen-containing carbon catalysts for oxygen reduction synthesized by thermal treatment of polypyridine-carbon black mixtures.* Electrochemistry Communications, 2011. **13**(6): p. 593-596.
488. Qiu, Y., et al., *Nitrogen-doped ultrathin carbon nanofibers derived from electrospinning: Large-scale production, unique structure, and application as electrocatalysts for oxygen reduction.* Journal of Power Sources, 2011. **196**(23): p. 9862-9867.
489. Wiggins-Camacho, J.D. and K.J. Stevenson, *Mechanistic Discussion of the Oxygen Reduction Reaction at Nitrogen-Doped Carbon Nanotubes.* The Journal of Physical Chemistry C, 2011. **115**(40): p. 20002-20010.
490. Kruusenberg, I., N. Alexeyeva, and K. Tammeveski, *The pH-dependence of oxygen reduction on multi-walled carbon nanotube modified glassy carbon electrodes.* Carbon, 2009. **47**(3): p. 651-658.

491. Yu, D., et al., *Metal-Free Carbon Nanomaterials Become More Active than Metal Catalysts and Last Longer.* The Journal of Physical Chemistry Letters, 2010. **1**(14): p. 2165-2173.
492. Higgins, D.C., et al., *Cyanamide derived thin film on carbon nanotubes as metal free oxygen reduction reaction electrocatalyst.* Electrochimica Acta, 2012. **59**(0): p. 8-13.
493. Nagaiah, T.C., et al., *Nitrogen-doped carbon nanotubes as a cathode catalyst for the oxygen reduction reaction in alkaline medium.* Electrochemistry Communications, 2010. **12**(3): p. 338-341.
494. Liu, R., et al., *Nitrogen-Doped Ordered Mesoporous Graphitic Arrays with High Electrocatalytic Activity for Oxygen Reduction.* Angewandte Chemie International Edition, 2010. **49**(14): p. 2565-2569.
495. Niwa, H., et al., *X-ray photoemission spectroscopy analysis of N-containing carbon-based cathode catalysts for polymer electrolyte fuel cells.* Journal of Power Sources, 2011. **196**(3): p. 1006-1011.
496. Sharifi, T., et al., *Formation of Active Sites for Oxygen Reduction Reactions by Transformation of Nitrogen Functionalities in Nitrogen-Doped Carbon Nanotubes.* ACS Nano, 2012. **6**(10): p. 8904-8912.
497. Biddinger, E., D. Deak, and U. Ozkan, *Nitrogen-Containing Carbon Nanostructures as Oxygen-Reduction Catalysts.* Topics in Catalysis, 2009. **52**(11): p. 1566-1574.
498. Chen, Z., et al., *Highly Active Nitrogen-Doped Carbon Nanotubes for Oxygen Reduction Reaction in Fuel Cell Applications.* The Journal of Physical Chemistry C, 2009. **113**(49): p. 21008-21013.
499. Kundu, S., et al., *Electrocatalytic Activity and Stability of Nitrogen-Containing Carbon Nanotubes in the Oxygen Reduction Reaction.* The Journal of Physical Chemistry C, 2009. **113**(32): p. 14302-14310.
500. Vazquez-Arenas, J., et al., *Mechanistic analysis of highly active nitrogen-doped carbon nanotubes for the oxygen reduction reaction.* Journal of Power Sources, 2012. **205**(0): p. 215-221.
501. Mo, Z., et al., *Preparation of nitrogen-doped carbon nanotube arrays and their catalysis towards cathodic oxygen reduction in acidic and alkaline media.* Carbon, 2012. **50**(7): p. 2620-2627.
502. Lin, Z., et al., *Facile preparation of nitrogen-doped graphene as a metal-free catalyst for oxygen reduction reaction.* Physical Chemistry Chemical Physics, 2012. **14**(10): p. 3381-3387.
503. Yang, S.-Y., et al., *A powerful approach to fabricate nitrogen-doped graphene sheets with high specific surface area.* Electrochemistry Communications, 2012. **14**(1): p. 39-42.
504. Kurak, K.A. and A.B. Anderson, *Nitrogen-Treated Graphite and Oxygen Electroreduction on Pyridinic Edge Sites.* The Journal of Physical Chemistry C, 2009. **113**(16): p. 6730-6734.
505. Ikeda, T., et al., *Carbon Alloy Catalysts: Active Sites for Oxygen Reduction Reaction.* The Journal of Physical Chemistry C, 2008. **112**(38): p. 14706-14709.
506. Gong, K., et al., *Nitrogen-Doped Carbon Nanotube Arrays with High Electrocatalytic Activity for Oxygen Reduction.* Science, 2009. **323**(5915): p. 760-764.
507. Biddinger, E.J. and U.S. Ozkan, *Role of Graphitic Edge Plane Exposure in Carbon Nanostructures for Oxygen Reduction Reaction.* The Journal of Physical Chemistry C, 2010. **114**(36): p. 15306-15314.

508. Matter, P.H., et al., *Oxygen Reduction Reaction Catalysts Prepared from Acetonitrile Pyrolysis over Alumina-Supported Metal Particles.* The Journal of Physical Chemistry B, 2006. **110**(37): p. 18374-18384.
509. Zhu, C. and S. Dong, *Recent progress in graphene-based nanomaterials as advanced electrocatalysts towards oxygen reduction reaction.* Nanoscale, 2013. **5**(5): p. 1753-1767.
510. Wang, H., T. Maiyalagan, and X. Wang, *Review on Recent Progress in Nitrogen-Doped Graphene: Synthesis, Characterization, and Its Potential Applications.* ACS Catalysis, 2012. **2**(5): p. 781-794.
511. Wang, S., et al., *BCN Graphene as Efficient Metal-Free Electrocatalyst for the Oxygen Reduction Reaction.* Angewandte Chemie International Edition, 2012. **51**(17): p. 4209-4212.
512. Yang, Z., et al., *Recent progress in doped carbon nanomaterials as effective cathode catalysts for fuel cell oxygen reduction reaction.* Journal of Power Sources, 2013. **236**(0): p. 238-249.
513. Lin, Z., et al., *Facile Synthesis of Nitrogen-Doped Graphene via Pyrolysis of Graphene Oxide and Urea, and its Electrocatalytic Activity toward the Oxygen-Reduction Reaction.* Advanced Energy Materials, 2012. **2**(7): p. 884-888.
514. Sun, Y., C. Li, and G. Shi, *Nanoporous nitrogen doped carbon modified graphene as electrocatalyst for oxygen reduction reaction.* Journal of Materials Chemistry, 2012. **22**(25): p. 12810-12816.
515. Hacker, V., et al., *Carbon nanofiber-based active layers for fuel cell cathodes – preparation and characterization.* Electrochemistry Communications, 2005. **7**(4): p. 377-382.
516. Kostowskyj, M.A., et al., *Silver nanowire catalysts for alkaline fuel cells.* International Journal of Hydrogen Energy, 2008. **33**(20): p. 5773-5778.
517. Cheng, Y., et al., *Modified multi-walled carbon nanotube/Ag nanoparticle composite catalyst for the oxygen reduction reaction in alkaline solution.* Electrochimica Acta, 2013. **111**(0): p. 635-641.
518. Hepel, M. and M. Tomkiewicz, *Study of the Initial Stages of Anodic Oxidation of Polycrystalline Silver in KOH Solutions.* Journal of The Electrochemical Society, 1984. **131**(6): p. 1288-1294.
519. Guo, J., et al., *Improving Oxygen Reduction Reaction Activities on Carbon-Supported Ag Nanoparticles in Alkaline Solutions.* The Journal of Physical Chemistry C, 2010. **114**(10): p. 4324-4330.
520. Tammeveski, L., et al., *Electrocatalytic oxygen reduction on silver nanoparticle/multi-walled carbon nanotube modified glassy carbon electrodes in alkaline solution.* Electrochemistry Communications, 2012. **20**(0): p. 15-18.
521. Maheswari, S., et al., *Carbon-supported Pd-Co as cathode catalyst for APEMFCs and validation by DFT.* Physical Chemistry Chemical Physics, 2012. **14**(27): p. 9683-9695.
522. Antolini, E., *Palladium in fuel cell catalysis.* Energy & Environmental Science, 2009. **2**(9): p. 915-931.
523. Shao, M., et al., *Origin of Enhanced Activity in Palladium Alloy Electrocatalysts for Oxygen Reduction Reaction†.* The Journal of Physical Chemistry B, 2007. **111**(24): p. 6772-6775.
524. Wang, Y. and P.B. Balbuena, *Design of Oxygen Reduction Bimetallic Catalysts: Ab-Initio-Derived Thermodynamic Guidelines.* The Journal of Physical Chemistry B, 2005. **109**(40): p. 18902-18906.

525. Fernández, J.L., D.A. Walsh, and A.J. Bard, *Thermodynamic Guidelines for the Design of Bimetallic Catalysts for Oxygen Electroreduction and Rapid Screening by Scanning Electrochemical Microscopy. M−Co (M: Pd, Ag, Au).* Journal of the American Chemical Society, 2004. **127**(1): p. 357-365.
526. Duong, H.T., et al., *Oxygen Reduction Catalysis of the Pt3Co Alloy in Alkaline and Acidic Media Studied by X-ray Photoelectron Spectroscopy and Electrochemical Methods.* The Journal of Physical Chemistry C, 2007. **111**(36): p. 13460-13465.
527. Jasinski, R., *A New Fuel Cell Cathode Catalyst.* Nature, 1964. **201**(4925): p. 1212-1213.
528. Claude, E., et al., *A new method for electrochemical screening basedon the rotating ring disc electrode and its applicationto oxygen reduction catalysts.* Journal of Applied Electrochemistry, 1998. **28**(1): p. 57-64.
529. Yu, E., et al., *Electrochemical reduction of oxygen with iron phthalocyanine in neutral media.* Journal of Applied Electrochemistry, 2009. **39**(5): p. 705-711.
530. Morozan, A., et al., *Catalytic activity of cobalt and iron phthalocyanines or porphyrins supported on different carbon nanotubes towards oxygen reduction reaction.* Carbon, 2011. **49**(14): p. 4839-4847.
531. Kruusenberg, I., et al., *Non-platinum cathode catalysts for alkaline membrane fuel cells.* International Journal of Hydrogen Energy, 2012. **37**(5): p. 4406-4412.
532. Chen, R., et al., *Unraveling Oxygen Reduction Reaction Mechanisms on Carbon-Supported Fe-Phthalocyanine and Co-Phthalocyanine Catalysts in Alkaline Solutions.* The Journal of Physical Chemistry C, 2009. **113**(48): p. 20689-20697.
533. Harnisch, F., et al., *Comparative study on the performance of pyrolyzed and plasma-treated iron(II) phthalocyanine-based catalysts for oxygen reduction in pH neutral electrolyte solutions.* Journal of Power Sources, 2009. **193**(1): p. 86-92.
534. Song, C., et al., *Temperature Dependence of Oxygen Reduction Catalyzed by Cobalt Fluoro-Phthalocyanine Adsorbed on a Graphite Electrode.* Fuel Cells, 2007. **7**(1): p. 9-15.
535. Mao, L., et al., *Mechanistic study of the reduction of oxygen in air electrode with manganese oxides as electrocatalysts.* Electrochimica Acta, 2003. **48**(8): p. 1015-1021.
536. Cao, Y.L., et al., *The mechanism of oxygen reduction on MnO2-catalyzed air cathode in alkaline solution.* Journal of Electroanalytical Chemistry, 2003. **557**(0): p. 127-134.
537. Yang, J. and J.J. Xu, *Nanoporous amorphous manganese oxide as electrocatalyst for oxygen reduction in alkaline solutions.* Electrochemistry Communications, 2003. **5**(4): p. 306-311.
538. Verma, A., A.K. Jha, and S. Basu, *Manganese dioxide as a cathode catalyst for a direct alcohol or sodium borohydride fuel cell with a flowing alkaline electrolyte.* Journal of Power Sources, 2005. **141**(1): p. 30-34.
539. Hu, F.-P., et al., *Oxygen reduction on Ag–MnO2/SWNT and Ag–MnO2/AB electrodes.* Carbon, 2005. **43**(14): p. 2931-2936.
540. Zhang, G.-Q., X.-G. Zhang, and Y.-G. Wang, *A new air electrode based on carbon nanotubes and Ag–MnO2 for metal air electrochemical cells.* Carbon, 2004. **42**(15): p. 3097-3102.
541. Bergmann, A., et al., *Electrochemical water splitting by layered and 3D cross-linked manganese oxides: correlating structural motifs and catalytic activity.* Energy & Environmental Science, 2013. **6**(9): p. 2745-2755.
542. Mette, K., et al., *Nanostructured Manganese Oxide Supported on Carbon Nanotubes for Electrocatalytic Water Splitting.* Chemcatchem, 2012. **4**(6): p. 851-862.
543. Cheng, F., et al., *MnO2-Based Nanostructures as Catalysts for Electrochemical Oxygen Reduction in Alkaline Media†.* Chemistry of Materials, 2009. **22**(3): p. 898-905.

544. Sun, W., A. Hsu, and R. Chen, *Carbon-supported tetragonal MnOOH catalysts for oxygen reduction reaction in alkaline media.* Journal of Power Sources, 2011. **196**(2): p. 627-635.
545. Lima, F.H.B., M.L. Calegaro, and E.A. Ticianelli, *Electrocatalytic activity of manganese oxides prepared by thermal decomposition for oxygen reduction.* Electrochimica Acta, 2007. **52**(11): p. 3732-3738.
546. Ohsaka, T., et al., *Bifunctional catalytic activity of manganese oxide toward O2 reduction: novel insight into the mechanism of alkaline air electrode.* Electrochemistry Communications, 2004. **6**(3): p. 273-277.
547. Cheng, F., et al., *Selective Synthesis of Manganese Oxide Nanostructures for Electrocatalytic Oxygen Reduction.* ACS Applied Materials & Interfaces, 2009. **1**(2): p. 460-466.
548. Qu, D., *Investigation of the porosity of electrolytic manganese dioxide and its performance as alkaline cathode material.* Journal of Power Sources, 2006. **156**(2): p. 692-699.
549. Roche, I. and K. Scott, *Effect of pH and temperature on carbon-supported manganese oxide oxygen reduction electrocatalysts.* Journal of Electroanalytical Chemistry, 2010. **638**(2): p. 280-286.
550. Klápště, B., J. Vondrák, and J. Velická, *MnOx/C composites as electrode materials II. Reduction of oxygen on bifunctional catalysts based on manganese oxides.* Electrochimica Acta, 2002. **47**(15): p. 2365-2369.